



UNIVERSITAT  
POLITÈCNICA  
DE VALÈNCIA

Department of Mechanical Engineering and Materials



# **Development of new high-performance Titanium alloys with Fe-addition for dental implants**

**Doctoral Thesis**

Prakash Mohan

Under guidance of:

Vicente Amigo Borrás

Valencia, March 2020





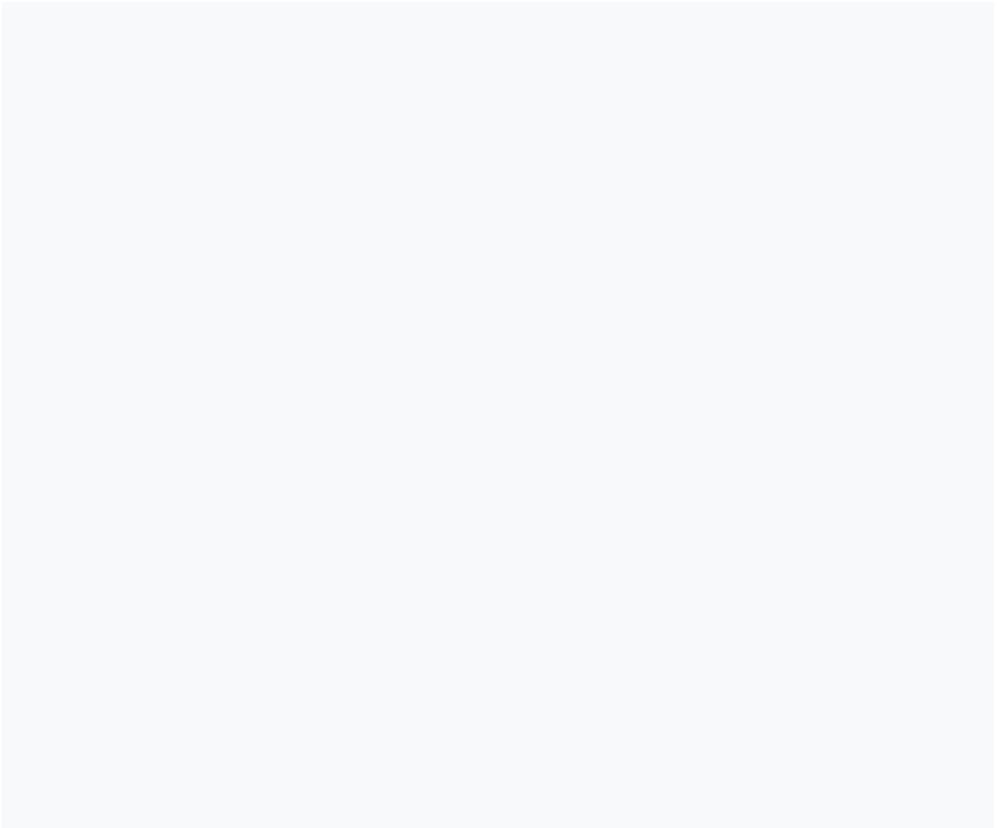


Memory presented by Prakash Mohan at the doctoral school of the polytechnic university of Valencia, doctoral program in engineering and industrial production, to qualify for the title of doctor.

This work has been developed in the department of material technology and mechanical and materials engineering department of Universitat Politecnica de Valencia, through the Spanish Ministry of Economy and Competitiveness under the Research Project PROMETEO 2016/040, MAT2018-53764-C3-1-R, and Erasmus-Mundus (Namaste) scholarship.



Dedicated to my family







## **Acknowledgement:**

First, I want to thank Dr. Vicente Amigo Borrás for all the knowledge and advice he has managed to convey to me and, above all, for his patience. He is always kind to me.

I want to express my gratitude to my family that always supports me unconditionally. They always supported me emotionally.

I also want to thank to scholarship program “Erasmus Mundus Action 2, Strand 1” (EMA 2) Namaste program and project 2018 from which they provide financially help during my research.

I also thank all the person who have supported me during my investigation, Angel, Paco, Montse, Esther, Jenny, Angelica, Juan carlos, Mauricio, Bakr, nelly, joan lario etc. I also want to thank all the lab assistant for helping me during my experiment.

There are many people who have influenced their bit in me and in this thesis during the time that I have been working on it. Thanks for everything.







# Resumen:

El titanio y sus aleaciones son los biomateriales principalmente usados debido a sus propiedades únicas como alta resistencia a la corrosión, bajo módulo de elasticidad, alta resistencia mecánica/densidad y buena biocompatibilidad. Las aleaciones Ti $\beta$  basadas en el sistema de aleación Ti-Mo muestran propiedades únicas para emplearse como biomateriales. Las aleaciones de Ti $\beta$  tienen un módulo de Young más bajo, menor apantallamiento de tensiones y menor reabsorción ósea. Esta investigación tiene como objetivo desarrollar un nuevo material biológico para un implante dental.

Esta investigación evalúa la adición de Zr y una pequeña cantidad de Fe sobre la estabilidad de fase  $\beta$  y las propiedades mecánicas de la aleación de Ti-Mo que se utilizará para las aplicaciones médicas. Estas aleaciones se han producido utilizando dos técnicas de pulvimetalurgia (PM); La primera técnica es la combinación de polvos elementales (EB) que se ha seleccionado porque mejora el contacto superficial entre el elemento de aleación y el titanio (Ti) con una ruta rentable. El comportamiento de diferentes composiciones de aleaciones de Ti se evaluó utilizando esta técnica. Las muestras se prensaron uniaxialmente a 600 MPa y se sinterizaron a 1250°C. La segunda técnica evaluada en este estudio fue la aleación mecánica (MA). Esta técnica tiene una mayor energía de mezcla que la mezcla elemental, lo que mejora el contacto mecánico entre las diferentes partículas y ayuda a la difusión durante el proceso de sinterización. Las muestras se prensaron, igualmente, a 600 MPa inicialmente, y después de evaluar las propiedades mecánicas, la presión de compactación se aumentó a 900 MPa para una mayor densidad en verde de los polvos.

Se realizaron diferentes pruebas mecánicas y estudios microestructurales para las muestras de mezcla elemental (EB) y las muestras de aleación mecánica (MA) para garantizar las propiedades adecuadas para aplicaciones biomédicas. Las diferentes

pruebas para MA han sido la fluidez, adecuada para conocer el flujo del polvo después del ciclo de molienda, y el análisis granulométrico, adecuado para el análisis de la distribución del tamaño de los polvos. Otras pruebas comunes como la determinación de la densidad por el método de Arquímedes, adecuada para calcular la porosidad de las muestras sinterizadas, el ensayo de flexión a tres puntos para conocer las propiedades mecánicas de las muestras sinterizadas y conocer la energía conservada por las muestras a rotura, y la dureza Vickers de las aleaciones. Mediante ultrasonidos se ha determinado el módulo elástico de las aleaciones. El análisis microestructural se ha realizado mediante microscopía electrónica de barrido y análisis por energías dispersivas de rayos X mediante los que se ha determinado la homogeneidad química de las aleaciones. La difracción de electrones retrodispersados (EBSD) ha permitido obtener la orientación cristalina de cada grano y su tamaño, pues resulta una excelente herramienta para el microanálisis del material.

La densidad en verde para aleaciones de mezcla elemental está en el rango del 77.42-78.11% y para las muestras de aleación mecánica se han obtenido densidades relativas del 74.94-78.58%. La densidad de los sinterizados, obtenida por el método de Arquímedes, está en el rango del 96.88-98.74%, para la mezcla elemental de polvos. La resistencia a la flexión obtenida a partir de la prueba de flexión a tres puntos está en un amplio rango de 666 a 2161 GPa, mientras que para los polvos de aleación mecánica se encuentra en el rango de los 371 a 1597 GPa. El módulo elástico determinado en las aleaciones obtenidas con polvos de mezcla elemental está en el rango de los 95.5 a los 103 GPa, mientras que, en las obtenidas con los polvos mezclados mecánicamente, su módulo elástico oscila entre los 66 y los 82 GPa, que sería más adecuado para un menor apantallamiento de tensiones. La microestructura de las muestras procesadas con polvos elementales con polvos mezclados mecánicamente, presentan diferencias sustanciales con un afinamiento del tamaño de grano con los polvos mezclados mecánicamente, aunque aparecen claramente diferenciadas dos fases distintas y una mayor proporción de fase  $\alpha$ . Debido a la menor densidad de las muestras procesadas con los polvos mezclados mecánicamente, estas presentan una menor resistencia mecánica y a su vez una menor plasticidad. Por ello se opta por utilizar técnicas de sinterización de alta densificación como el *Spark Plasma Sintering* (SPS) a pesar de lo cual no

obtenemos mejora en el comportamiento mecánico de las mismas. Sin embargo, en los ensayos de corrosión y liberación de iones si se ha encontrado una sustancial mejor en las muestras obtenidas por SPS.





# Resum:

El titani i els seus aliatges són utilitzats, principalment, com a biomaterials per les seves propietats úniques com alta resistència a la corrosió, baix mòdul d'elasticitat, alta resistència mecànica específica i bona biocompatibilitat. Els aliatges  $\beta$  Ti basades en el sistema d'aliatge Ti-Mo mostren propietats úniques per a emprar-se com biomaterials. Els aliatges de  $\beta$  Ti tenen un mòdul de Young més baix, menor apantallament de tensions i menor reabsorció òssia. Aquesta investigació té com a objectiu desenvolupar un nou material biocompatible per a la seva aplicació com a implants dentals.

Aquesta investigació avalua l'addició de Zr i petites quantitats de Fe sobre l'estabilitat de la fase  $\beta$  i les propietats mecàniques dels aliatges Ti-Mo que s'utilitzaran per a aplicacions biomèdiques. Aquests aliatges s'han produït utilitzant dues tècniques pulvimetalúrgiques (PM); La primera tècnica és la mescla elemental de pols (EB) que s'ha seleccionat perquè millora el contacte superficial entre l'element d'aliatge i el titani (Ti) amb una ruta rendible. El comportament de diferents composicions d'aliatges de Ti s'ha avaluat utilitzant aquesta tècnica. Les mostres es van premsar uniaxialment a 600 MPa i es sinteritzaren a 1250°C. La segona tècnica avaluada en aquest estudi va ser l'aliatge mecànic (MA). Aquesta tècnica té una major energia de mescla que la mescla elemental, el que millora el contacte mecànic entre les diferents partícules i ajuda a la difusió durant el procés de sinterització. Les mostres es van premsar a 600 MPa inicialment, i després d'avaluar les propietats mecàniques, la pressió de compactació es va augmentar a 900 MPa per a una major densitat en verd de les pols.

Es van realitzar diferents proves mecàniques i estudis microestructurals per a mostres de mescla elemental (EB) i per a mostres d'aliatge mecànic per garantir les propietats adequades per a aplicacions biomèdiques. Les diferents proves per MA són la prova de fluïdesa (adequada per conèixer el flux de la pols després del cicle d'aliatge mecànic) i l'anàlisi granulomètric (la prova és adequada per a l'anàlisi de distribució de la mida de les pols). S'han realitzat altres proves comunes com la prova d'Arquímedes, adequada per a calcular la porositat de les mostres sinteritzades. La

prova de flexió de tres punts és adequada per conèixer la resistència a la flexió de les mostres sinteritzades i conèixer l'energia conservada per les mostres durant el seu trencament. Mitjançant ultrasons s'ha determinat el mòdul elàstic dels aliatges i la duresa s'ha realitzat per calcular la duresa Vickers de l'aliatge. S'ha realitzat l'anàlisi per SEM per conèixer la microestructura i l'anàlisi per EDX (mitjançant el qual es coneixeria la mescla adequada de l'element d'aliatge amb l'element central). EBSD (difracció d'electrons retro dispersats) també es realitza per a un més complet anàlisi sobre la microestructura, orientacions cristal·lines, mida de gra, mescla de diferents elements en els aliatges. EBSD és una excel·lent eina per al microanàlisi del material.

De la secció de resultats es determinen la densitat en verd de l'aliatge, fluïdesa de la pols mòlta, granulometria de la pols, densitat de l'aliatge sinteritzada (prova d'Arquímedes), resistència a la flexió i mòdul a flexió de l'aliatge, mòdul elàstic per ultrasons, microestructura de l'aliatge (per SEM i EBSD). La densitat en verd per als aliatges de mescla elemental està en el rang dels 77.42-78.11%, mentre que per a les mostres d'aliatge mecànica van ser d'un 74.94-78.58%. La densitat dels sinteritzats, obtinguda pel mètode d'Arquímedes, està en el rang dels 96.88-98.74%, per la mescla elemental de pols. La resistència a la flexió obtinguda a partir de la prova de flexió de tres punts es troba en el rang dels 666-2161 MPa, mentre que per a les mostres de aliat mecànic el seu rang és molt ampli, des dels 371 als 1597 MPa. A partir de l'assaig d'ultrasons, el mòdul elàstic determinat per als aliatges de mescla elemental està en el rang de 95.5 a 103 GPa i per a les sinteritzades amb pols aliats mecànicament, es troba en el rang dels 66-82 GPa, que seria més adequat per a aplicacions biomèdiques. A partir de les anàlisis per SEM i EBSD, es confirma que l'aliatge mecànica és una mescla més homogènia en comparació amb la mescla elemental dels pols.

La densitat en verd (just després de la compactació) per a la mescla elemental és més gran que en l'aliatge mecànica, de manera que la densitat sinteritzada per a la mescla elemental és major igualment que en l'aliatge mecànica. A causa d'una major densitat dels sinteritzats, la porositat és menor en el cas de la mescla elemental. A més, a causa d'una major porositat, la resistència a la flexió és baixa en cas d'aliatge mecànica amb els mateixos paràmetres de sinterització que els aliatges de mescla elemental. El valor de microduresa és major en el cas de la mescla elemental en

comparació amb l'aliatge mecànica. El mòdul elàstic també resulta més gran en el cas d'una mescla elemental comparat amb l'aliatge mecànica, que en aquest cas resultaria més adequat per a aplicacions biomèdiques. Els grans són més regulars i més petits en el cas de l'aliatge mecànica, a causa d'una distribució més homogènia dels elements en comparació amb la mescla elemental i als efectes de recristal·lització durant la sinterització.

L'aliatge mecànica va produir una mescla més homogènia dels elements d'aliatge, a causa de la mòlta a alta velocitat amb una relació boles/pols més alta que genera una major energia dins de les gerres i obté partícules de pols més petites. S'ha realitzat una combinació de diferents velocitats i temps de mòlta, optimitzant aquests paràmetres per a les nostres aliatges.



# Abstract:

Ti and its alloys are mostly used biomaterials due to its unique properties like (high corrosion resistance, low elastic modulus, high mechanical strength/ density and good biocompatibility). Ti  $\beta$  alloys based on the Ti-Mo alloy system shows unique properties to employ as biomaterials. Ti $\beta$  alloys have lower Young Modulus, shielding stress and lower bone reabsorption. This research aims to develop a new biomaterial for a dental implant.

This research evaluates the addition of Zr and a small amount of Fe on the  $\beta$ -phase stability and the mechanical properties of Ti-Mo alloy to be employed for the medical applications. These alloys had been produced using two powder metallurgy (PM) techniques; first technique is elemental blending (EB) which had been selected because it enhanced the surface contact between the alloying element and Titanium (Ti) with a cost-effective route. The behavior of different Ti alloys composition was evaluated using this technique. Samples were uniaxial pressed at 600 MPa and sintered at 1250°C. Second technique evaluated in this study was Mechanical alloying (MA). This technique has higher mixing energy than elemental blend which improves mechanical contact between different particles, and it helps diffusion during the sintering process. Samples were pressed at 600 MPa initially, and after evaluating mechanical properties, compaction pressure is changed to 900 MPa for a high green density of powders.

Different mechanical tests and microstructural studies were performed for elemental blend (EB) samples and for mechanical alloying samples to ensure the properties suitable for biomedical applications. Different tests for MA are Fluidity test (suitable to know about the flow of the powder after milling cycle) and Granulometric Analysis (test is suitable for powder distribution analysis). Other tests are common like Archimedes test which is suitable for calculating the porosity of the sintered samples, Three-point bending test is suitable for knowing Bending strength of the sintered samples and to know energy conserved by the breaking samples, Ultrasonic

test performed for knowing elastic modulus of the alloys, Hardness test performed for calculating the Vicker's hardness of the alloy, SEM analysis performed to know about microstructure and EDX analysis (by which proper mixing of the alloying element with the central element would be known). EBSD (Electron Beam Scattered Diffraction) is also performed for more analysis about microstructure, grain size, mixing of different elements in alloys. EBSD is an excellent tool for microanalysis of the material.

From the results section, Green density of the alloy, fluidity of the milled powder, Granulometry of the powder, sintered density of the alloy (From Archimedes test), bending strength and bending modulus of the alloy, Elastic modulus by Ultrasonic test, Microstructure of the alloy (By SEM and EBSD Analysis of the sintered part.) are determined. Green density for elemental blend alloys is in the range of (77.42-78.11%) and for Mechanical alloying samples were (74.94-78.58%). Sintered density obtained by Archimedes' test for the elemental blend is in the range of (96.88-98.74%). Bending strength obtained from three-point bending test is in range of (666-2161 MPa), and mechanical alloying is in range of (371-1597 MPa). From the high test, Determined Elastic modulus of the alloy is in range of (95.5-103 GPa) and for Mechanical Alloying elastic modulus was in the range of (66-82 GPa), which would be more suitable for biomedical applications. (From the SEM and EBSD analysis Mechanical alloying are more homogeneous mixing in comparison to Elemental Blend.

Green density (just after compaction) for the elemental blend is more than mechanical alloying so that Sintered Density for Elemental Blend is more than Mechanical Alloying. Due to higher sintered density, porosity is more in case of the elemental blend. Also, due to higher porosity, bending strength is low in case of mechanical alloying with same sintering parameters as Elemental blend alloys. Micro-Hardness value is more in case of elemental blend in comparison to Mechanical Alloying. Elastic modulus is more in case of elemental blend in comparison to mechanical alloying; lower elastic modulus is more suitable for biomedical applications. Grains are more regular and smaller in case of Mechanical alloying which is due to a more homogeneous distribution of the elements in comparison to elemental blend.

Powder processing technique is changed from Elemental Blend to Mechanical Alloying due to the improvement of homogeneity of green powders. Mechanical Alloying produced more homogeneous mixture due to high-speed milling with higher Ball to powder ratio (which generates higher energy within the jars and breaks the powders into smaller particles). Different combination of milling speed and milling time performed for our results and the effects of a combination of different parameters observed.





# Index

Resumen .....	i
Resum .....	v
Abstract .....	ix
Chapter 1: Introduction .....	1
1.1: Motivation .....	1
1.2: Objectives .....	4
Chapter 2: State of the art .....	7
2.1 Metallic biomaterials.....	7
2.2 Ti and its alloys .....	9
2.2.1 Low modulus Titanium alloys .....	10
2.3 Ti-Mo alloys .....	12
2.4 Process Selection.....	16
2.4.1 Casting process .....	16
2.4.2 Powder metallurgy (P/M) Technology.....	17
2.4.2.1 Elemental Blend (EB): .....	18
2.4.2.2 Mechanical alloying (MA) .....	19
2.4.2.3: Spark plasma sintering (SPS):.....	24
2.5: Corrosion:.....	27
Chapter 3: Material and methods .....	29
3.1: Phase 1: To see the effect of Mo and Fe on Ti-Mo alloy by Elemental Blend .....	30
3.1.1: Task 1: Selection of elemental powders:.....	31

3.1.2: Task 2: Mixing of the powder .....	36
3.1.3: Task 3: Compaction of the mixed powder.....	38
3.1.4: Task 4: Sintering of the green sample .....	39
3.1.5: Task 5: To know geometrical properties of the sintered samples like porosity by Archimedes' test .....	40
3.1.6: Task 6: Determination of Mechanical properties of the sintered part of samples: .....	41
3.1.7: Task 7: Microstructural characterization of the sintered part of the alloy: .....	43
3.2: Phase 2: To perform mechanical alloying technique.....	49
3.2.1: Task 1: Mixing of powder without process control agent (PCA).....	49
3.2.2: Task 2: Mixing of powder with process control agent (PCA) .....	53
3.3: Phase 3: for obtaining full density samples with spark plasma sintering Method.....	54
3.4: Phase 4: for obtaining $I_{\text{corr}}$ , open circuit potential (OCP), potential by corrosion test.....	56
3.4.1: Ion Release Study: .....	56
3.4.2: Study of resistance against corrosion .....	56
Chapter 4: Results.....	65
4.1. Elemental blend (EB) .....	65
4.1.1. Green Density (GD).....	65
4.1.2. Porosity, Sintered Density and relative density: .....	66
4.1.3. Shrinkage calculation: .....	67
4.1.4. Bending strength (MPa), Tenacity(J) and elongation (%) of sintered samples .....	68
4.1.5. Elastic modulus EU (GPa), Eccentricity and hardness (HV) of sintered samples .....	70

4.1.6. Surface fracture characterization .....	72
4.1.6.1. Ti-Mo base alloys sintered at 1250°C .....	73
4.1.6.2. Fractography analysis of Ti-Mo-Zr-Fe quaternary alloys .....	73
4.1.7. Grain size analysis:.....	73
4.1.8. Microstructure characterization.....	74
4.1.8.1. Ti-Mo base alloys sintered at 1250°C.....	74
4.1.8.2. Microstructure analysis of Ti-Mo-Zr-Fe Quaternary alloys at 1250°C.....	75
4.1.8.3. EDS analysis of Ti-12Mo-6Zr-2Fe .....	76
4.1.9: XRD Analysis .....	78
4.1.10: EBSD analysis.....	80
4.2. Mechanical Alloying (MA): .....	81
4.2.1: MA for Ti-12Mo-6Zr-2Fe with different compaction pressure .....	81
4.2.1.1. Mechanical properties with short milling time.....	81
4.2.1.2. Fractography analysis.....	82
4.2.1.3. Micro-Structural analysis .....	83
4.2.1.4. EBSD analysis of Ti-12Mo-6Zr-2Fe with MA at 900 MPa.....	83
4.2.2. MA with short milling time.....	84
4.2.2.1. Fluidity test:.....	84
4.2.2.2. Granulometry: .....	85
4.2.2.3. Mechanical properties: .....	87
4.2.3: Mechanical alloying with 180 RPM-52 Min. for different alloys.....	89
4.2.4: Mechanical alloying with Process control agent (PCA): .....	90
4.3: Spark Plasma Sintering (SPS) Results: .....	93

4.3.1: Mechanical test result: .....	93
4.3.2: Micro hardness of Ti-Mo alloys with different conditions:.....	94
4.3.3: DRX analysis of SPS samples with different conditions.....	95
4.3.4: EBSD analysis of Ti-Mo alloys by SPS with different conditions.....	96
4.4 Corrosion Test: .....	98
Chapter 5: Discussion of the result.....	105
Chapter 6: Conclusion .....	129
6.1: By Elemental Blend (EB) process:.....	129
6.2: By Mechanical alloying (MA) process:.....	130
6.3: By Spark plasma sintering (SPS) process: .....	131
6.4: From corrosion test:.....	131
Chapter 7: Future Developments: .....	133
References .....	135
List of publications .....	149

## List of Tables:

Table 2.1 Mechanical properties of biomedical titanium alloys .....	8
Table 2.2 Different elastic modulus values of various medical titanium materials .....	12
Table 2.3: Microhardness and bending properties of c.p. Ti and Ti alloys fabricated .....	14
Table 2.4: Physical properties for elements used during our research .....	15
Table 2.5: Important milestones in the development of mechanical alloying .....	20
Table 3.1: Elemental powder with its suppliers and quality.....	32
Table 3.2: Typical chemical analysis of supplier powder Ti, Mo and Fe .....	34
Table 3.3: Granulometry of Ti, Mo, ZrH <sub>2</sub> and Fe supplied powder.....	36
Table 3.4: Elemental powder weight (real) for EB 1250°C.....	37
Table 3.5: Elemental powder weight (real) for EB 1300°C.....	37
Table 3.6: Mechanical Alloying powder weight (real) with different parameters ..	50
Table 3.7: Different combinations of milling time and milling speed with different ball size for MA technique (with PCA).....	54
Table 3.8: Processing parameters for SPS .....	55
Table 3.9: Chi-square values obtained for the adjustment of the electric models of compact layer and double porous layer .....	59
Table 3.10: Template to illustrate the calculation of the corrosion rate .....	62
Table 3.11. Template to illustrate the calculation of polarization resistance .....	63
Table 4.1: Theoretical density, green density and relative green density of elemental blended samples.....	66
Table 4.2: Theoretical density, close and open porosity, sintered density and relative green of elemental blended samples.....	67

Table 4.3: Volumetric shrinkage (%), Bulk shrinkage (%) and linear shrinkage (%) of elemental blended samples .....	68
Table 4.4: Bending strength (MPa), Toughness (J) and Elongation (%) of elemental blended samples.....	70
Table 4.5: Table 4.5: Elastic modulus (EU), Poisson's coefficient and Hardness of elemental blended samples. ....	71
Table 4.6: Grain Size Analysis of Ti-Mo alloy .....	74
Table 4.7: Elemental Composition calculated by smart map analysis.....	75
Table 4.8: Elemental Composition calculated by smart map analysis of Ti-12Mo-6Zr-XFe. ....	78
Table 4.9: Phase analysis by XRD analysis.....	79
Table 4.10: Phase fraction for different alloys with EB .....	81
Table 4.11 Relative density of Ti-12Mo-6Zr-2Fe with different conditions.....	82
Table 4.12 Elastic modulus of Ti-12Mo-6Zr-2Fe with different conditions .....	82
Table 4.13: Phase distribution and internal porosity .....	83
Table 4.14: Phases analysis with EBSD for Ti-12Mo-6Zr-2Fe with MA at 900 MPa.....	84
Table 4.15: Fluidity (For Ti-15Mo and Ti-15Mo-6Zr-2Fe) with different milling condition .....	85
Table 4.16: Particle size analysis (For Ti-15Mo and Ti-15Mo-6Zr-2Fe) with different milling conditions .....	86
Table 4.17: Green density (%), sintered density (%) and bending strength of (For Ti-15Mo and Ti-15Mo-6Zr-2Fe) with different milling conditions.....	87
Table 4.18: Elastic modulus (GPa) (For Ti-15Mo) with different milling conditions .....	88
Table 4.19: Particle size analysis of Ti-Mo with 180 rpm-52 min.....	89
Table 4.20: green density, Sintered density and bending strength of Ti-Mo with 180 rpm-52 min .....	89

Table 4.21: Elastic modulus of Ti-Mo with 180 rpm-52 min .....	90
Table 4.22: Powder utility (%) of Ti-15Mo-6Zr-2Fe with 1% PCA .....	91
Table 4.23: Fluidity of Ti-15Mo-6Zr-2Fe with 1% PCA.....	91
Table 4.24: Particle size analysis of Ti15Mo6Zr2Fe with 1% PCA .....	91
Table 4.25: Elemental analysis of Ti-15Mo-6Zr-2Fe with 1% PCA by SEM image .....	92
Table 4.26: Mechanical properties of sintered Ti-15Mo-6Zr-2Fe with 1% PCA by SEM image.....	93
Table 4.27: Different mechanical test of Ti-Mo alloys by SPS with different temperatures .....	94
Table 4.28: Micro hardness of Ti-Mo alloys by SPS with different temperatures.....	94
Table 4.29: Phase analysis table of Ti-Mo alloys with different parameters .....	97
Table 4.30: Grain size with EBSD table of Ti-Mo alloys with different parameter .....	97
Table 4.31: Corrosion result with different parameters $I_{\text{corr}}$ ( $\text{A}/\text{cm}^2$ ), $E_{\text{corr}}$ (V), $\beta_c$ (V/dec) and $\beta_a$ (V/dec) for different process .....	98
Table 4.32: Corrosion result with different parameters OCP (V), $R_p$ ( $\text{K}\Omega.\text{cm}^2$ ) and $V_{\text{corr}}$ ( $\mu\text{m}/\text{year}$ ) for different process.....	99
Table 4.33: Ion-release rate of different particle with different parameters for corrosion.....	102
Table 4.34: Corrosion velocity with ion-release rate .....	103





## List of figures:

Figure 2.1 Comparison of Young's modulus of cortical bone, $\beta$ type Ti–13Nb–13Zr, $\alpha + \beta$ type Ti–6Al–4V, 316L stainless steel and Co–Cr–Mo alloy for biomedical applications .....	8
Figure. 2.2: Phase stability index diagram based on Bo and Md parameters .....	13
Figure. 2.3: Microstructure of the Ti–10Mo–5Fe for MA alloy (SEM) .....	19
Figure 2.4: Typical current and potential applications of mechanically alloyed products .....	20
Figure: 2.5: An ON-OFF pulsed current path through the spark plasma sintering machine .....	25
Figure 3.1: Flow diagram of overall project.....	30
Figure 3.2: Supplied powder of Ti, Mo, ZrH <sub>2</sub> and Fe with different magnification.....	33
Figure 3.3: Granulometric analysis of Ti, Mo, ZrH <sub>2</sub> and Fe supplied powder .....	35
Figure 3.4: (a) Press of compaction with the floating matrix between the compression plates, (b) detail of the cavity of the rectangular matrix of 12x30mm and (c) detail of the punch of the cylindrical matrix of 20 mm diameter.....	39
Figure 3.5: proposed sintering curve. Presents a heating 15°C /min up to a temperature of 750°C, idle time of 30 min to homogenise the temperature of the material and the oven, another cycle up to 1250°C and 10°C/min, 3 hours sintering and cooling in furnace .....	40
Figure 3.6: Micro hardness equipment Shimadzu HMV 2T .....	44
Figure 3.7: Fractured surface and after cut for microstructural analysis.....	45
Figure 3.8: (A) Optical microscopy equipment (NIKON elipse LV 100) (B) SEM Jeol JSM 6300 .....	46
Figure 3.9: EBSD Oxford Instruments.....	47
Figure 3.10: Bruker D2PHASER diffractometer. ....	48
Figure 3.11: Glove box for mixing of powders for compaction.....	51

Figure 3.12: Planetary ball milling equipment (RETSCH PM 400/2) .....	51
Figure 3.13: Malvern instruments mastersizer 2000 dispersion unit AWM 2002. ....	53
Figure 3.14: (A) FAST HP D 5/1 equipment (model S8451) from FCT (B) Setup for sintering with charcoal disk (C) Sample during sintering.....	55
Figure 3.15: Scheme of the proposed routine for the study of resistance against corrosion.....	57
Figure 3.16. Scheme of a potentiodynamic polarization curve.....	61
Figure 4.1: Fractography analysis of A) Ti-12Mo B) Ti-15Mo C) Ti-12Mo-6Zr D) Ti-15Mo-6Zr with 500x magnification .....	72
Figure 4.2: Fractography analysis of (A) Ti-12Mo-6Zr-1Fe B) Ti-12Mo-6Zr-2Fe with magnification 250x and (C) Ti-12Mo-6Zr-3Fe (D) Ti-12Mo-6Zr-4Fe with 500x magnification.....	73
Figure 4.3: Microstructure of Ti-Mo base alloy with magnification 500X BS (a) Ti-12Mo (b)Ti-15Mo (c) Ti-12Mo-6Zr (d)Ti-15Mo-6Zr .....	75
Figure 4.4: Microstructure of Ti-Mo quaternary alloy with magnification 500X BS (A) Ti-12Mo-6Zr-1Fe (B) Ti-12Mo-6Zr-2Fe (C) Ti-12Mo-6Zr-3Fe (D) Ti-12Mo-6Zr-4Fe at 1250°C .....	76
Figure 4.5: Smart map analysis of Ti-12Mo-6Zr-2Fe with 500x BS (A) General mixing of the alloying element (B) map of Ti, Mo K , Zr L and Fe K elemental mixing and (C) Spectrum obtained with EDS analysis .....	77
Figure 4.6: Phase analysis by XRD analysis of Ti-Mo alloys.....	79
Figure 4.7: IPF X mixed image by EBSD analysis of (A) Ti-12Mo (B) Ti-12Mo-6Zr (C) Ti-12Mo-6Zr-3Fe at 1250°C (D) Ti-12Mo-6Zr-3Fe at 1300°C.....	80
Figure 4.8: Fractography image of Ti-12Mo-6Zr-2Fe (A) with MA method under 900 MPa compaction pressure (B) with EB method under 600 MPa compaction pressure.....	82
Figure 4.9: Microstruture of Ti-12Mo-6Zr-2Fe: Mechanical alloying method with (A) 600 MPa compaction pressure (B) with 900 MPa compaction pressure .....	83

Figure 4.10: (A) IPF X color image and (B) phase color of Ti-12Mo-6Zr-2Fe with MA at 900 MPa.....	84
Figure 4.11: Granulometry for Ti-15Mo and Ti-15Mo-6Zr-2Fe (MA, P & S).....	87
Figure 4.12: Bending strength of Ti-15Mo with different combination of parameters .....	88
Figure 4.13: Figure 5.13: SEM analysis of mechanical alloying powder with (a) 6h-5mm (b) 6h-10 mm (c) 24h-5 mm (d) 24h-10mm.....	92
Figure 4.14: DRX analysis of Ti-Mo SPS samples with different Temperature (a) of Ti-15Mo-6Zr (b) Ti-15Mo-6Zr-2Fe.....	95
Figure 4.15: IPF X analysis of SPS samples (A) Ti-15Mo with 1100°C (B) Ti-15Mo-6Zr-2Fe with 1100°C (C) Ti-15Mo-6Zr-2Fe with 1200°C.....	96
Figure 4.16: Different graphs for corrosion results of MA samples (A) Log(i) vs E for samples without PCA (B) E vs t for samples without PCA .....	100
Figure 4.17: Different graphs for corrosion results of MA samples (A) Log(i) vs E for samples with PCA (B) E vs t for samples with PCA .....	101
Figure 5.1: Shrinkage of Ti-Mo alloy .....	106
Figure 5.2: (A) Relative sintered density of Ti-Mo alloy (B) Relative sintered density of Ti-Mo-Zr-xFe at different temperatures .....	107
Figure 5.3: (A) Bending strength of Ti-Mo alloy (B) Bending strength of Ti-Mo-Zr-xFe at different temperatures.....	109
Figure 5.4: (A) Elastic modulus of Ti-Mo alloy (B) Elastic modulus of Ti-Mo-Zr-xFe at different temperatures.....	111
Figure 5.5 (A) Hardness of Ti-Mo alloy (B) Hardness of Ti-Mo-Zr-xFe at different temp.....	112
Figure 5.6: (A) Elongation to fracture of Ti-Mo alloy (B) Elongation to fracture of Ti-Mo-Zr-xFe at different temperatures.....	114
Figure 5.7: Grains size of Ti-Mo alloy.....	115
Figure 5.8: Fractography of Ti-12Mo-6Zr-4Fe.....	116

Figure 5.9: Euler color image of Ti12Mo (a) IPF X image of Ti12Mo (c) Phases image of Ti12Mo (d) Euler color image of Ti12Mo6Zr (e) IPF X image of Ti12Mo6Zr (f) Phases image of Ti12Mo6Zr.....	118
Figure 5.10: IPFX colour image by EBSD analysis of Ti-12Mo-6Zr-3Fe at 1250 <sup>0</sup> C .....	119
Fig.5.11: Relative sintered density of SPS samples with different sintering samples .....	123
Fig.5.12: Bending strength of SPS samples with different sintering samples .....	124
Fig.5.13: Elastic modulus of SPS samples with different sintering samples.....	125
Fig.5.14: Hardness of SPS samples with different sintering samples .....	126
Fig.5.15: E <sub>Corr</sub> of EB samples with 1300 <sup>0</sup> C sintering samples.....	127

## **Abbreviations and Symbols:**

%  $V_{cl}$ : Closed porosity

$\alpha$ : Hexagonal phase of Titanium

$\beta$ : Cubic phase of Titanium

$\gamma$ : Austenite phase of Titanium

$\alpha'$ : Alpha prime phase or martensite hexagonal of Titanium

$\alpha''$ : Alpha double prime phase or martensite orthorhombic of Titanium

$\epsilon$ : Deformation

$\nu$ : Poisson's coefficient

$\rho$ : Density

$\rho_T$ : Theoretical density

$\rho_{sint}$ : Sintered density

$\mu m$ : Micro-meter

$B_o$ : Bond order

$b$ : width of the sample

$\beta_a$ : Anodic slope of Tafel

$\beta_c$ : Cathodic slope of Tafel

$B_w$  real: Real ball weight

$D$ : Dry mass of sample

d: Thickness of the sample

D: Maximum deflection of the center of the sample

$E_b$ : Potential for breaking the passive layer

$E_v$ : Elastic modulus

F: Force applied on the sample

F: Faraday constant

$I_{corr}$ : Corrosion current density

i: current density

$i_a$ : Partial anodic current density

$i_b$ : Partial cathodic current density

$i_p$ : Passivation current density

Hz: Hertz

kN: kilo Newton

L: Length of the sample

M: Mass of the sample in the air after eliminating excessive water

$M_d$ : Metal d-orbital energy level

P: % open porosity

$P_w$  real: Real powder weight

$R_p$ : Passive layer resistance

$R_{ct}$ : Load transfer resistance

xxvi

S: Mass immersed in water after saturation

t: Thickness of the sample

V: Volume

$V_{cl}$ : Closed pore volume

$V_{corr}$ : Corrosion velocity

$V_{external}$ : External volume

$V_{green}$ : Green volume of sample

$V_L$ : Longitudinal velocity

$V_{op}$ : Open pore volume

$V_{sint}$ : Sintered volume of sample

$V_T$ : Transversal velocity

$V_{Theoretical}$ : Theoretical volume

$W_{sint}$ : Sintered weight of sample

ASTM: American Society for Testing and Materials

BCC: Body centered Cubic

BPR: Ball to powder ratio

BS: Backscattered Electron detector

CP: Commercial pure

EB: Elemental blend

EBSD: Electron beam scattered diffraction

EDS: Energy dispersive spectroscopy

EIS: Electrochemical impedance spectroscopy

HA: Hydroxy apatite

HCP: Hexagonal close packed

HIP: Hot isostatic pressing

IM: Ingot metallurgy

LSV: Linear sweep voltammetry

MA: Mechanical Alloying

MIM: Metal injection molding

MM: Mechanical mixing

OCP: Open circuit potential

ODS: Oxide dispersion-strengthened

OM: Optical microscopy

PAS: Plasma active sintering

PCA: Process control agent

P/M: Powder metallurgy

PVD: Physical vapor deposition

rpm: Revolution per minute

SEI: Secondary electron image

SEM: Scanning electron microscopy



SiC: Silicon carbide

SPS: Spark plasma sintering

XRD: X-ray diffraction







# Chapter 1: Introduction

## 1.1: Motivation

It has been estimated that 90% of population over the age of 40 suffers from degenerative diseases and the aged people's population has increased tremendously in recent past and it is estimated there would be a seven times increase (from 4.9 million which was in 2002 to 39.7 million by 2010 (Jackson-Leach and Lobstein, 2006). Musculoskeletal disorders are most widespread human health problem which is costing around 254 billion dollars to the society (Ekpenyong, C.E., Udokang, N.E., Akpan, E.E., Samson, 2012).

Artificial biomaterials are the solutions for these problems, as surgical implantation of these artificial biomaterials of suitable shapes helps in restoring the function of the otherwise functionally compromised structures.

There is a tremendous increase in the demand for the new long-lasting implants, as the data collected on total joint replacements surgery by the end of 2030, the number of total hip replacements would rise by 174% (572,000 procedures) and total knee arthroplasties is projected to grow by 673% from the present rate (3.48 million procedures). The reason for joint replacements attributed to diseases such as osteoporosis (weakening of the bones), osteoarthritis (inflammation in the bone joints) and trauma. Replacement surgeries only have not been increased, simultaneously the revision surgery of hip and knee implants have also been increased (Kurtz *et al.*, 2007).

The revision in surgeries which causes more pain for the patient is very expensive and the lesser success rate. The total number of hip revision surgery is expected to increase by 137% and knee revision surgery by 607% between the years 2005 and 2030 (Kurtz *et al.*, 2007; Correa *et al.*, 2018). Thus, a very high boom in implant manufacturing is expected in coming years. An ever-increasing demand for implants

makes it imperative that development efforts on biomaterials have accelerated. The materials used for orthopedic implants especially for load-bearing applications should possess excellent biocompatibility, superior corrosion resistance in body environment, excellent combination of high strength and low modulus, high fatigue and wear resistance, high ductility and no cytotoxicity (Niinomi, 2002).

Metals and their alloys are widely used as biomedical materials. Ceramics or polymers cannot replace metallic biomaterials due to the inferiority of mechanical strength and toughness, which are most crucial safety requirements for biomaterials. Sometimes, metallic materials show toxicity and fracture because of their corrosion and mechanical damages (Hanawa, 2006) which is the ultimate reason for the trial of the new biomaterials. There is some specific purpose for development of novel Biomaterials. There should be some improvement which is necessary for biomaterials including toxicity elements elimination, decreased elastic modulus to avoid stress shield effect in bone fixation, enhanced biocompatibility.

Development of appropriate material with high longevity and excellent biocompatibility is highly essential. While several materials are currently in use as biomaterials, titanium alloys are fast emerging as the first choice for most applications.

So, development of new biomaterial is an exciting field of research in future due to its increasing demand, so the present research is carried out, and Ti  $\beta$ -alloy has better properties for this research.

The development of new alloy must be on a better balance between mechanical properties and microstructure of the resultant alloys. Ti and its alloys are most suitable alloys due to its superior comprehensive properties and satisfy the requirements of implantation materials better than other competing materials, such as stainless steels, Cr-Co alloys, CP niobium and Tantalum (Li *et al.*, 2014).

The development of Ti and its alloys as implant material is perfectly reflecting the research goal of biomaterials. So, initially CP Ti was proposed as an alternative for the 316L stainless steel and Co-Cr alloys (Li *et al.*, 2014), which contains some harmful elements, such as Ni, Co and Cr. When there is need for high strength usage like hard tissue replacement or under intensive wear use, mechanical properties of

CP Ti could not satisfy the requirement (Van Noort, 1987). For this reason, CP Ti replaced by  $\alpha+\beta$  Ti alloys, particularly Ti-6Al-4V but Ti-6Al-4V is composed of cytotoxic elements like Al and V, which may cause several problems once released into the human body (Alves *et al.*, 2009). To overcome the potential V toxicity, V was replaced by Nb and Fe, leading to two new V- free  $\alpha+\beta$  Ti-based alloys, i.e., Ti-6Al-7Nb and Ti-5Al-2.5Fe (Fellah *et al.*, 2015). Both alloys show better mechanical and metallurgical properties comparable to Ti-6Al-4V. Several studies confirmed that the elastic modulus of  $\alpha$  and  $\alpha+\beta$  alloys are much higher than that of human bone, which also causes stress shielding effect (Geetha *et al.*, 2009)

In order to overcome these problems, low modulus  $\beta$  type Ti based alloys have been developed on a bigger scale to alleviate stress shielding effect, among those representatives are Ti-15Mo, Ti-13Nb-13Zr, Ti-12Mo-6Zr-2Fe, Ti-35Nb-5Ta-7Zr and Ti-29Nb-13Ta-4.6Zr (Geetha *et al.*, 2009; Drahansky *et al.*, 2016; Lampman 2018).

Powder metallurgy technology (P/M) allows  $\beta$  Titanium alloys to be produced with non-soluble phases, where the microstructure is achieved through solid-state diffusion. An elemental blended (EB) method is potentially the lowest-cost titanium components manufacturing process and Mechanical alloying (MA) is a P/M processing technique involving cold welding, fracturing and rewelding of powder particles in a high-energy ball mill, and has now become an established commercial technique to produce oxide dispersion strengthened (ODS) nickel- and iron-based materials.

Developing Ti- $\beta$  alloy started with Ti-Mo alloy having better mechanical properties and developing different Ti-Mo based alloy with different process techniques. Hence it is decided to develop this composition (Ti-Mo-Zr-Fe) with a different stoichiometric ratio like Ti-12Mo-6Zr-xFe (where x=1, 2, 3, 4) with two techniques of powder processing (Mechanical Alloying & Elemental Blend), and this alloy is developed and found all the mechanical properties. Effect of sintering temperature (1250°C and 1300°C) analyzed. There are some ideas for developing the better  $\beta$ -alloy. After successful development of these alloys, it is planned to work on Ti-15Mo-6Zr-xFe (where x=2, 3) because Ti-15Mo gives better results than Ti-12Mo,

and Ti-15Mo-6Zr also gives better mechanical properties than Ti12Mo6Zr. So, it is for a better implant alloy in the field of biomedical applications like dental purpose.

This Project mainly focuses on the development of an alloy which is suitable for Biomaterials. The requirements are low elastic modulus, higher bending strength, lower porosity, good surface, better corrosion resistance, Biocompatibility. Ti and its alloy are a promising candidate for this research.  $\beta$ - Ti alloy is a suitable for dental implant due to its lower elastic modulus, excellent corrosion resistance and biocompatible. They are the most necessary properties of the biomaterial. So, it is decided to work with Ti-Mo alloy, due to Mo as it is a good  $\beta$ -stabilizer. Further developing of more ternary and quaternary alloy is feasible.

## **1.2: Objectives:**

The main objective is Development of a new high-performance Titanium alloy (Mainly  $\beta$ -alloy) for dental implants and for this we are developing different specific objectives.

### **Specific objectives:**

- Develop Ti-Mo binary, ternary alloys with addition of Zr and quaternary alloy with addition of different (1,2,3,4) % of Fe by weight by elemental blend (EB) and mechanical alloy (MA) powder processing technique.
- Determine the effects of compaction pressure (600 MPa and 900 MPa) on TMZF alloys with different powder processing Alloys.
- Sintering temperature has a more impact on the final mechanical, microstructure and corrosion properties of the alloy, so we also explore different sintering temperature for the alloy (1250°C and 1300°C). The sintering temperature is the leading cause for better diffusion. So, if sintering temperature is proper, then diffusion is also proper.



- Determine elastic modulus of the alloy with different techniques (like the addition of Fe reduces elastic modulus), higher porosity also has a lower elastic modulus, but this is not suitable for implants.
- For mechanical alloying (MA); Analyse the effect of milling speed and milling time for Ti-Mo alloy with MA technique. Also, choose one proper combination for work further.
- For MA technique; Study the effect of process control agent (PCA) with high-speed milling with different ball size (5mm and 10 mm respectively).
- Improvement of mechanical properties with full density techniques like spark plasma sintering (SPS) technique.
- Analyse microstructure with one of best technique like SEM, XRD and EBSD. Analyse phase, grain boundary analysis of the alloys, mixing of the element inside the alloys after sintering processing.
- Corrosion resistant is a must characterization of the biomaterials, so we must determine  $I_{\text{corr}}$  [A/cm<sup>2</sup>],  $E_{\text{corr}}$  [V], Open circuit potential (OCP)[V], Corrosion velocity [ $\mu\text{m}/\text{year}$ ], ion release rate [ $\mu\text{g}/\text{L cm}^2 \text{ h}$ ] of the sintered alloys.

*Development of new high-performance Titanium alloys with Fe-addition for dental implants*

# Chapter 2: State of the Art

The present study focuses on developing new Ti  $\beta$  alloys for biomedical application with powder metallurgy route and searching of metallic materials including Stainless steel alloys, Ti- alloys, Co-Cr alloys. Metallic implant materials, their usability and suitability for the present research is discussed.

## 2.1 Metallic biomaterials

Presently 70-80% biomaterials are mostly metallic implants; it's important for the reconstruction of the failed tissue especially for the reconstruction of the hard tissue failure. Presently world population is getting older at the earliest, and they need hard tissue implant for the long run. The metallic implant needs much improvement for the natural and mechanical biocompatibility. After all, bio-functionality of metallic biomaterials is at present inadequate and needs to improve a lot. Presently representative metallic biomaterials are stainless steel, Cobalt (Co)-Chromium (Cr), Titanium and its alloys. Within these available metallic biomaterials, Ti alloys show the highest biocompatibility, corrosion resistance and specific resistance (Ratio of the tensile strength to density), in comparison to stainless steel and Co-Cr alloys. Among these metallic biomaterials, Co-Cr alloys exhibit the highest wear resistance and relatively higher strength compared with stainless steels and Ti alloys. Stainless steels generally exhibit higher ductility and cyclic twist strength compared with Co-Cr and Ti alloys. Co-Cr has the highest stiffness than Ti alloys. Magnesium (Mg) alloys, Iron (Fe), Tantalum (Ta) and Niobium (Nb) are also important. Highly intense research and development are being carried out globally on each type of metallic biomaterials which is tabulated in table 2.1 and shown in figure 2.1. The elemental components of metallic biomaterials are mainly non-toxic. Min representative elements are Ti, Ta, Nb, Molybdenum (Mo) and Zr. (Niinomi, Nakai and Hieda, 2012; Liu *et al.*, 2014).

Development of new high-performance Titanium alloys with Fe-addition for dental implants

Table 2.1 Mechanical properties of biomedical titanium alloys (Geetha *et al.*, 2009)

Material	Standard	Modulus (GPa)	Tensile strength (MPa)	Alloy type
First generation biomaterials (1950–1990)				
Commercially pure Ti (Cp grade 1–4)	ASTM 1341	100	240-550	$\alpha$
Ti–6Al–4V ELI wrought	ASTM F136	110	860-965	$\alpha+\beta$
Ti–6Al–4V ELI Standard grade	ASTM F1472	112	895-930	$\alpha+\beta$
Ti–6Al–7Nb Wrought	ASTM F1295	110	900-1050	$\alpha+\beta$
Ti–5Al–2.5Fe	-	110	1020	$\alpha+\beta$
Second generation biomaterials (1990-till date)				
Ti–13Nb–13Zr Wrought	ASTM F1713	79-84	973-1037	Metastble $\beta$
Ti–12Mo–6Zr–2Fe (TMZF)	ASTM F1813	74-85	1060-1100	$\beta$
Ti–35Nb–7Zr–5Ta (TNZT)	-	55	596	$\beta$
Ti–29Nb–13Ta–4.6Zr	-	65	911	$\beta$
Ti–35Nb–5Ta–7Zr–0.40 (TNZTO)	-	66	1010	$\beta$
Ti–15Mo–5Zr–3Al	-	82	-	$\beta$
Ti–Mo	ASTM F2066	-	-	$\beta$

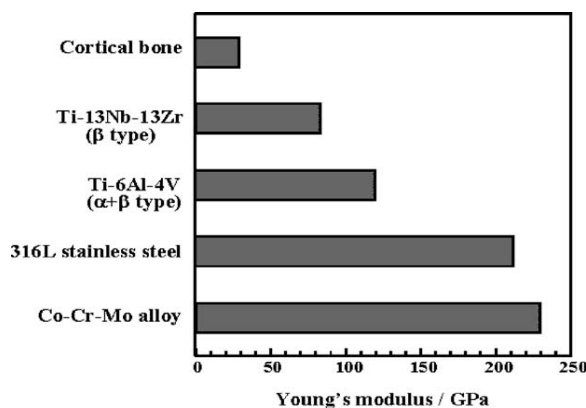


Figure 2.1 Comparison of Young's modulus of cortical bone,  $\beta$  type Ti–13Nb–13Zr,  $\alpha + \beta$  type Ti–6Al–4V, 316L stainless steel and Co–Cr–Mo alloy for biomedical applications (Niinomi, 2003b)

## 2.2 Ti and its alloys

Among all the available metallic biomaterials, Ti (pure Ti) and its alloys have the highest biocompatibility, corrosion resistance. Stainless steels and Co-Cr alloys have inferior properties concerning Ti (pure Ti) and its alloy. (Niinomi, 2002; Zhao *et al.*, 2012). Therefore, Ti and its alloy get attention by biomaterial scientists since last decade. Initially for the development of V free Ti alloys for biomedical applications, scientists developed Ti6Al7Nb and Ti5Al2.5Fe, because due to V present in Ti6Al4V ELI was toxic. After that Scientists started developing V and Al-free Ti alloys like Ti-Zr and Ti-Sn alloys which cause Alzheimer's disease due to Al (still it is unclear). Nowadays stress shielding effect also got a lot of attention which are mostly metallic implants. (Niinomi, 2002). The leading cause of stress shielding is the mismatch or inhomogeneous transfer of stress between the implant and bone. Due to a much higher difference of Young's modulus of implants made of metallic implants and bones; stress predominantly transferred through the implant. It is the primary cause of bone absorption; it results in loosening of the implant or re-fracture of the bone after eliminating of the implant. For this reason, metallic implants with similar Young's modulus with bone, i.e., low modulus metallic implants are suitable for implant. Among the main metallic biomaterials, the modulus of Ti alloys is the smallest (Niinomi, 2002). From the figure 1, the elastic modulus of Ti alloy Ti6Al4V which is ( $\alpha+\beta$ ) alloy having modulus 110 GPa and much lower than stainless steel and Co-based alloys (180 and 210 GPa, respectively). Ti alloys divided into three groups like  $\alpha$ -alloys, ( $\alpha+\beta$ ) type and  $\beta$ -type alloys. B-type Ti alloys have a lower modulus of elasticity than  $\alpha$ -alloys and ( $\alpha+\beta$ ) alloys. The main reason behind the difference between elastic modulus because of the crystal structure of the  $\alpha$ -phase, which is the primary component phase of  $\alpha$ -type Ti alloys, which is hexagonal close-packed (hcp), but for the  $\beta$ -phase, which is the primary component phase of  $\beta$ -type Ti alloys, is body centered cubic (bcc). All those above reasons, lowest modulus  $\beta$ -Ti alloys developing still is exciting research for biomaterial scientists.

### 2.2.1 Low modulus Titanium alloys

Mainly alloys developed for biomedical applications are low modulus  $\beta$ -Ti alloys composed of non-toxic elements. Ti-13Nb-13Zr (Mishra *et al.*, 1996) was the first low modulus  $\beta$ -type Ti alloys developed for biomedical applications. Then after developing different low modulus  $\beta$ -ti alloys like Ti-12Mo-6Zr-2Fe (TMZF) (I, I, and I 2017), Ti-15Mo (Zardiackas, Mitchell and Disegi, 2017), Ti-16Nb-10Hf (Wang, 1996) Ti-15Mo-5Zr- 3Al, Ti<sub>35</sub>Nb<sub>7</sub>Zr<sub>5</sub>Ta (TNZT) (Kwasniak *et al.*, 2014), and Ti-29Nb- 13Ta-4.6Zr (TNTZ) (Niinomi, 2003a). After these alloys, a lot of low modulus  $\beta$ -type alloys developed or development in progress. Nowadays biomaterials scientists focused on Ti alloys which mainly contains low-cost elements such as Fe, Cr, Mn, Sn and Al which might reduce consumption of high-cost factors such as the rare materials like Nb, Ta, Mo and Zr. Some of the alloys with these elements are Ti-10Cr-Al (Hatanaka *et al.*, 2010), Ti-Mn (Ikeda *et al.*, 2009), Ti-Cr- Al (Sugano and Ikeda, 2005), Ti-Sn-Cr (Ashida, Kyogoku and Hosoda, 2012), Ti-(Cr, Mn)-Sn (Kusano *et al.*, 2010), and Ti-12Cr (Nakai *et al.*, 2011).

Now a days  $\beta$ -type Ti alloys containing Nb, Zr, Ta, Mo, Sn, Fe etc., have attracted considerable attention mainly for orthopaedic implants' applications due to their unique combination of better mechanical properties like low elastic modulus, higher flexural strength, Superior biocorrosion resistance, allergy free implants, and superior biocompatibility. Some scientists also confirmed that elastic modulus of the alloy could significantly reduce by adjusting the concentration of  $\beta$ -stabilizing element. (Niinomi, 2002; Ikehata *et al.*, 2004; Abdel-Hady, Hinoshita and Morinaga, 2006). New  $\beta$ -type Ti alloys mainly are made from the above elements, and they are non-allergic and non-toxic elements (Niinomi, 1998).

Depending upon its ability to achieve biological passivity and capacity of reducing the elastic modulus, the addition of  $\beta$  stabilizing elements is preferred to produce safe Ti-based alloys for biomedical applications (Yang and Zhang, 2005).

Main features which should be in a metallic biomaterial is listed below.

1. Outstanding biocompatibility.
2. Better Osseo integration (bone ingrowth).

3. Improved mechanical properties such as specific strength, fatigue resistance, impact strength, flexibility and low Young's modulus.
4. Superior corrosion behavior in body fluid.
5. Encouraging tribological characteristics, i.e., low friction and high wear resistance.
6. Long-term dimensional stability.
7. Processability (casting, plastic deformation, powder metallurgy, machinability, and welding).

All properties found in the alloys as mentioned earlier are mainly low elastic modulus  $\beta$ -Ti alloys.(Mohammed, 2014) .

Alloying elements for Ti alloys also play a vital role in properties of biomaterial which divides mainly into different categories like:

$\alpha$ -stabilizers such as Al, O, N, C

$\beta$ -stabilizers such as V, Nb, Ta, Mo (isomorphous)

Fe, W, Cr, Ni, Si, Co, Mn, H (Eutectoid)

Neutrals such as Zr and Sn.

The main mechanical properties of the biomaterial are elastic modulus. The lowest value from table 2.2 is for porous alloy Ti-19Nb-14Zr (14 GPa), which is like the modulus of cortical bone.

Ti alloy with different beta – stabilizing elements, and two alloying parameters was determined theoretically. First one is the bond order (denoted as  $B_o$ ) which is a measure of the covalent bond strength between Ti and an alloying element. The second is the metal d-orbital energy level ( $M_d$ ) which correlates with the electronegativity and the metallic radius of elements. For alloys, the average values of  $B_o$  and  $M_d$  are defined by taking the compositional averages of the parameters and denote them  $B_o$  and  $M_d$ , respectively.  $B_o$  and  $M_d$  values and the chemical compositions of the designed alloys in this study given in Table 2.2. Fig. 2.2 is a phase stability map (called the  $B_o$ – $M_d$  map)(Kuroda *et al.*, 1998) in which the areas of  $\alpha$ ,  $\alpha+\beta$  and  $\beta$  type alloys separated clearly. The stability region of the  $\beta$  type alloys

extends to the higher  $B_o$  and the lower  $M_d$  region. Positions of titanium and titanium alloys shown by the numbers surrounded by the open circles in Fig. 2.2. The values of moduli of elasticity also shown in parentheses. The benefits of moduli of flexibility for these alloys are decreased with increasing  $B_o$  and  $M_d$  values in  $\beta$  type alloys region on the  $B_o$ – $M_d$  map. The alloy position moves in the  $B_o$ – $M_d$  map as the alloy composition varies as shown in Fig. 2.2.

Table 2.2 Different elastic modulus values of various medical titanium materials

Alloy Designation	Type alloy	E (GPa)	Reference
Ti19Nb14Zr(porous)	Near $\beta$	14	(Ma, Cheng and Chung, 2013)
Ti–24Nb–4Zr–7.9Sn(porous)	$\beta$	33	(Hao <i>et al.</i> , 2007)
Ti–29Nb–6Ta–5Zr(porous)	$\beta$	43	(Laheurte <i>et al.</i> , 2010)
Ti–35Nb–4Sn(porous)	$\beta$	44	(Miura <i>et al.</i> , 2011)
Ti25Ta25Nb	$\beta$	55	(Bertrand <i>et al.</i> , 2010)
Ti–10Zr–5Ta–5Nb	$\beta$	51.97	(Raducanu <i>et al.</i> , 2011)
Ti–(18–20)Nb–(5–6)Zr	Near $\beta$	45–55	(Brailovski <i>et al.</i> , 2011)
Ti25Nb11Sn	Near $\beta$	45–55	(Miura <i>et al.</i> , 2011)
Ti–35Nb–7Zr–5Ta	Near $\beta$	55	(Oldani and Dominguez, 2007)
Ti–35Nb–5.7Ta–7.2Zr	$\beta$	57	(Majumdar, Singh and Chakraborty, 2008)
Ti–28Nb–13Zr–0.5Fe	Near $\beta$	58	(Cui and Guo, 2009)
Ti–29Nb–11Ta–5Zr	$\beta$	60	(Laheurte <i>et al.</i> , 2010)
Ti–29Nb–13Ta–2Sn	$\beta$	62	(Dalmau <i>et al.</i> , 2015)
Ti–12Mo–5Zr	$\beta$	64	(Zhao, Zhang and Cao, 2011)
Ti–29Nb–13Ta–4.6Zr	$\beta$	65	(Tane <i>et al.</i> , 2008)
Ti–25Nb–2Mo–4Sn	Near $\beta$	65	(Guo <i>et al.</i> , 2013)
TLM Alloy	$\beta$	67	(Zhentao and Lian, 2006)
Ti12Mo5Ta	Near $\beta$	74	(Gordin <i>et al.</i> , 2005)
Ti–29Nb–13Ta–6Sn	$\beta$	74	
Ti–12Mo–6Zr–2Fe	$\beta$	74–85	(I, I and I, 2017)
Ti–13Nb–13Zr	Near $\beta$	77	(Majumdar, Singh and Chakraborty, 2008)
Ti–15Mo	$\beta$	78	(Sabeena <i>et al.</i> , 2016)

### 2.3 Ti-Mo alloys

After analyzing and going through different literature review, we started working with Ti-Mo binary alloy, Ternary alloy and quaternary alloy. So, it is necessary to discuss Ti-Mo alloying system. Suitability of the  $\beta$ -Ti alloys depends on some factors like implant should have a less low elastic modulus, lower notch sensitivity



and better biocompatibility than Ti-6Al-4V. As it discussed that Vanadium and Al were purposely avoided due to its toxic effect while the elements, i.e., Mo, Zr, and Fe introduced. The new titanium alloy, Ti-12Mo-6Zr-2Fe (TMZF), is unique in having a modulus of elasticity as low as 74 GPa, excellent mechanical strength and corrosion resistance coupled with reasonable wear and notch fatigue resistance.

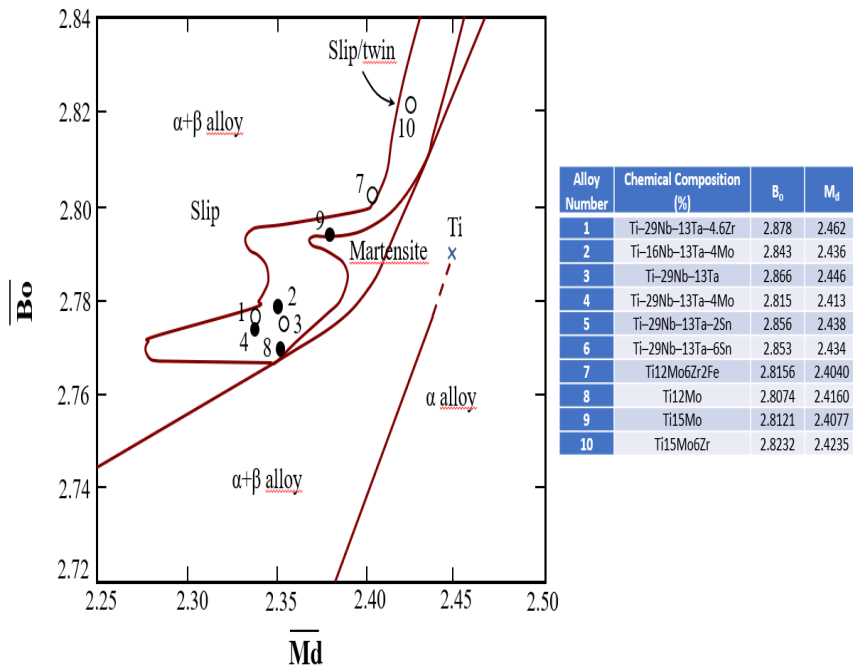


Figure 2.2: Phase stability index diagram based on  $B_0$  and  $M_d$  parameters. (Kuroda *et al.*, 1998)

Molybdenum (Mo) is an isomorphous  $\beta$  stabilizing element. For stabilizing 100%  $\beta$  retention at room temperature, a minimum of 10% Mo content needed in a Titanium plus Mo alloys. From the Ti-Mo equilibrium phase diagram indicates that  $\alpha+\beta$  phase to  $\beta$ -phase transformation occurs at approximately 750°C for a binary composition containing 15% Mo. For a Ti-Mo system, for example, it moves to the left (the lower  $M_d$  region) with increasing Mo content. (As we can see in fig 2.2), it is shown that Ti-12Mo have less  $B_0$  values than Ti-15Mo. Ti (12,15)Mo, Ti-(12,15)Mo-6Zr, Ti-(12,15) Mo-6Zr-xFe are the alloys which were used by our team for research. So, it's interesting to compare the results with each fusion. Such a vector varies in

Development of new high-performance Titanium alloys with Fe-addition for dental implants

direction and magnitude, depending on alloying elements, as shown in the map. Once a specific  $B_o$ - $M_d$  region and an alloy system set in the plan, the similar alloy composition is determined merely following the rule of the vector sum. The trial and error experiments no longer needed to optimize the alloy composition.

From the figure 2.2, it clearly is shown that increase of % of Fe decreases the value of  $B_o$  and decreases the amount of  $M_d$ . Addition of Zr increases the value of  $B_o$  and increases the value of  $M_d$ .

Different scientists (Ho, Ju and Chern Lin, 1999) worked with Ti-Mo binary alloys with different % of Mo (6,7.5,9,10,12.5,15,17.5,20) by weight. The metastable  $\beta$  phase Ti-15Mo alloy is being evaluated for orthopedic implant applications by Synthesis USA. The rapidly quenched Ti-15Mo alloy was reported to have  $\alpha''$  grained bcc structure with a lower modulus (77.7 GPa) than that of 316L stainless steel, Grade IV Ti, Ti-6Al-4V and Ti-6Al-7Nb (Zardiackas, Mitchell and Disegi, 1997).

Table 2.3: Microhardness and bending properties of CP Ti and Ti alloys fabricated (Zardiackas, Mitchell and Disegi, 1997)

	Microhardness (HV)	Bending strength (MPa)	Bending modulus (GPa)
CP Ti	156	884	92
Ti6Al4V	294	1857	105
Ti15Mo	307	1348	71
Ti7.5Mo	263	1395	55

From the table 2.3, Ti-Mo alloys have less bending modulus than CP Ti, Ti-6Al-4V and higher bending strength than the CP Ti. Microhardness for Ti-Mo alloys are larger than CP Ti and like Ti-6Al-4V, which makes Ti-Mo alloys more suitable for biomaterials.

From the table 2.4, it clearly shown that melting point and density of Mo are the highest among all elements used during our research.

Table 2.4: Physical properties for elements used during our research (Li *et al.*, 2015)

Elements	Melting point(°C)	Density(g/cc)
Ti	1668	4.506
Mo	1538	10.28
ZrH <sub>2</sub>	800	5.6
Fe	2623	7.87

Molybdenum has strong  $\beta$ -stabilizing properties on titanium alloys, and small content should be enough to gain and stabilize a  $\beta$ -phasic titanium alloy. According to Eq. (2.1) (Park *et al.*, 2017), the  $\beta$ -stabilizing effect of molybdenum can be obtained.

$$[\text{Mo}]_{\text{eq}} = [\text{Mo}] + \frac{1}{5}[\text{Ta}] + \frac{1}{3.6}[\text{Nb}] + \frac{1}{2.5}[\text{W}] + \frac{1}{1.5}[\text{V}] + 1.25[\text{Cr}] + 1.25[\text{Ni}] + 1.7[\text{Mn}] + 1.7[\text{Co}] + 2.5[\text{Fe}] \quad (2.1)$$

In this equation, a large  $\beta$ -stabilizing character is recognized for eutectoid  $\beta$  elements, such as Fe. However, elements such as Ta or Nb have a stabilizing power of  $\beta$ -phase lower than Mo, so that a greater amount of these elements is used to obtain  $\beta$ -Ti alloys. The issue of elements biocompatibility becomes important upon choosing its composition. On the other hand, elements such as Cr, Mn, Ni, Co and very less % of Fe may be useful to strongly improve the stabilizing character of the alloy (Geetha *et al.*, 2009).

Ti-Mo alloys are one of most reliable alloys for bio-medical applications. There are lots of scientists who worked with Ti-Mo alloys like (Zhao, Zhang and Cao, 2011; Gao *et al.*, 2012; Tsai *et al.*, 2012; Zhang *et al.*, 2015).

Density of Ti is 4.51 g/cm<sup>3</sup> (Correa *et al.*, 2018) and addition of Zr and Mo increases the density of alloy whose density values are (6.51 g/cm<sup>3</sup>) and (10.22 g/cm<sup>3</sup>) (Correa

*et al.*, 2018). Density is an important parameter for bio materials due to its need specific strength (mechanical strength to density ratio) (Mishnaevsky *et al.*, 2014).

## **2.4 Process Selection**

For dental implants or orthopedic implants, there are many conventional and advanced technologies available, including casting, milling, spark erosion, forging, powder metallurgy (P/M), and a combination of milling or spark erosion. From earlier studies and suitability for our research, work with powder metallurgy technology (P/M) is chosen. In P/M technology, different powder processing technology like Elemental blend (EB), mechanical mixing without process control agent (PCA), mechanical mixture with process control agent (PCA) and Full density sintering like Spark Plasma Sintering (SPS) techniques are used. It started at EB and then proceed to other technology for overcoming the problems faced during our research. Casting also plays vital roles for the implant but using the process depends on its suitability, mechanical compatibility etc.,

### **2.4.1 Casting process**

There are some unusual features associated with titanium casting. Unlike another metal casting, there are no commercial Ti alloys developed strictly for casting; therefore (i) Casting of all titanium alloys have compositions based on those of the standard wrought alloys and (ii) titanium castings are equal or nearly equal in strength to their wrought counterparts. The cast of titanium dental appliances noted by numerous studies in Japan, Europe, and the United States on the precision casting of dental prostheses, and the development of casting machines and suitable investment materials. The cast ability of Titanium and its alloys can be metallurgical improved (Yoda *et al.*, 2001). For control, the casting defects especially with Titanium alloy (which cannot be 100% eliminated when using a casting process). The major flaws are shrinkage cavities, pinholes, or voids and these are all problems for denture bases. It's challenging to cast Titanium alloys, it's due to melting temperature difference between Titanium alloying element, reaction with oxygen, formation of  $\alpha$ -phase on the top layer of the alloys etc., Porosity is also a big problem for titanium casting, for example, some authors (Oshida, 2013) discussed that Ti-6Al-4V have (60.86%) cast ability and CP Ti have lower (48.44%) cast ability.

Powder metallurgy techniques would be the better option to improve the mechanical properties.

#### **2.4.2 Powder metallurgy (P/M) Technology**

The Powder Metallurgy (P/M) process is a near-net or net-shape manufacturing process that combines the features of shape-making technology for powder compaction with the development of final material and design properties (physical and mechanical) during subsequent densification or consolidation processes (e.g., sintering). It is critical to recognize this interrelationship at the outset of the design process because a subtle change in the manufacturing process can cause a remarkable difference in material properties. Titanium alloys' output improves day by day, but still, titanium alloys faced an issue of high-cost P/M techniques have the advantages including elimination of the casting defects, less segregation and short process time. P/M processing route also results in parts as close as Near Net shape (NNS) forming which reduces the overall cost of the parts.

Some P/M design found to be into considerations.

**Size:** For some powder processes, the product size is quite limited (such as metal injection molding, MIM), while for hot-isostatic pressing (HIP), extent not considered as a severe constraint.

**Shape Complexity:** It's easy to change the shape of the green part (Un-sintered) part of the alloy, it depends only on the die or mold shape.

**Tolerances:** Powder characteristics, compaction parameters and the sintering cycle are the main factors for determining the tolerances. In comparison to another process' parts like HIP parts, press and sintering P/M parts have very less amount of size change during sintering; it's the main reason of the products typically have the closest dimensional tolerances.

**Material systems:** powder shape, size and purity are also the primary factors during P/M manufacturing process. For example, conventional press and sintering method required irregular powder shape and distribution of particle size for better green

strength and sinter ability. Hot isostatic pressing needs spherical powders (gas atomized) for lowest impurities and good particle packing.

Properties: The physical and mechanical properties are primary characteristics of the functional response.

Quality and cost: The number of pieces produced is main factors of economic feasibility. For press and sintering, minimum 1000 to 10000 or even larger sections should produce for desired tooling investment.

The P/M manufacturing methods can divide into two main categories: conventional press-and-sinter methods and full-density processes.

Conventional press and sintering methods: This process includes compaction (compaction pressure depends on the dimensional usability and processing, sintering (according to requirement and alloying elements). Optional machining like grinding, cutting etc., could be performed with the sintered part.

For the present research, elemental blend and mechanical mixing or high energy ball milling process was used.

#### **2.4.2.1 Elemental Blend (EB):**

The elemental blend is a simple and cost-effective technique in which fewer powders are used for the part production. The main problem faced during EB techniques is lack of homogeneity and confirmed by microstructure.

Elemental blend technique is useful where cost is a significant constraint and number of parts would be more. But for costlier parts where surface quality and homogeneity of the alloy are the constraints then this technique is not very useful. High energy ball milling or mechanical mixing or mechanical alloying (MA) are used for the homogenized microstructure as shown in figure 2.3.

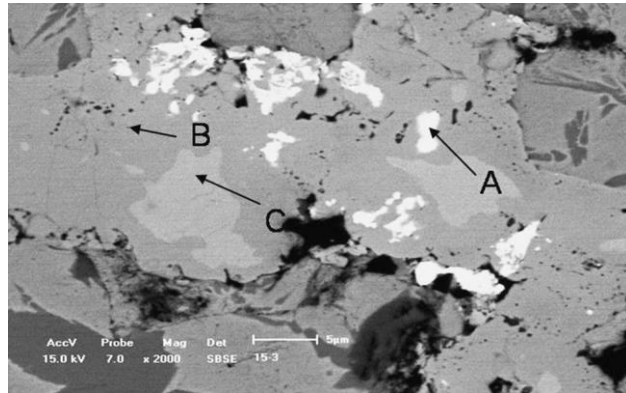


Figure 2.3: Microstructure of the Ti–10Mo–5Fe for MA alloy (SEM) (X. Li *et al.*, 2015)

#### 2.4.2.2 Mechanical alloying (MA)

Mechanical alloying (MA) is a P/M processing technique involving cold welding, fracturing and re-welding of powder particles in a high energy ball mill (Suryanarayana, Ivanov and Boldyrev, 2001). MA is a dry powder processing technique which is employed to synthesize both equilibrium and metastable phases of commercially useful and scientifically useful materials. This technique was developed by Benjamin (Benjamin, 1976) around 1966 to form an alloy combining oxide dispersion strengthening with  $\gamma'$  precipitation hardening intended for gas turbine applications in a nickel-based superalloy as shown in table 2.5. Oxide-dispersion could not be possible in the liquid phase so that solid-state processing technique is necessary; for this reason, MA is started using for industrial uses. The main advantage of using MA technique is that it produces different alloys, e.g. alloying of immiscible elements which are not possible with other technology.

The process of mechanical alloying consists of loading of powder mix and grinding mix (mainly of Co-Cr or tungsten carbide balls) in a stainless-steel container sealed under a protective Argon atmosphere (for avoiding/ minimizing oxidation and nitration during milling) and milling for the estimated length of the time. Approximately 1-2% of process control agent (PCA) added during milling for protection of the cold welding. There is a different type of milling equipment like Spex mills, Fritsch mills or planetary ball mills. In case of planetary ball mills,

control milling time and dwell time can be monitored after each small milling cycle and milling speed as shown in figure 2.4.

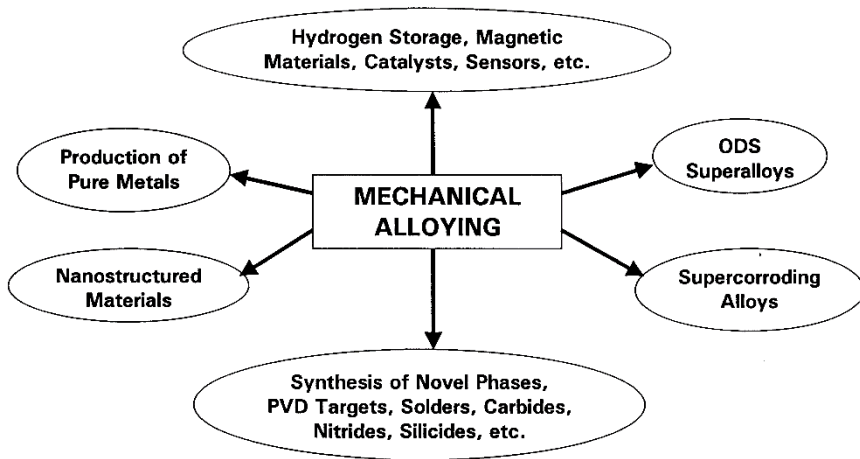


Figure 2.4: Typical current and potential applications of mechanically alloyed products (Suryanarayana, Ivanov and Boldyrev, 2001)

Agglomeration is also a phenomenon which is reported in mechanically alloyed powder mixtures. The phase has been obtained starting from elemental blend powders or mixtures of intermetallic (MA), or stoichiometric compounds (pre-alloyed intermetallic or even pure elements) (referred to as mechanical milling, MM)(Suryanarayana, Ivanov and Boldyrev, 2001).

Table 2.5: Important milestones in the development of mechanical alloying (Herr, 1995)

1966	Development of ODS nickel-base alloys
1981	Amorphization of intermetallics
1982	Disordering of ordered compounds
1983	Amorphization of blended elemental powder mixtures
1987/88	Synthesis of nanocrystalline phases
1989	Occurrence of displacement reactions
1989	Synthesis of quasicrystalline phases

In literature, there is mainly two ball mills powder processing with high energy discussed. Former is Mechanical alloying and latter is mechanical mixing.



Mechanical alloying (MA) primarily deals with the process when powders of (different metals or alloys/compounds) are milled together. In this process, the main reason for homogeneity is material transfer. But for the latter, i.e., Mechanical mixing (MM) deals with the uniform milling (even stoichiometric) composition powders, such as pure metals, intermetallic, or pre-alloyed powders, where the material transfer does not require for homogeneity. The advantage of MM over MA is less process time for MM; it's due to alloyed MM powders and powders are just needed for particle reduction and other transformations need to be induced mechanically. For example, MM requires approximately half of the time in comparison to MA.

Mechanical Alloying process depends on a lot of factors which need optimization of the process variables for better microstructure, or for achieving the desired products. Mainly process variables affect the quality of powder, or final product are:

Type of mill: There are the different type of mills available in the market like mixer mills, planetary mills, attritors, Uni-ball mills etc., These mills differ in their Capacity, ability to Control the process and temperature inside jars etc.,

Milling container: The material used for milling container is essential due to the impact of grinding medium of the inner walls of the container. If the substance of the vessel is different from the powder used, some material might be dislodged and get incorporated into the powder. It might be contaminating the powder.

Milling speed: The usual concept is **Milling energy  $\propto$  Milling speed** i.e. if the milling speed is high, milling energy is also high and vice versa. But milling speed depends on the design of the mill. Above a certain speed (Critical Speed) balls might be pinned to the inner walls of the vials. More speed also generates high heat inside the Jar. In some cases, it might be useful like where diffusion is required to promote homogenization or alloying in the powders. But in some cases, increased temperatures accelerate the process a lot and change the phases.

Milling time: This is the most critical parameter. Mainly the time is so chosen as to achieve a steady state between the fracturing and cold working of the powder

particles. It depends on the type of mills used, the intensity of milling, ball to powder ratio (BPR) and temperature of milling.

Type, size, and size distribution of the grinding medium: Hardened steel, hardened Chromium steel, tool steel, WC-Co and bearing steel are the mainly used materials for the abrasive medium. The density of the abrasive medium should be high enough so that balls can create enough impact force onto the powder. The size of the grinding medium also plays a vital role in the milling efficiency. In general, a significant proportion (high density) grinding balls is more useful because it can transfer more impact energy onto the powder particles.

Ball-to-powder (BPR) weight ratio: It is an essential variable in the milling process. It might be from 1:1 to 220:1 depends on the investigators. Usually 10:1 is used for small mills but for large mills BPR should be 50:1 to 100:1. Higher the BPR, shorter the milling time required. For the present study, BPR would be 10:1 to 15:1.

The extent of filling the vial: Alloying among the powder particles mainly occurs due to the impact forces applied on them, so it is necessary that there should be enough space for the balls and the powder particles to move freely around in the container. Usually, 50% of the Vial space is left empty in most of the milling. For our research, vial approximately is filled with one-third.

Milling atmosphere: The main effect of the milling atmosphere is for the contamination of the powder. For this reason, the powders milled in those containers which have been either evacuated or filled with an inert gas such as Argon (Ar) or Helium (He). In the present study, jars filled with Argon for avoiding contamination.

Process control agent (PCA): A process control agent (PCA) is added to the powder mixtures during milling to reduce the effect of cold welding. It may be solid, liquid or gases. The stearic acid used as PCA.

All the above variables are not independent, like milling speed and milling time depends on the type of mill.

Few reported that any alloy could be made amorphous under the appropriate milling conditions. Amorphous phases form from EB powders either directly or via the formation of an intermetallic phase.

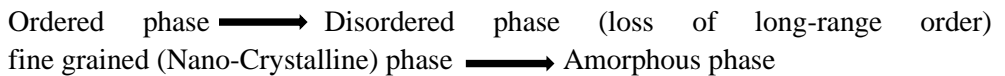
For example:



In some other instances, it may be like,



n intermetallic or a solid solution forms before amorphization depends on the relative free energies of the two competing phases. On the other side, amorphization in ordered alloys seems to follow the sequence.



The time required for amorphization is dependent on the process variables, but they are typically shorter in case of MM than MA, due to alloying which does not need for MM.

Problems during MA:

There is a lot of advantages of using MA, but still, there are some disadvantages. It divides into three groups:

**Powder Contamination:** This is a significant problem during this process. It may be due to grinding medium, Vial, milling atmosphere etc.; It should minimize by using high purity metals, uses of balls and container of the same material and proper milling atmosphere etc.,

**Limited Science content:** The problem is not very clear about this technique. It may be due to a lot of variables involved in this process.

Limited application: The industrial applications of MA is very few. Mainly demand seems to be about 350t of ODS materials, 200t of solder alloy, and 5t of Physical vapor deposition (PVD) target (Cr-V) alloys per year. The use of mechanochemical reactions in producing metals, alloys and compounds, catalyst materials, needs to be explored more.

The primary application of MA products is in the form of ODS alloys, which is very difficult to process with conventional ingot metallurgy (IM) methods. Due to a high homogeneous distribution of alloying elements during MA provides robust solution strengthened and precipitation- hardened alloys having more stability at elevated temperatures and overall improvement in properties.

Mechanochemistry is the term applied to the process in which chemical reactions and phase transformations take place due to applications of mechanical energy. This reaction might be utilized to produce pure metals, alloys and compounds at room temperature both in the laboratory and in large scale.

#### **2.4.2.3: Spark plasma sintering (SPS):**

Spark plasma sintering is one of the full densification processing routes to process biomaterials in the laboratory.

SPS is a new technique which takes place in lesser time (few minutes) to complete a sintering process compared to conventional sintering which may take hours or even days for the same. Due to high heating rate, it can attain for SPS process, high sintering rate is possible. Another reason is less holding time (5 to 10 min) for SPS and for regular sintering holding time maybe 2-3 hours. Usually, heating rate attained in conventional furnaces is 5 to 8°C or maximum 10°C, but in SPS heating rate might exceed 300°C. For example, if the temperature of 1200°C is needed, then with conventional sintering it takes 3-4 hours minimum, but for SPS it takes only 4 minutes (Shen *et al.*, 2002).

For conventional sintering, usually, a green compact need to be prepared externally using a suitable die and hydraulic m/c for applying the necessary pressure. After that, the green compact sintered in a furnace. For SPS, the powder directly fed into the

graphite dies and the die enclosed with suitable punches. Due to the advantage of high heating rate and less holding time, SPS can restrict the unwanted sintering reactions in highly reactive systems as opposed to conventional sintering and hence the formation of undesirable product phases can be avoided.

In 1990 Sumitomo heavy industries ltd. (Japan), commercially operated first plasma activated sintering (PAS) developed and Spark Plasma Sintering (SPS) machines with punches and dies made from electrically conductive graphite (Suárez, Fernández and Menéndez, 2013).

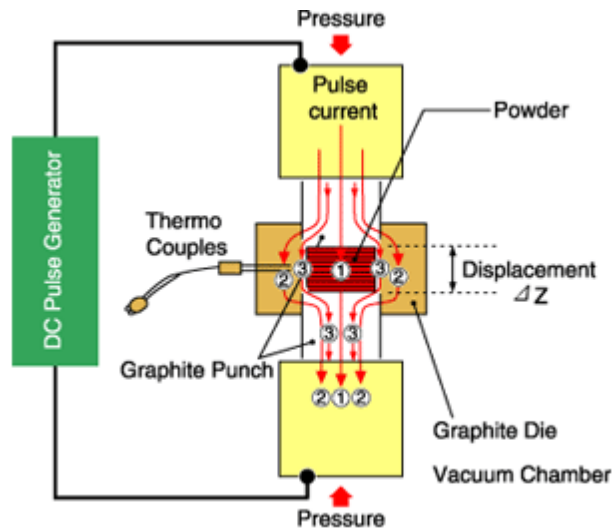


Figure: 2.5: An ON-OFF pulsed current path through the spark plasma sintering machine (Basu, 2011)

The SPS process is an electrical sintering technique which applies an ON-OFF DC pulse. The action of the electrical field causes rapid diffusion due to rapid migration of ions.

SPS process use for different specific purposes:

(1) For biomaterial: Erik O. Martz found a wide variety of applications in implantology with bulk Hydroxyapatite (HA) compacts and composites with HA (Martz *et al.*, 1997). Aerospace engineering; New York Confirmed that HA shows

limited stability at high temperatures and would dissociate into Tricalcium phosphate and tetra-calcium phosphate at 1300°C in the air or 1000°C in a vacuum (Engineering and York, 1994). High temperatures and long sintering duration are required for consolidation of HA powders by conventional techniques resulting in extreme grain coarsening or surface contamination, which can reduce the required mechanical properties. These problems can be minimized or eliminated by using Spark Plasma Sintering to avoid exposing the compacts to high temperatures for a long duration. Some scientists confirmed that it is possible to sinter HA powders by SPS at a temperature as low as 950°C, and good performance regarding fracture toughness, Young's modulus and toughness. The obtained density is 99.6%.

(2) For nuclear energy applications: from different literature, it is shown that SPS can densify the materials at lower temperatures and shorter times than those required in conventional processes. Spark plasma sintering minimizes grain growth, and it is, therefore, suitable to be used in materials requiring better machine performance. (O'Brien *et al.*, 2009) reported about other works on encapsulation of plutonium dioxide or americium dioxide within a tungsten-based cermet using SPS technique.

(3) Materials with a low coefficient of thermal expansion: The ceramic materials obtained by using the conventional method of pressure less natural sintering have ordinarily low mechanical properties and Young's modulus. SPS is a solution for fabrication of sub-micron Las-Alumina composites (García-Moreno *et al.*, 2011) and they also found that it is possible to sinter the composites up to theoretical density and even reach higher strength values at less current temperatures than required by conventional sintering. There are also different fabrication technologies like additive manufacturing, electron beam melting etc.,

Additive manufacturing or 3D printing is a process of making 3D solid objects from a digital model. This technology also used in the field of jewellery, footwear, industrial design, architecture, engineering and construction, automotive, aerospace, dental and medical industries, education, geographic information systems, civil engineering and many others.

The significant applications of additive manufacturing are the prosthesis, which replaces damaged tissue with a non-living material (usually a metal alloy) in a form that at least approximates natural function. The best examples could be including dental crowns and bridges, heart valves and stents, knee and hip replacements (Oshida, 2013).

### **2.5: Corrosion:**

For biomedical applications corrosion properties is very important. Alloys should be corrosion resistant. For  $\beta$ -Ti alloys normally corrosion behavior is better in comparison to CP Ti and Ti-6Al-4V which is also discussed by different authors (Niespodziana, Jurczyk and Jurczyk, 2008; Nishimura, 2011). Some authors also confirmed corrosion resistant character of Ti-15Mo which makes the alloy suitable for biomedical application (Kumar and Narayanan, 2008).

*Development of new high-performance Titanium alloys with Fe-addition for dental implants*



# Chapter 3: Material and methods

There are mainly four phases carried out to achieve the main objective. For obtaining mainly three phases, we divided into different tasks which followed one by one:

**Phase 1: To see the effect of Mo and Fe on Ti-Mo alloy by Elemental Blend**

**Phase 2: To perform mechanical alloying technique**

**Phase 3: for obtaining full density samples with spark plasma sintering Method**

**Phase 4: for obtaining  $I_{\text{corr}}$ , open circuit potential (OCP), Corrosion velocity, ion release rate by corrosion test**

It is shown the overall project planning in flow diagram of our research work in figure 3.1.

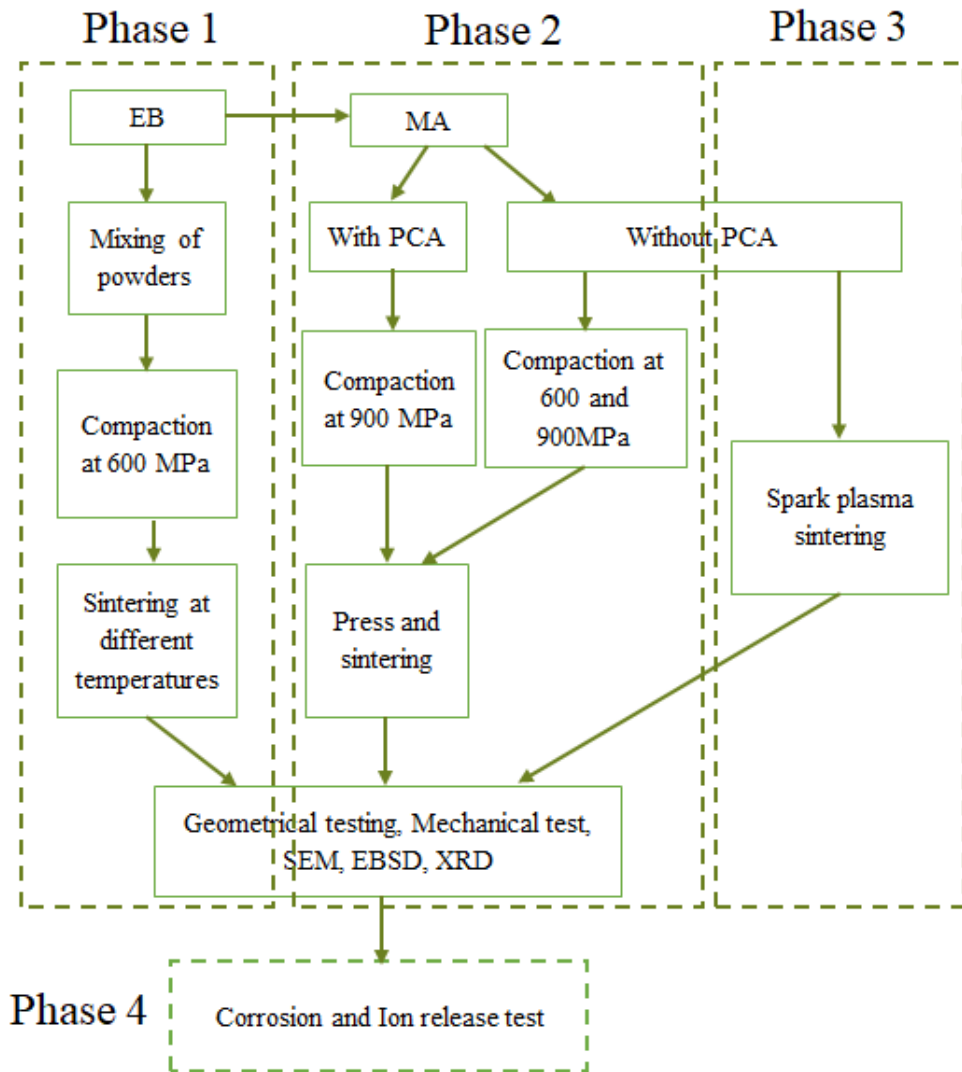
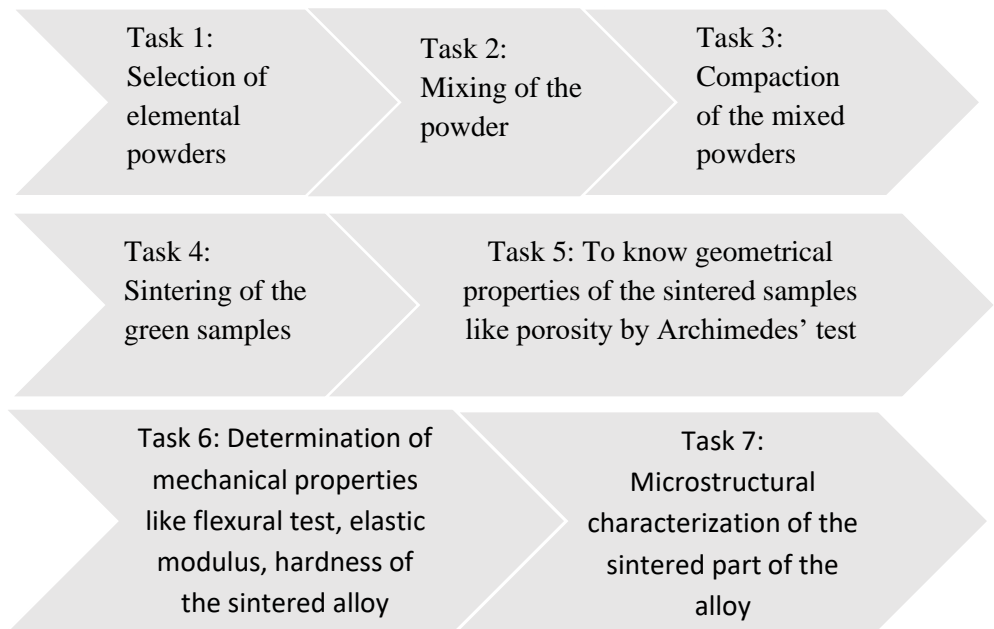


Figure 3.1: Flow diagram of overall project

### 3.1: Phase 1: To see the effect of Mo and Fe on Ti-Mo alloy by Elemental Blend

Elemental Blend (EB) is a technique for mixing of elemental powders. It is a very simple and cost-effective technique, but the problem is lack of homogeneity due to less intense process. For this process powders needs to be mixed as per the weight calculated and then after if necessary, mixed the powders in tubular mixer with 150 rpm.

For obtaining different properties of alloy with Elemental Blend we have done different tasks:



#### 3.1.1: Task 1: Selection of elemental powders:

The main objective is to develop  $\beta$ -Ti alloys for biomedical uses.  $\beta$ -stabilizing elements (Zr, Mo, Fe) are the better candidates for designing new  $\beta$ -type Ti-based alloys with lower elastic modulus, greater strength and corrosion resistance. Initially

Development of new high-performance Titanium alloys with Fe-addition for dental implants

selection of elemental powders is the most important step towards development of new Ti-β biomaterial alloys. Ti-Mo based biomaterials would be a promising candidate for the present study. It is started from Ti-Mo binary alloy followed by Zr with Ti-Mo alloy for better diffusion and further with Ti-Mo-Zr addition of Fe with different %(w/w) and shown the effect of adding different % of Fe (1,2,3,4).

Ti-(12,15) Mo, Ti-(12,15) Mo-6Zr, Ti-(12,15) Mo-6Zr-(1,2,3,4) Fe is developed.

For obtaining this task we must select power supplier company of Ti, Mo, ZrH<sub>2</sub> with high purity.

Supplier for the Titanium, Molybdenum is from Atlantic Equipment Engineers and Zirconium powders are Alfa Aesar with purity and powder size are listed in table 3.1. Supplier for Fe are Atlantic Equipment Engineers with purity 99.8% and powder size are (1-9) μm.

Table 3.1: Elemental powder with its suppliers and quality

<b>Powder</b>	<b>Supplier</b>	<b>Purity (%)</b>	<b>Powder size</b>
Titanium	Atlantic Equipment Engineers	99.7	45 μm
Molybdenum	Atlantic Equipment Engineers	99.95	2-8 μm
Zirconium Hydride	Alfa Aesar	99.95	44 μm
Iron	Atlantic Equipment Engineers	99.8	1-9 μm

During this study different alloys were developed with Elemental blend with different percentage of Fe. Initially Ti-(12,15% w/w) Mo, Ti-(12, 15% w/w) Mo-6Zr and Ti-(12, 15% w/w) Mo-6Zr-x(1,2,3,4)Fe Elemental powder were used with high purity (> 99.7%) for better geometrical properties and produces less problems during compaction and sintering process. Powder quality of the raw element can be seen in Figure 3.2 with different magnification analyzed in Scanning electron microscopy (SEM).

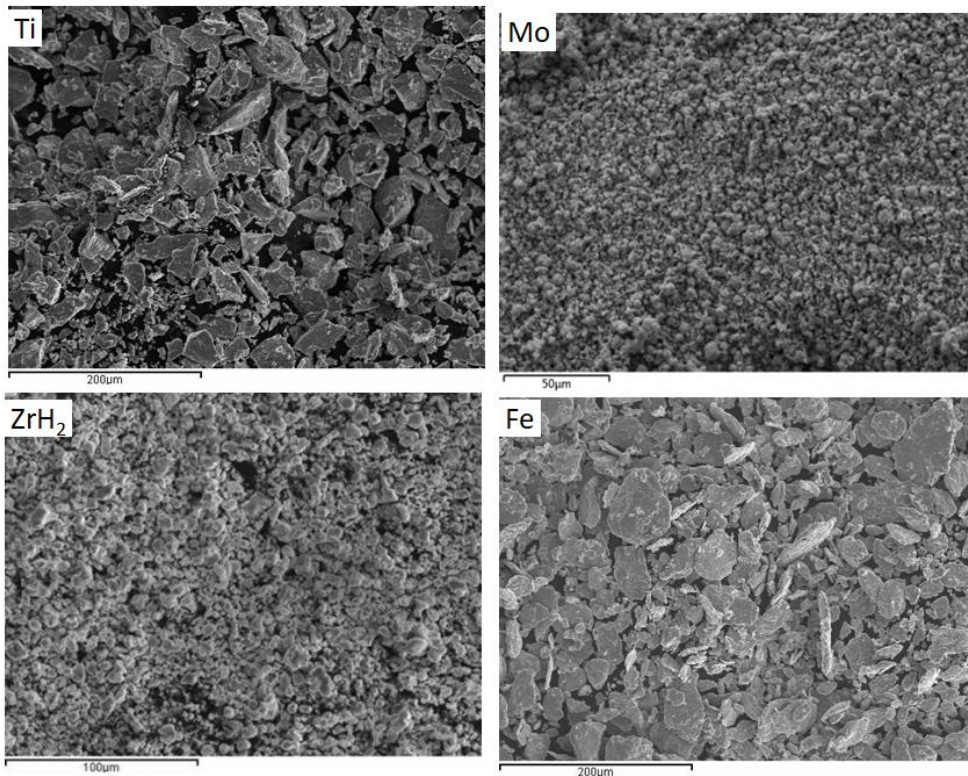


Figure 3.2: Supplied powder of Ti, Mo, ZrH<sub>2</sub> and Fe with different magnification

Chemical analysis of Ti, Mo and Fe elemental powders is summarized in table 3.2, which shows different contents of element available in the raw material. In Ti powder, gases were present as main impurities. Mo powder was almost pure whereas Fe powder had acid insoluble in it.

Table 3.2: Typical chemical analysis of supplier powder Ti, Mo and Fe

Element	For Ti % by w/w	For Mo % by w/w	For Fe % by w/w
Oxygen	0.22900	-	-
Nitrogen	0.01600	-	-
Hydrogen	0.02220	-	-
Iron	0.01000	0.00200	99.90000 min metals basis
Silicon	<0.01000	0.00600	-
Aluminum	<0.01000	<0.00100	-
Sulfur	<0.00100	<0.00100	-
Carbon	0.01800	0.00300	-
Magnesium	0.01000	<0.00100	-
Manganese	0.01000	<0.00100	-
Sodium	<0.01000	-	-
Chlorine	<0.01000	-	-
Phosphorus	<0.00200	-	-
Titanium	99.90000 min metals basis	<0.00100	-
Calcium	-	<0.00100	-
Chromium	-	<0.00100	-
Copper	-	<0.00100	-
Nickel	-	0.00300	-
Lead	-	<0.00100	<0.00040
Tin	-	<0.00100	-
Molybdenum	-	99.98000 min metals basis	-
Arsenic	-	-	<0.00030
Mercury	-	-	<0.00020
Acid insolubles	-	-	0.03000

The above analysis is carried out as part of our internal quality control testing and is based upon our analysis methods. The granulometric analysis of the supplied powder has been shown in figure 3.3.

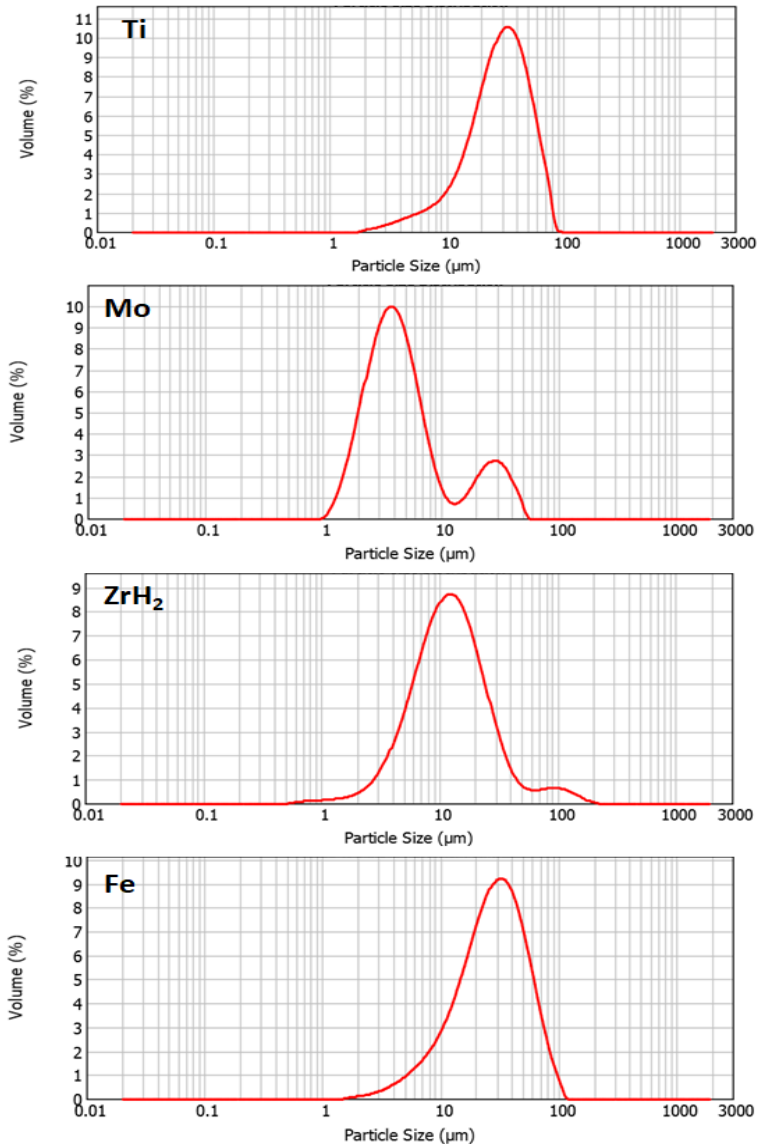


Figure 3.3: Granulometric analysis of Ti, Mo, ZrH<sub>2</sub> and Fe supplied powder

### **Granulometry of raw powder:**

D (0.1), D (0.5), D (0.9) data provide by supplier as shown in table 3.3, we mainly see the value of D (0.5) for average particle size.

Table 3.3: Granulometry of Ti, Mo, ZrH<sub>2</sub> and Fe supplied powder.

Material	size (µm)		
	D (0.1)	D (0.5)	D (0.9)
Ti	11.064	29.227	55.929
Mo	2.086	4.255	24.501
ZrH <sub>2</sub>	4.757	12.074	30.436
Fe	9.850	28.110	59.888

Selection of material is an essential step for powder metallurgy process. The first thing is to obtain alloys for powder metallurgy using selective raw material. The suppliers of metallic powder materials in our research are Alfa Aesar and Atlantic Equipment Engineers.

After selection of the elemental powder with higher purity, it is required to weight the powders according to stoichiometric relations.

#### **3.1.2: Task 2: Mixing of the powder**

In this step we must calculate the mass of the powder according to stoichiometric relation and composition of the required alloy. Mixing of the powder done in Bioengineering tubular mixer.



Table 3.4: Elemental powder weight (real) for EB 1250°C

Alloy	%Ti real	%Mo real	% ZrH <sub>2</sub> real	%Fe real	ρt Real
Ti12Mo	88.01	11.99	0	0	4.83
Ti12Mo6Zr	82.00	12.00	6.00	0	4.93
Ti15Mo	85.00	15.00	0	0	4.92
Ti15Mo6Zr	79.01	14.98	6.00	0	5.02
Ti12Mo6Zr1Fe	81.00	12.00	6.00	1.00	4.95
Ti12Mo6Zr2Fe	80.00	12.00	6.00	2.00	4.98
Ti12Mo6Zr3Fe	79.00	12.00	6.00	3.00	5.00
Ti12Mo6Zr4Fe	78.00	12.00	6.00	4.00	5.02
Ti15Mo6Zr2Fe	77.00	15.00	6.00	2.00	5.07
Ti15Mo6Zr4Fe	75.00	15.00	6.00	4.00	5.12

Table 3.5: Elemental powder weight (real) for EB 1300°C

alloy	%Ti real	%Mo real	% ZrH <sub>2</sub> real	%Fe real	ρt Real
Ti12Mo6Zr1Fe	81.00	12.00	6.00	1.00	4.95
Ti12Mo6Zr2Fe	80.01	11.99	6.00	2.00	4.98
Ti12Mo6Zr3Fe	79.01	11.99	6.00	3.00	5.00
Ti12Mo6Zr4Fe	78.00	12.00	6.01	4.00	5.02

Powder weight: normally weighing of powders done according to alloy (depends upon density), number of samples (normally 5), dimension of sample etc. (30\*12\*6 mm<sup>3</sup>). Density of alloy calculated according to stoichiometric relation of alloying powder. %Ti<sub>real</sub>, %Mo<sub>real</sub>, % ZrH<sub>2</sub> real and % Fe<sub>real</sub>. Real powder weight with different composition with both temperatures are tabulated in table 3.4 and 3.5.

### **3.1.3: Task 3: Compaction of the mixed powder**

Compaction is an important part of powder metallurgy. Powder filling is by manual method inside the compaction matrix. This equipment is Uni-axial compaction equipment which have a higher range of compaction pressure which we can use according to need or powder quality. This is suitable for compacting.

After getting mixtures of elemental powders by different method, it is needed to compact, press uniaxial with floating matrix. Compaction is important for production of green samples to achieve a better distribution of pressure applied on both sides of the Compact (top and bottom). For this purpose, it is determined the force to be applied according to the area exposed to each of the arrays. Knowing that  $P = F/S$ , where P is the considered pressure, F is the force applied and the surface of the test piece S. The force must be applied to maintain the pressure of compaction constant, in all samples, 600 MPa obtaining.

The application of force to the compaction of the samples, is held at a constant speed and keeping the charge needed in each case for 15 s.

After compaction of samples, green density of samples was analyzed which signifies the elemental powder bonding with another alloying element.

The compaction matrix is used for making samples for flexural samples. Normally 8-9 g powders were kept inside the slot made in this metal matrix. The volume of this slot is 32mm\*12mm\*x mm (where x is thickness of samples), which is adjustable by the movement of both part of the matrix. During research, normally thickness is maintained as 5-6 mm. Matrix was properly cleaned with ethanol and lubricant before its use and after that properly covered with plastic to eliminate any possible chance of contamination from outside environment. The equipment used for compaction is Instron model 1343 equipped with a 500 kN load cell which is shown in figure 3.4 (A), matrix for the bending sample compaction is shown in figure 3.4 (B) the punch of the cylindrical matrix of 20 mm diameter shown in figure 3.4 (C).

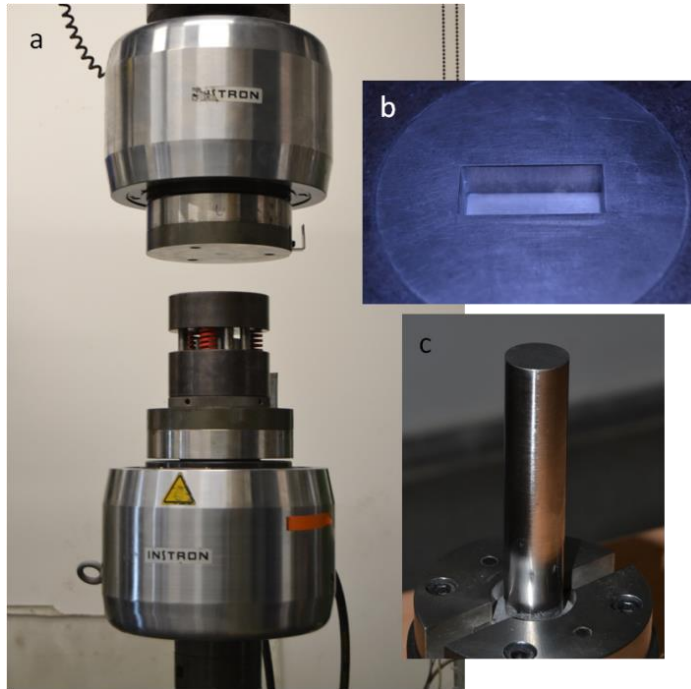


Fig 3.4: (a) Press of compaction with the floating matrix between the compression plates, (b) detail of the cavity of the rectangular matrix of 12x30mm and (c) detail of the punch of the cylindrical matrix of 20 mm diameter

After compaction of samples, green density of samples was analyzed which signifies the elemental powder bonding with another alloying element.

#### 3.1.4: Task 4: Sintering of the green sample

From the literature, it is found that the mechanical properties is superior at 1250°C due to better dissolution of  $\alpha$ -particles into  $\beta$  alloy (Guo *et al.*, 2014). So, it is planned to use 1250°C temperature for our alloy or near to this temperature. 1250 and 1300°C are employed for better diffusion of the elements inside the alloy. Inside the furnace, vacuum is maintained to restrict the oxidation of the alloy. Argon atmosphere inside the furnace tube and vacuum pressure ( $10^{-3}$  to  $10^{-4}$  mbar) are retained. Sintering cycle plays very important role for the mechanical properties of the alloy and the microstructure of the alloys.

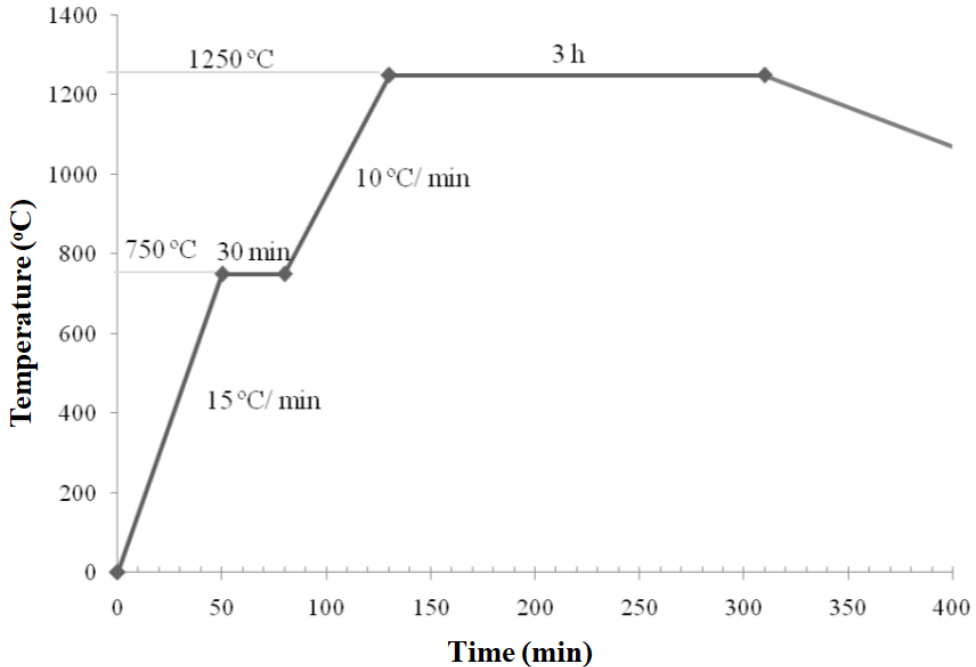


Figure 3.5: proposed sintering curve. Presents a heating 15C/min up to a temperature of 750°C, idle time of 30 min to homogenize the temperature of the material and the oven, another cycle up to 1250°C and 10°C/min, 3 hours sintering and cooling in furnace

The sintering cycle is maintained like figure (3.5) and the 1<sup>st</sup> cycle is from (0°C to 750°C) with 15°C/min and 30 min holding time, then (750°C-1250°C) with 10°C/min heating rate and then holding time for 3 hours and then after cooling of the alloy. Vacuum sintering was done in the Furnace CARBOLITE HVT 15 75 450. This technique of sintering was used for specimen produced by elemental blend and Mechanical alloying technique.

### **3.1.5: Task 5: To know geometrical properties of the sintered samples like porosity by Archimedes' test**

Relative density/porosity is the primary characteristics of the sintered alloy. There are two type of porosity i.e., one is open porosity and other is closed porosity. Open

porosity signifies porosity on the upper surface of the samples, closed porosity signifies the porosity inside the samples. Closed porosity also signifies the diffusion quality of the samples.

Porosity is determined by the Archimedes' test. From this test, closed porosity, open porosity, relative density is determined. Archimedes' test was done and then the specimen was kept inside the vacuum chamber with water for extraction of bubbles (approx. 30 min.) and after that calculation ( $S = \text{Mass immersed in water after saturation}$  and  $M = \text{weight in the air after removing excess water}$ ) was done.

After calculation of relative density, porosity could be calculated very easily.

Porosity =  $100 - \text{relative density}$

So, if relative density is higher that means porosity should be smaller which is ambient for this study.

### **3.1.6: Task 6: Determination of Mechanical properties of the sintered part of samples:**

For mechanical properties determination we must perform different mechanical test like flexural strength of the sintered part, determine elastic modulus of the alloy, Determination of Alloy Hardness.

#### **(Step 1)-flexural strength of the sintered part**

The flexural strength is the primary stage of the alloys to determine after sintering, flexural samples should be  $30 \times 12 \times 6 \text{ mm}^3$ . Flexural strength, flexural modulus, stress, strain is determined. Basic mechanical properties of the samples are analyzed.

Flexural tests were done by Universal Shimadzu Autograph AG-100 kN Xplus. In this equipment, samples were kept horizontally (cross) to assure the break of samples. Initially data of displacement and force were taken, then the data of tests were recorded by Trapezium software and after that analysis of data were done as per the available information. With these results stress, strain, bending modulus and bending energy were analyzed.

Note: For our experiment  
 $L = 22 \text{ cm}$

H= thickness of the sample

D=displacement

**(Step 2)-: Determine elastic modulus of the alloy**

Elastic modulus is the main mechanical properties for the biomaterials. It should be less (up to 30 GPa) approximately for hard tissue replacement. From the literature, it is found that most of the present alloys have more elastic modulus which is the main cause of stress shielding effect due to mismatching the modulus of the implant materials and the hard tissue. The main concern is to focus on minimizing the elastic modulus with the addition of different  $\beta$  stabilizing elements like Mo, Zr and Fe. Elastic modulus is calculated by Ultrasonic test with the calculation of longitudinal velocity ( $V_L$ ), Transversal velocity ( $V_T$ ). With the help of these two parameters, elastic modulus and Poisson's ratio are calculated for that alloy. These steps are followed for the calculation of parameters.

Note: for the longitudinal velocity and transversal velocity we need better surface contact, so we need to grind break samples after bending test with 220, 500, 1000 SiC grit size paper for 15 s approximately.

Experimental density is calculated by Archimedes' test ( $\rho_{exp}$ ), then thickness of sintered samples (t), and 2t, 3t and 4t are calculated respectively followed by calculation of longitudinal velocity ( $V_L$ ) and Transversal velocity ( $V_T$ ) using ultrasonic equipment with different setup. After getting the value of  $V_L$  and  $V_T$ , E (elastic modulus) and Poisson's ratio are assessed.

The measurement of the modulus of elasticity by ultrasound is carried out in a Karl Deutsch Echo-graph 1090 equipment. After the preparation of the surface the measurements of the thickness of the samples have been taken, using a micro-meter of RS components with a distance between 0 and 25 mm and a sensitivity of 0.001 mm, and the double and triple thickness values have been calculated. For the measurement of the longitudinal velocity, a DS 6 PB 4-14 probe with a longitudinal wave coupling 1571 of the Echo-trace houses was used. The transverse speed is measured using a YS 12 HB1 probe with a transverse wave coupling 1898.025 from the Karl Deutsch echo-graph.

Method for determine elastic modulus:

- Measure the thickness as it has been shown in micrometre and adjust the thickness as it can be.
- Density used is  $t$  obtained by the method of Archimedes.
- If it is deformed due to the sintering, search the area of best contact.
- To place the sensor in the part convex.

### **(Step 3)-Determination of Alloy Hardness**

Hardness is a measurement of the materials for the resistant quality to the compressive load for the shape change of those materials. Hardness of the metals should be larger than the plastics and polymers. Macroscopic hardness is generally characterized by strong intermolecular bonds, but the behavior of solid materials under force is complex; therefore, there are different measurements of hardness: scratch hardness, indentation hardness, and rebound hardness. For the metallurgic uses, indentation hardness is used. Common indentation hardness scales are Rockwell, Vickers, Shore, and Brinell. It would depend on the availability of the equipment in the laboratory. But preferred hardness would be Vickers's hardness. Nowadays most of the equipment provides the values automatically and some are still semi-automatic.

Note: We would perform 10 reading( start from 0  $\mu\text{m}$  of the sample and after each reading move 25  $\mu\text{m}$  and so on) for one sample and for one alloy we normally select 2 samples which is near to mean bending strength due to similar to that alloy. After that we normally take average of all the reading.

First, hardness was calculated with Rockwell Hardness equipment and then after it was converted into Vickers's hardness (HV).

Determination of Rockwell hardness (HRN 15N) was done by equipment Durometer-2-Centaur-model-HD 9-45. Normally for one specimen Rockwell hardness was calculated at 5-6 different point of the specimen. After that Rockwell hardness was converted into Vickers's hardness according to conversion table and average of all the values were taken.

**3.1.7: Task 7: Microstructural characterization of the sintered part of the alloy:**

For analyzing microstructural properties of the sintered part, we have to perform different analysis like microhardness of the sintered part, fractography of the sintered part, back scattered/ secondary image with SEM, phase analysis of the alloy with the help of DRX, SEM and EBSD analysis.

**(Step 1): Microhardness of the alloy**

The micro harness values were calculated with Shimadzu HMV 2T equipment, figure 3.6, test force was 90.07 mN, image in rhombus shape was fixed and the area of the rhombus was hardness values.

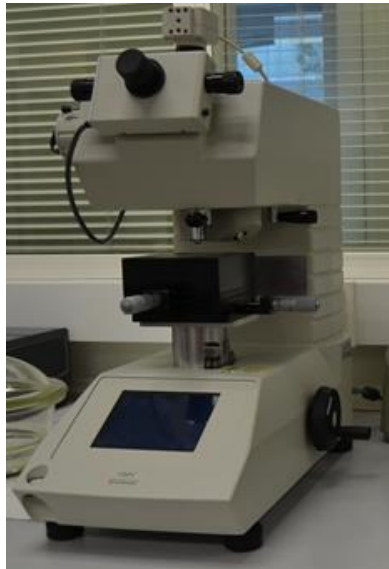


Fig 3.6: Microhardness equipment Shimadzu HMV 2T

Normally 10 reading were noted for one sample from 25  $\mu\text{m}$  of the starting point of the sample and move towards right direction to 25  $\mu\text{m}$  for each reading and then the average of the all the values were taken.



**(Step 2): Fractography analysis and Back scattered/ secondary image with Optical microscopy/SEM:**

For Back scattered image (BSE) and secondary image of the alloy, all the samples are prepared followed by different steps like cutting of the samples, mounting of the samples and metallographic preparation of the samples. Select the sample which bending strength value is near to average value of 5 samples. Then cut the samples transversally 2mm for analyses the fracture surface, then 1.5 mm for the SEM, after 1.5 mm cut for the DRX samples. After cutting of sample we should mount the samples with non-conductive resins with height 8 mm approx. Then after we must grind the samples with 220, 500, 1000 SiC grit size paper. Then after we must polish with 9 $\mu$ m and then 1 $\mu$ m. Then it will be better to clean with Ultrasonic and very good dry with dryer.

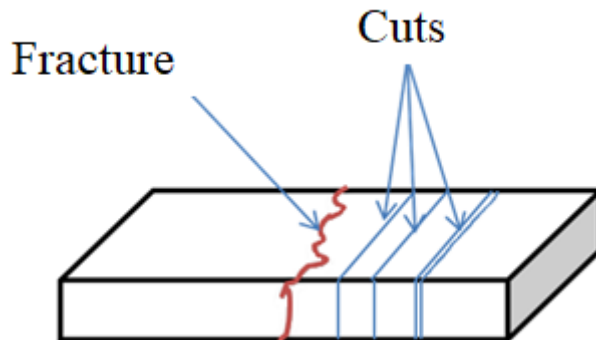


Figure 3.7: Fractured surface and after cut for microstructural analysis

Energy Dispersive Spectroscopy (EDS) is the main tool for analyzing the chemical composition of the alloy and mapping also done for the elemental analysis after mixing. Mixing of the different elements is observed by the different software like INCA, AZTEC. Percentage of different elements inside the alloy atomically and by weight is calculated. Fracture surface after break are shown in figure 3.7.

### Scanning Electron Microscopy (SEM):

Optical microscopy equipment available for our research is Nikon elipse LV 100 shown in figure 3.8 (A) and SEM equipment available in our lab is Jeol 6300 JSM shown in figure 3.8 (B).

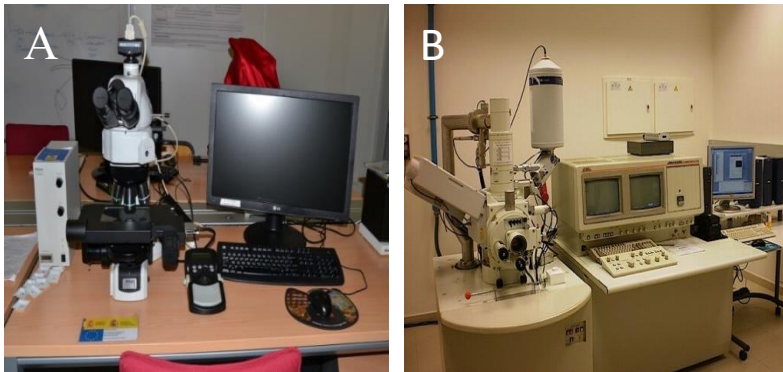


Figure 3.8: (A) Optical microscopy equipment (NIKON elipse LV 100) (B) SEM Jeol JSM 6300

During SEM First of all fractography of the samples were analyzed, then microstructure of the samples was done (Back scattered image and secondary image) with different magnification (100x/250x for general aspects), 500 x for grain structure for the alloy, 1000x/2500x for specific analysis for some part of the microstructure. Inca software was applied for SEM analysis.

#### **(Step 3): Phase analysis of the alloy with the help of DRX, SEM and EBSD analysis**

Phase analysis is the important step for the alloy. It is focused to increase the percentage % of  $\beta$ -phase or to reach the 100 %  $\beta$ -phase. Phases would be determined by different techniques like XRD and EBSD analysis. The peaks in XRD technique show the effect of different elements on the alloy. XRD is a good tool to know about different phases. Different phases with different conditions of the alloy is compared like phase change due to change in sintering temperature, change in alloying element, change in percentage (%) of alloying element and change in powder processing techniques. Shifting of the peak due to changing parameters of the alloys is seen.

Preparation for EBSD samples is little bit different from SEM samples preparation. For EBSD samples we must use conductive resin for mounting and height of sample should be 8 mm. We must dry sample very good for better analysis.

Depending on the microstructure observed in the cross sections of the samples, the crystalline orientation is studied using EBSD. With the help of pole figure and inverse pole figure, the orientation of the crystal present in the alloy is determined. There is a discussion briefly about the planar orientation of the crystal inside the alloy (Tarzimoghadam *et al.*, 2015).

### **Electron Back scatter Diffraction (EBSD)**

EBSD helps to view better microstructure and to determine disorientation of the alloy. Pole figure and inverse pole figure helps to know about orientation of the alloy. It also helps to calculate  $\alpha/\beta$  phase of the alloy. Both techniques were very useful during this study; equipment available is Oxford instruments as shown in figure 3.9.



Fig. 3.9: EBSD Oxford Instruments.

AzTec and channel 5 software was used for EBSD analysis during research.

### **XRD Analysis**

In order to have better surface finishing, the appropriate intensity in XRD (X ray diffraction) was measured. Half part of the obtained specimen after breaking during flexural tests been prepared metallographically, following the same steps of assembly, thinning Grinding and polishing explained before. The measurements are

performed on a Bruker D2Phaser device as shown in figure 3.10; using 30 kV and a 0.05 ° step every 10 seconds.

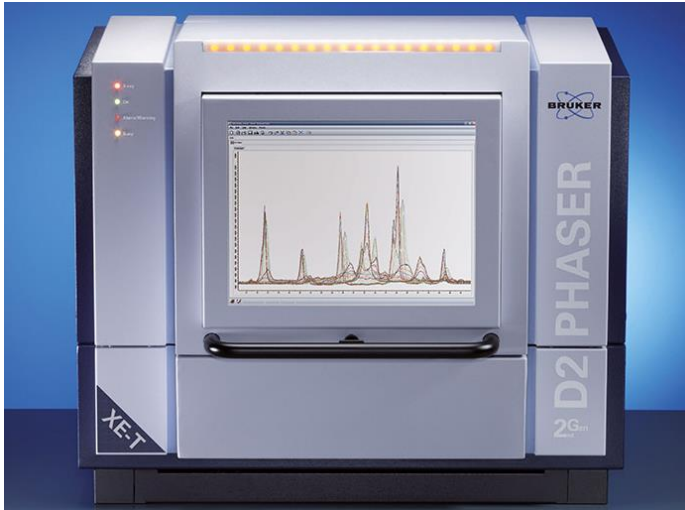


Figure 3.10: Bruker D2PHASER diffractometer.

The determination of the phases is done with the EVA software program. The amount of phase was determined for some cases through the application of the Rietvel method which requires the deconvolution of the peaks assigning the intensities to each of the phases, realized in the TOPAS software. The measurements were performed over the  $2\theta$  range from 20 to 90 degrees at room temperature.

### **3.2: Phase 2: To perform mechanical alloying technique**

Mechanical alloying: (MA) is a solid-state powder processing technique involving repeated welding, fracturing, and re-welding of powder particles in a high-energy ball mill.

EB have lack of diffusion so, for overcome this problem we started work with MA techniques with different combinations. The sample we can work with mechanical alloying technique for better homogeneity, because this technique has more impact with high speed and more time. Starting we prefer to work without process control agent (PCA) due to Ti alloy got contaminated with PCA so, for neglect the contamination. We can start with less time and same compaction pressure.



#### **3.2.1: Task 1: Mixing of powder without process control agent (PCA)**

For obtain this task we have done mixing of different combination of milling speed and milling time without PCA. First, we planned to work with Ti-12Mo-6Zr-2Fe with 600 and 900 MPa, after the analysis of the results it is found that 900 MPa have better mechanical properties in comparison to 600 MPa. All combination of mechanical alloying technique is shown in table 3.6.

Main parameters for mechanical alloying process are milling speed (in rpm), milling time (in min or h), Ball to powder ratio (BPR), Ball size (Diameter in mm) and milling cycle.

During experiment different combination of milling speed and milling time were used for best homogeneous, better mechanical properties and better microstructure of the powder.

During experiment powder mixing for mechanical alloying was done in Camera gloves (Jacomex GPT2) as shown in figure 3.10. The equipment was used for

weighing the elemental powder inside the glove box, restricted contamination and it is most important for Ti-alloy, because Ti is very reactive and mixing of elemental powders outside the glove box can lost powders and in some cases it may cause fire to avoid the addition of oxygen to the powder, which may modify the properties of Ti alloy. So, this equipment is utmost required to control such type of problems. This equipment is not available easily in each laboratory, so this is new and innovative idea to restrict the accidents like fire, lost or contamination of powders.

Table 3.6: Mechanical Alloying powder weight (real) with different parameters

Alloy	PW <sub>Real</sub>	BW <sub>Real</sub>	(BPR) <sub>Real</sub>	Milling speed	Milling Time	Compaction pressure
Ti12Mo6Zr2Fe	398.53	39.14	10.18	300	45	600
Ti12Mo6Zr2Fe	398.05	39.26	10.14	300	45	900
Ti15Mo	349.09	23.28	15	300	45	900
Ti15Mo	348.21	23.28	14.96	300	37	900
Ti15Mo	366.42	24.281	15.09	300	52	900
Ti15Mo	365.38	24.281	15.05	240	45	900
Ti15Mo	363.88	24.282	14.99	180	45	900
Ti15Mo	364.14	24.281	15	180	52	900
Ti15Mo	364.15	24.282	15	240	52	900
Ti15Mo	366.26	24.283	15.08	180	60	900
Ti15Mo6Zr2Fe	360.26	23.492	15.35	180	45	900
Ti15Mo6Zr2Fe	360.43	24.112	15.2	210	45	900
Ti15Mo6Zr2Fe	359.23	23.982	14.98	180	52	900

PW<sub>Real</sub> = Powder weight during milling in real

BW<sub>Real</sub> = Ball weight during milling in real

(BPR)<sub>Real</sub> = ratio of ball weight to powder weight in real during milling



Figure 3.11: Glove box for mixing of powders for compaction



Figure 3.12: Planetary ball milling equipment (Retsch PM 400/2)

Retsch PM 400/2, as shown in figure 3.12, is used for mechanical alloying powder mixing process. The movement of the vial are in both direction i.e clockwise and

anti-clockwise direction. For one whole cycle, we can put small cycles. For examples if we put one cycle for 1 hour, we can put small cycle for 5 min movement and 30 Sec idle. After each small cycle, direction of the vial change, like if starting cycle is clockwise then next cycle is anticlockwise direction and like that. We can control milling time and milling speed with this equipment. We also controlled small cycle (5 min.) and ideal time (30 Sec) after each cycle. After each small cycle direction of rotation changed like from clockwise to anti-clockwise and vice-versa.

This equipment is suitable for homogeneous mixing of the powders, we put two jars (approx. one third filled) of powders and balls (made from Fe-Cr Steel). For MA, we mixed the powders in planetary ball milling equipment Retsch Pm 400/2 with two jars. Each jar should fill maximum one third with the ball and powders together. Weight of both jars should be equal approximately for balancing the rotating disk. We maintain the argon atmosphere inside the jars for minimizing the contamination problems. After finishing the milling cycle, it is needed to cool the jar for 45 minutes. Then after we opened the jar inside the chamber for minimizing the risk of fire. We extract the milling powders and done some test for analyzing the mixing quality of the alloy.

### **Granulometry analysis**

This test is suitable for determining granulometric characteristics of the mixed powders. This test is suitable for all mixed powders, but we mainly used for mechanical mixing powders. It provides mainly D(0.1), D (0.5) and D (0.9) values. D (0.1) signifies the diameter values which less than 10% values of entire lot of powders, D (0.5) signifies the diameter values of mixed powders is approximately 50% of the powders and D (0.9) signifies the diameter values of mixed powders is approximately 90% of the powders. D (0.5) values used the most due to it is approx. mean of all the powders lot value.

We put approx. 0.5 gram to the slot of granulometry and after each cycle of granulometric analysis, we need to clean properly to the entire slot with distilled water. The equipment for this test is Granulometry Malvern instruments Mastersizer 2000 dispersion unit AWM 2002 as shown in figure 3.13.



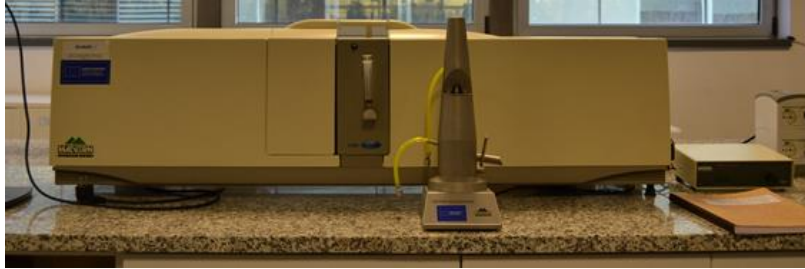


Figure 3.13: Malvern instruments Mastersizer 2000 dispersion unit AWM 2002.

### **Fluidity**

Method for determination of flow rate of free-flowing metal powders using the hall apparatus with MPIF standard 03.

Mixed powder was kept in the matrix.

### **3.2: Task 2: Mixing of powder with process control agent**

During literature survey most of the scientists used wax which maybe a cause of contamination for Ti alloy. Stearic acid was used as PCA during research. PCA was mixed with the Ti-15Mo-6Zr-2Fe the effects of grinding balls on the powders was analyzed. PCA was also used for controlling the heat generated during milling and timing was changed from (45 min, 52 min, 60 min-6 h, 24h) also shown in table 3.7. After 24h there was a generation of more heat inside the jar and Weld powders with each other, but on 6 h better result was observed, and microstructure was also more homogenous than without PCA. Effect of ball size i.e. 5 mm dia. and 10mm dia. was also observed. Effects of changing ball to powder ratio (BPR) from (10:1-15:1) were also visualized. Therefore, mechanical alloying provides a lot of possibility for more homogenized powders with different combination of parameters.

Table 3.7: Different combinations of milling time and milling speed with different ball size for MA technique (With PCA)

Alloy	Pressure	Milling condition
Ti-15Mo-6Zr-2Fe MA	900 MPa	6h-180 rpm (5 mm dia)
Ti-15Mo-6Zr-2Fe MA	900 MPa	6H-180 rpm (10 mm dia)
Ti-15Mo-6Zr-2Fe MA	900 MPa	24H-180 rpm (5 mm dia)

After mixing of the powder with PCA 1<sup>st</sup> we must calculate ratio of obtained powder weight after mixing and initial powder weight; by this we can see the powder loss.

We analyzed mixing powder granulometry, fluidity (explained in section 3.2.1) and geometrical test (like Archimedes' test), mechanical test (flexural test, micro hardness, elastic modulus) and microstructure according to section 3.1.

### **3.3: For obtaining full density samples with spark plasma sintering Method**

There is a possibility with mechanical alloying technique to found lots of porosity inside the sample, so for overcome this problem we can use some full density technique like spark plasma sintering (SPS).

One of the greatest challenges faced in powder metallurgy is identifying an appropriate sintering technique that can retain the developed microstructure while preventing or minimizing undesirable grain growth. Conventional sintering techniques usually lead to undesirable grain growth, reduced densification and loss of mechanical strength due to the long sintering time and high temperature required. Among the sintering processes that have been developed thus far, SPS is proofing to be effective in yielding fully dense metallic materials at relatively low temperatures and in very short sintering times. Such conditions are capable of preventing/reducing grain growth and minimizing the formation of undesired secondary phases that degrade the properties (Li *et al.*, 2015).

For preparation of Spark plasma sintering powder firstly produce powders mix with mechanical alloying technique with 180 rpm and 52 min and then sintered with SPS technique. During research, we explored with Ti-15Mo, Ti-15Mo-6Zr, Ti-15Mo-6Zr-2Fe, Ti-12Mo-6Zr-2Fe with different parameters which are listed in table 3.8.

Table 3.8: Processing parameters for SPS

Alloy	Temperature	Pressure	Time
Ti15Mo	1100°C, 1150°C,1200°C	50MPa	5 min
Ti15Mo6Zr	1100°C, 1150°C,1200°C		
Ti15Mo6Zr2Fe	1100°C, 1150°C,1200°C		
Ti12Mo6Zr2Fe	1200°C		

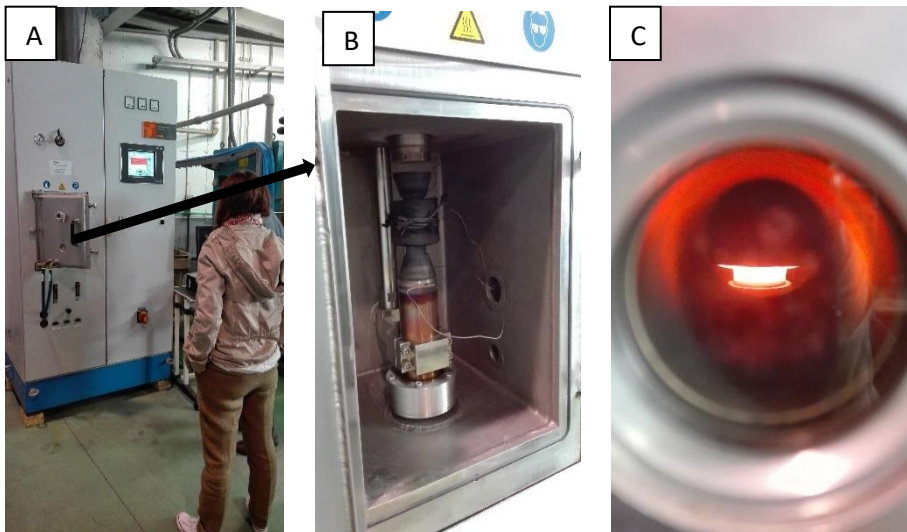


Figure 3.14: (A) FAST HP D 5/1 equipment (model S8451) from FCT (B) Setup for sintering with charcoal disk (C) Sample during sintering

The mechanical alloy has been made in a Retsch PM400 / 2 planetary mill at 180 rpm for 52 minutes and a dust / ball mass ratio 1/15. The sintering was carried out at 1100°C, 1150°C,1200°C for 5 min on a FAST HP D 5/1 equipment (model S8451) from FCT, obtaining sintered products with a diameter of 30 mm and a thickness of 5 mm. Disk for sintering is charcoal. This equipment is available in Tecnalia, San Sebastian, Spain; shown in figure 3.14.

### **3.4: Phase 4: for obtaining $I_{\text{corr}}$ , open circuit potential (OCP), Corrosion velocity, ion release rate by corrosion test**

A determining objective in the study of biomaterials is to check the behavior of these materials in a corrosive environment and determine their ability to release concentrations of harmful ions to the human body in working conditions.

#### **3.4.1: Ion Release Study:**

Regardless of their composition, all metal implants release different amounts of their components in the surrounding tissues where they have been inserted.

The samples will be prepared metallographically as explained above and the edges between resin and metal will be enameled to avoid penetration of the electrolyte into that opening, altering the test results. The test will consist of the complete immersion of the samples in a sealed bottle with 50mL of artificial saliva at 37 ° C in the 2000207 SELECTA stove for 730 hours. These test conditions simulate a real time of 20 years with a defined cycle of 3 brushings of 2 min a day. The electrolyte to be used will be artificial saliva with the modification of Fusayama.

After the specified time, the samples will be carefully cleaned with distilled water and stored in a desiccator for further microscopic analysis. On the other hand, the artificial saliva solution will be analyzed by the ICP-OES VARIANT-715ES plasma spectroscopy equipment located in the ITQ, with which the concentrations of the different titanium, molybdenum, zirconium and iron ions released during immersion will be recorded. The analyzes will be carried out in collaboration with the Institute of Chemical Technology of the UPV. The results of this study should be as representative and reliable as possible, so each triplicate test will be carried out for each alloy.

#### **3.4.2: Phase 2: Study of resistance against corrosion**

In this stage several electrochemical tests will be carried out that allow us to characterize the processes that occur when Ti-Mo alloys are in contact with physiological environments that can be corrosive and try to identify the influence of surface fusion to this behavior. The Ti-Mo alloy is widely used in biomedical

research today, so its behavior against corrosion in electrolytes such as NaCl or even artificial saliva is known. Not knowing to what extent, the properties of our samples are altered with superficial fusion in a corrosive environment like the buccal, it is interesting to study their behavior in artificial saliva at a controlled temperature (37 ° C).

The study will be carried out by means of a corrosion test with a three-electrode assembly, so that the sample will be the working electrode, the reference electrode will be Ag / AgCl, 3M KCl and the counter electrode will be platinum. The corrosion test will follow the routine proposed in Figure 3.15.



Figure 3.15. Scheme of the proposed routine for the study of resistance against corrosion.

#### TASK 1: Cathodic Cleaning

The first task of this stage will be the application of -1.1V for 5 minutes in order to activate the surface to be studied. First, within cathodic cleaning a potentiostatic test mode, a current range of 1mA was defined along with the order to save the signal obtained for 300s. This stage is performed simply to homogenize the tested surfaces and achieve more representative results. The tested area of each sample was 1cm in diameter, that is, 0.785cm<sup>2</sup>. Three electrodes were assembled: working electrode (sample), reference electrode (Ag / AgCl, 3MKCl) and counter electrode (platinum). When using the reference electrode Ag / AgCl with a potential of -0.205V with respect to the hydrogen electrode (SHE, Standard Hydrogen Electrode), all the potentials were registered with respect to said potential. The necessary parameters (applied potential, voltammetry, applied current, definition of the hardware configuration) that allow the subsequent calculation of the searched parameters  $E_{\text{corr}}$ ,  $I_{\text{corr}}$  and  $R_p$  were defined.

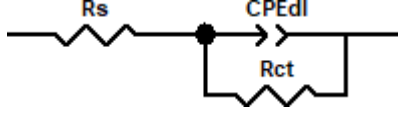
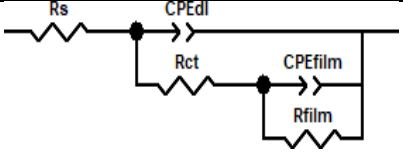
## TASK 2: Open Circuit Potential (OCP)

The determination of the open circuit potential allows us to know the surface state of the alloy studied, that is, the 'nobility' of the sample. It should be considered that the values obtained are completely dependent on the test conditions and can only be considered for comparison between the samples tested in this study. In this way, the value of the OCP will be obtained after the stabilization of the circuit potential without the passage of current for 30 minutes. Once the OCP curve is registered, the data we are looking for will be calculated using the average of the last 300 recorded values of the stabilized potential. The AUTOLAB AU51095 potentiostat was used together with the Nova 2.1.1 program to register and work with the test data. In this way, the potential in the absence of external current was recorded during 1800s, starting at - 1.1V from the previous step. The result is a potential vs. curve. time, of which the average value of the last 300 values recorded as the value of the OCP is used.

## TASK 3: Electrochemical Impedance Spectroscopy (EIS)

Next, the necessary parameters for the third step of the program were defined within the Frequency Response Analyzer (FRA) command to carry out the study of electrochemical impedance spectroscopy (EIS). Electrochemical impedance spectroscopy will quantify the response of the sample to a modulation at different frequencies of small amplitude sinusoidal potential. A frequency range of 104-0.005Hz with an amplitude of 0.01V was established. The results will be studied by a modelling software with which the necessary parameters that define the behavior of the interface between the metal and the electrolyte will be obtained.

Table 3.9: Chi-square values obtained for the adjustment of the electric models of compact layer and double porous layer.

Compact layer circuit		$\chi^2 = 200$
Porous double layer circuit		$\chi^2 = 10^{-3}$

The interpretation of the electrochemical behavior of the surface of the alloys is not simple, so it is necessary to consider an equivalent circuit that simulates the behavior against the corrosion test. The equivalent circuit that was proposed by Randles (Randles, 1947) has a great application in many electrochemical systems due to its simplicity (compact layer circuit). In this way, the data obtained in the impedance spectroscopy were analyzed with the Z View 2.0 software and they tried to adjust to the circuits of the table 3.9. In almost all samples, the diagram did not fit the results obtained, so it was necessary to test with other electrical circuits until it was found suitable for modeling the electrolytic behavior of the passive layers present in the alloys studied. In addition, it should be noted that the modification of the starting circuit was necessary since it could not really explain the electrolytic behavior of the material by modeling the passive layer as an ideal capacitor. Finally, the circuit that achieved a value of  $\chi^2$  less than  $10^{-3}$  was the electrical circuit that simulates a double porous layer, as will be explained in the subsequent results and discussion sections.

#### TASK 4: Linear Sweep Voltammetry (LSV, Linear Sweep Voltammetry)

The last task of the corrosion test routine consists of a linear scan voltammetry at  $0.0002\text{V} / \text{s}$ . This technique is a potential sweep through which the current density will be recorded based on the applied potential that increases linearly. Faraday's law dictates that the reaction rate is proportional to the density of current flowing through the electrode / electrolyte interface. The curve obtained from the current density as a function of the potential will provide information on the kinetic processes of the electrochemical reactions that occurred during the test (Landolt, 2007).

The current density ( $i$ ) corresponds to the sum of the partial anodic current density ( $i_a$ ) and the partial cathodic current density ( $i_c$ ). The concrete potential in which the total current changes from cathodic current to anodic current, is called corrosion potential ( $E_{\text{corr}}$ ). Thus, the corrosion current density ( $i_{\text{corr}}$ ) is the value of the current density when  $E_{\text{corr}}$  is obtained, and it is characterized in that the current density of both half-reactions is equivalent ( $i_a = i_c$ ), as shown in figure 3.15.



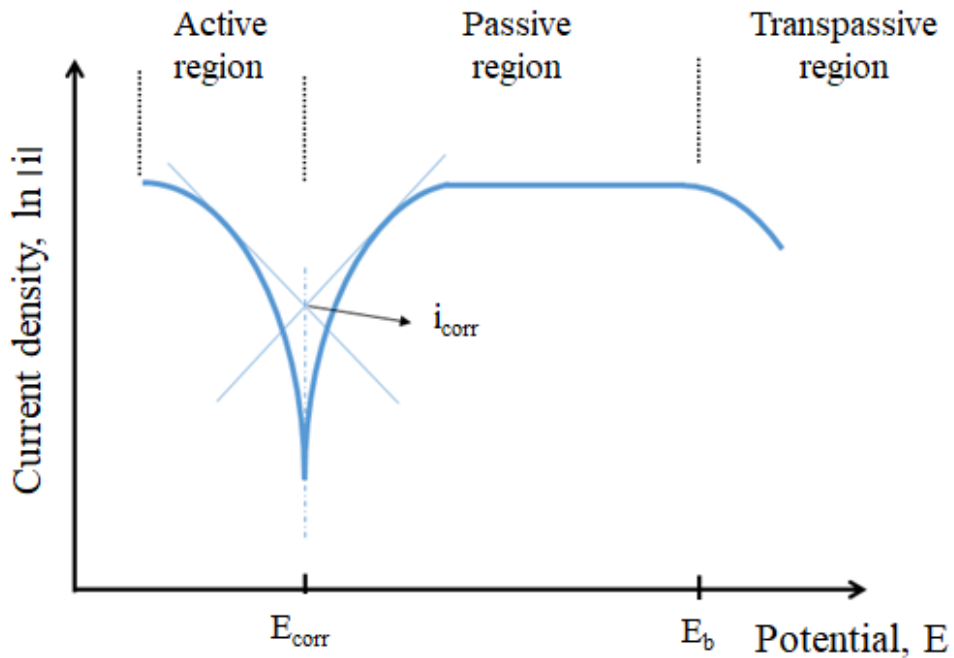


Figure 3.16: Scheme of a potention dynamic polarization curve.

The corrosion rate of a material is a very interesting parameter to compare the corrosion behavior of the different alloys studied. It is directly related to the corrosion current density, so the material loss ratio will finally be obtained following equation (3.1) and the template in table 3.10. We assume that the polarization curves of the alloys studied follow the Butler-Volmer equation, where the lines that intersect at the point  $(E_{\text{corr}}, i_{\text{corr}})$  of the representation of the logarithm of the current intensity versus the potential are the slopes of Tafel ( $\beta_a$  and  $\beta_c$ ).

$$v_c = \frac{i_{\text{corr}} \cdot M \cdot S}{\eta \cdot F \cdot \delta} \times 4.02 \times 10^{11} \quad (3.1)$$

Table 3.10: Template to illustrate the calculation of the corrosion rate

obtaining the corrosion speed, Vc (µm / year)	
$i_{corr}$	Corrosion current density obtained by Tafel
M	Atomic mass (g / mol) calculated through atomic% and weight Atomic of each element.
S	Exposed area (cm <sup>3</sup> ), in our case 0,785 cm <sup>2</sup>
n	Valence number of titanium (in our case it is 4)
F	Faraday constant, 96500 A s / mol
δ	Alloy Density (g / cm <sup>3</sup> )

Figure 3.16 shows the three regions that can be differentiated in a polarization curve: cathodic (active), anodic (passive) and transpassive region. The cathodic domain encompasses the potentials above  $E_{corr}$  and the current is defined by the reduction of water and dissolved oxygen. At potentials below the  $E_{corr}$  is the active region, characterized by the ionic dissolution of the metal in the medium. On the other hand, the passive domain is characterized by the appearance of an oxide film that determines the dissolution rate of the metal to a specific potential. Finally, the properties of the passive film change in the transpassive domain and an increase in dissolution rate is observed. The transpassivation potential  $E_b$  marks the end of the passive domain and the transition from the passive to the trans passive region.

$$R_p = \frac{\beta_a \beta_c}{2.3 I_{corr} (\beta_a + \beta_c)} \quad (3.2)$$

Table 3.11. Template to illustrate the calculation of polarization resistance

obtaining polarization resistance, $R_p$ ( $\Omega$ )
Anodic Tafel slope ( $\beta_a$ )
Earring of cathodic Tafel (V / A)
Corrosion Current Intensity (A)

Once the tests have been carried out and the potentiodynamic curves obtained, the values of the corrosion potential ( $E_{\text{corr}}$ ) and the corrosion current density ( $i_{\text{corr}}$ ) will be obtained. After this, the polarization resistance ( $R_p$ ) will be calculated using the mathematical ratio of equation 3.2, explained by the template in Table 3.11, and finally, an electrical model will be adjusted to try to understand the behavior of the metal / electrolyte. If the potentiodynamic curves allow it, it would be interesting to study other data such as passivation current density ( $i_p$ ) or the potential for breaking the passive layer ( $E_b$ ).

Development of new high-performance Titanium alloys with Fe-addition for dental implants

# Chapter 4: Results

In this chapter, different mechanical test, microstructural characterization produced by different method such as Elemental Blend (EB), Mechanical Alloying (MA) and Spark plasma sintering (SPS) method are summarized.

First, Ti-xMo (x=12 and 15 in weight %) binary alloys were obtained, followed by ternary alloys with 6%, in weight of Zr, and quaternary alloys of the type Ti-xMo-6Zr-yFe (where x=12 & 15 and y=1, 2, 3 & 4 in weight %). As mentioned before, the mixing of the alloys was performed by two different routes: EB and MA. After analysing the mechanical alloying samples, big porosity was found inside the samples. So, for overcome this problem we start working with one of the full density method spark plasma sintering (SPS).

This chapter is divided in mainly 4 parts:

- **Elemental blend (EB)**
- **Mechanical Alloying (MA)**
- **Spark plasma sintering (SPS)**
- **Corrosion test**

## 4.1. Elemental blend (EB)

It started working with EB powder processing technique with Ti-Mo binary, ternary and quaternary alloy.

### 4.1.1. Green Density (GD)

After compaction, first step is to analyse green density by which compaction quality of the alloy could be understood.

Green density signifies density of the samples after compaction or density of the green sample. Theoretical density, Green density and relative green density of Ti-12Mo, Ti-15Mo, Ti-12Mo-6Zr, Ti-15Mo-6Zr and Ti-12Mo-6Zr-xFe are tabulated in table 4.1. Theoretical density is calculated with stoichiometric relation

according to weight % of different powder elements present in the powder mix of the alloy. Green density is calculated with help of ratio of mass of green sample and volume of green samples and relative green density is calculated with ratio of green density and theoretical density. Lowest green density is calculated for Ti-12Mo-6Zr revealing powder packing for this alloy is lower comparatively than to other base alloys. From table 4.1; relative green density for all the alloy is near to 78%.

Table 4.1: Theoretical density, green density and relative green density of elemental blended samples

Alloys	Theoretical density (g/cm <sup>3</sup> )	Green density (g/cm <sup>3</sup> )	Relative green density (%)
Ti-12Mo	4.83	3.77 ± 0.02	78.00 ± 0.43
Ti-15Mo	4.92	3.84 ± 0.01	78.11 ± 0.19
Ti-12Mo-6Zr	4.93	3.82 ± 0.01	77.55 ± 0.16
Ti-15Mo-6Zr	5.02	3.90 ± 0.01	77.64 ± 0.30
Ti-12Mo-6Zr-1Fe	4.95	3.83 ± 0.01	77.42 ± 0.12
Ti-12Mo-6Zr-2Fe	4.98	3.86 ± 0.02	77.48 ± 0.34
Ti-12Mo-6Zr-3Fe	5.00	3.89 ± 0.01	77.70 ± 0.27
Ti-12Mo-6Zr-4Fe	5.02	3.90 ± 0.01	77.64 ± 0.13

**4.1.2. Porosity, Sintered Density and relative density:**

Porosity is mainly of two types (1) open porosity and (2) close porosity. Both type of porosity is calculated by Archimedes method Porosity. Sintering density is the most important parameter for the confirmation of the alloys for further analysis. It is calculated after sintering of the samples. It is the ratio of sintered mass with the sintered volume of the samples. Sintered density is calculated with Archimedes’ method during our experiment. Relative sintered density is the ratio of sintered density and theoretical density of each sample. Open porosity (%), close porosity (%), sintered density (kg/m<sup>3</sup>) and relative sintered density (%) of Ti-12Mo, Ti-15Mo, Ti-12Mo-6Zr, Ti-15Mo-6Zr and Ti-12Mo-6Zr-xFe (1250°C and 1300°C) are tabulated in table 4.2. Open porosity is minimum in case of Ti-12Mo-6Zr-1Fe sintered at 1250°C; which is 0.58% as shown in table 4.2 and maximum open porosity for Ti-12Mo-6Zr-3Fe sintered at 1300 °C, which is 1.36%. Close porosity is minimum in case of Ti-12Mo-6Zr-1Fe sintered at 1300 °C, which is 0.97% and maximum open porosity for Ti-15Mo sintered at 1250°C; which is 1.93%. Relative

sintered density is maximum for Ti-12Mo-6Zr-1Fe sintered at 1250°C which is 98.05 %; as shown in last column of the table 4.2. Total porosity is the addition of close porosity and open porosity, which is reciprocal of the sintered density.

Table 4.2: Theoretical density, close and open porosity, sintered density and relative green of elemental blended samples

Alloys	Temperature	Theoretical density (kg/m <sup>3</sup> )	Open porosity (%)	Close porosity (%)	sintered density (kg/m <sup>3</sup> )	Relative sintered density (%)
Ti-12Mo	1250°C	4.83	1.19	1.74	4.69 ± 0.03	97.07 ± 0.63
Ti-15Mo		4.92	1.19	1.93	4.77 ± 0.03	96.88 ± 0.70
Ti-12Mo-6Zr		4.93	0.90	1.13	4.83 ± 0.01	97.97 ± 0.29
Ti-15Mo-6Zr		5.02	1.53	1.18	4.89 ± 0.04	97.29 ± 0.82
Ti-12Mo-6Zr-1Fe		4.95	0.58	1.37	4.86 ± 0.02	98.05 ± 0.49
Ti-12Mo-6Zr-2Fe		4.98	0.94	1.44	4.86 ± 0.04	97.62 ± 0.73
Ti-12Mo-6Zr-3Fe		5.00	0.62	1.67	4.89 ± 0.03	97.70 ± 0.56
Ti-12Mo-6Zr-4Fe		5.02	0.71	1.89	4.89 ± 0.02	97.40 ± 0.39
Ti-12Mo-6Zr-1Fe	1300 °C	4.95	1.12	0.97	4.85 ± 0.03	97.91 ± 0.62
Ti-12Mo-6Zr-2Fe		4.98	1.11	1.23	4.86 ± 0.02	97.66 ± 0.43
Ti-12Mo-6Zr-3Fe		5.00	1.36	1.35	4.86 ± 0.03	97.29 ± 0.64
Ti-12Mo-6Zr-4Fe		5.02	1.26	1.42	4.89 ± 0.06	97.32 ± 1.10

#### 4.1.3. Shrinkage calculation

Shrinkage is the reduction of dimension of any material either it is solid or plastic. There are three types of shrinkage (1) volumetric shrinkage (%) (2) Bulk shrinkage (%) and (3) Linear shrinkage (%). Volumetric shrinkage is calculated by the dimension loss after sintering, means contraction after compaction to sintering. Average value for volumetric shrinkage is 19.50 % for alloys Ti-12Mo, Ti-15Mo, Ti-12Mo-6Zr, Ti-15Mo-6Zr and Ti-12Mo-6Zr-xFe as seen in table 4.3. Bulk

shrinkage is the dimension loss with the area either length and width wise or length and thickness wise or width and thickness wise. For our case we calculated with length and width wise. On average bulk shrinkage is approximately 14 % (little bit less than 14). Maximum bulk shrinkage is for Ti-12Mo-6Zr-2Fe which is 13.87 with deviation 0.16. Linear shrinkage is the unit dimensional loss with length, width or thickness; here we calculated with length dimension loss. Linear shrinkage is less in case of binary and ternary alloys in comparison with quaternary alloys. Maximum linear shrinkage is for Ti-12Mo-6Zr-2Fe which is 7.74 with deviation 0.13. All the values are quite similar irrespective of the alloys.

Note: Deviation is calculated with 5 samples for each alloy.

Table 4.3: Volumetric shrinkage (%), Bulk shrinkage (%) and linear shrinkage (%) of elemental blended samples

alloys	Volumetric shrinkage (%)	Bulk Shrinkage (%)	Linear Shrinkage (%)
Ti-12Mo	18.57 ± 0.63	13.74 ± 0.35	6.67 ± 0.26
Ti-15Mo	18.51 ± 0.34	13.71 ± 0.33	6.62 ± 0.21
Ti-12Mo-6Zr	19.50 ± 0.21	13.64 ± 0.25	6.56 ± 0.14
Ti-15Mo-6Zr	19.38 ± 0.35	13.63 ± 0.24	6.53 ± 0.14
Ti-12Mo-6Zr-1Fe	19.10 ± 0.63	13.84 ± 0.14	7.71 ± 0.14
Ti-12Mo-6Zr-2Fe	19.07 ± 0.53	13.87 ± 0.16	7.74 ± 0.13
Ti-12Mo-6Zr-3Fe	18.97 ± 0.34	13.83 ± 0.10	7.69 ± 0.13
Ti-12Mo-6Zr-4Fe	18.84 ± 0.14	13.60 ± 0.07	7.62 ± 0.10

#### 4.1.4. Bending strength (MPa), Toughness (J) and elongation (%) of sintered samples

Flexural strength, also known as modulus of rupture, or bend strength, or transverse rupture strength is a material property, defined as the stress in a material just before it yields in a flexure test.

Bending strength of different Ti-Mo alloys are shown in table 4.4, Bending strength for Ti-15Mo is higher which is approx. (2161 MPa), but this is much higher, for biomedical applications (650-850 MPa). But higher strength is not a big problem;



even it is better for long term implant. From the table 5.4, addition of Zr reduced the bending strength.

Bending strength of Ti-12Mo-6Zr-xFe alloys with 1250°C and 1300°C are also shown in table 5.4. Increase of % of Fe reduced the value of bending strength i.e. value for Ti-12Mo-6Zr-1Fe is highest and Ti-12Mo-6Zr-4Fe is lowest among quaternary alloys. With increase in temperature from 1250°C to 1300°C the increment in strength found for Ti-12Mo-6Zr-1Fe and for Ti-12Mo-6Zr-2Fe as shown in table 4.4 and vice versa for Ti-12Mo-6Zr-3Fe and Ti-12Mo-6Zr-4Fe.

Bending strength decreases from 2023 MPa (for Ti-15Mo) to 766 MPa (for Ti-15Mo-6Zr-4Fe) approximately 62% decrement. In all the alloys listed in the table 4.4; it is clearly shown that addition of Zr and Mo reduces bending strength.

Toughness is energy involved in breaking samples during bending test. The value is maximum for Ti-12Mo which value is 50.37 J and the lowest value is for Ti-12Mo-6Zr-4Fe (sintered at 1300°C) which value is 6.05J which is approx. 90% less than Ti-12Mo. Normally from the table, it is clear that increment of % of Fe decreases the value of tenacity.

Elongation is maximum in case of Ti-12Mo-6Zr which is 5.95% (sintered at 1300 °C) and least for Ti-12Mo-6Zr-4Fe which value is 2.42%, which is approx. 60% less than Ti-12Mo-6Zr.

Note: Standard deviation calculated with 5 samples for each test.

Table 4.4: Bending strength (MPa), Toughness (J) and Elongation (%) of elemental blended samples

Alloys	Temperature	Bending Strength (MPa)	Toughness (J)	Elongation (%)
Ti-12Mo	1250°C	2023 ±107	50.37 ± 10.36	5.67 ± 0.96
Ti-15Mo		2161 ± 28	48.52 ± 2.37	5.28 ± 0.40
Ti-12Mo-6Zr		1932 ±106	36.59 ± 5.03	5.95 ± 0.13
Ti-15Mo-6Zr		1659 ±131	26.07 ± 4.48	4.27 ± 0.34
Ti-12Mo-6Zr-1Fe		1521 ± 71	23.31 ± 2.13	4.60 ± 0.28
Ti-12Mo-6Zr-2Fe		1195 ± 71	14.90 ± 1.80	3.96 ± 0.25
Ti-12Mo-6Zr-3Fe		971 ± 88	10.28 ± 1.70	3.34 ± 0.21
Ti-12Mo-6Zr-4Fe		766 ± 87	7.13 ± 1.65	2.70 ± 0.30
Ti-12Mo-6Zr-1Fe	1300°C	1725 ±134	32.53 ± 5.52	4.86 ± 0.36
Ti-12Mo-6Zr-2Fe		1390 ± 46	20.43 ± 1.24	4.34 ± 0.12
Ti-12Mo-6Zr-3Fe		929 ± 55	9.79 ± 0.85	3.12 ± 0.30
Ti-12Mo-6Zr-4Fe		666 ± 114	6.05 ± 1.35	2.42 ± 0.28

**4.1.5. Elastic modulus  $E_U$  (GPa), Poisson’s coefficient and hardness (HV) of sintered samples**

Table 4.5 denotes the values of elastic modulus of elemental blend samples, Poisson’s coefficient during elastic modulus testing which is denoted as  $\nu$  and hardness of the samples which is tabulated in column 1, column 2 and column 3 of the table 5.5 respectively. Elastic modulus is the main property for the biomedical applications which should be less like approx. 28-35 GPa.

Table 4.5: Elastic modulus ( $E_U$ ), Poisson's coefficient and Hardness of elemental blended samples

Alloys	Temperature	$E_U$ (GPa)	$\nu$	Hardness (HV)
Ti-12Mo	1250°C	$104.89 \pm 1.38$	$0.33 \pm 0.0033$	$283 \pm 28$
Ti-15Mo		$103.84 \pm 0.82$	$0.33 \pm 0.0018$	$309 \pm 19$
Ti-12Mo-6Zr		$102.90 \pm 0.86$	$0.34 \pm 0.0019$	$309 \pm 30$
Ti-15Mo-6Zr		$98.55 \pm 0.83$	$0.34 \pm 0.0017$	$322 \pm 29$
Ti-12Mo-6Zr-1Fe		$103.58 \pm 0.81$	$0.33 \pm 0.0009$	$542 \pm 12$
Ti-12Mo-6Zr-2Fe		$100.70 \pm 1.31$	$0.33 \pm 0.0025$	$512 \pm 36$
Ti-12Mo-6Zr-3Fe		$95.23 \pm 0.60$	$0.34 \pm 0.0031$	$493 \pm 19$
Ti-12Mo-6Zr-4Fe		$96.85 \pm 0.58$	$0.34 \pm 0.0007$	$467 \pm 23$
Ti-12Mo-6Zr-1Fe	1300°C	$103.69 \pm 0.76$	$0.33 \pm 0.0020$	$500 \pm 26$
Ti-12Mo-6Zr-2Fe		$102.74 \pm 0.33$	$0.33 \pm 0.0013$	$499 \pm 29$
Ti-12Mo-6Zr-3Fe		$95.00 \pm 1.42$	$0.33 \pm 0.0031$	$472 \pm 26$
Ti-12Mo-6Zr-4Fe		$97.62 \pm 0.99$	$0.33 \pm 0.0007$	$451 \pm 27$

Maximum value of elastic modulus for Ti-12Mo which is 104.89 (approx. 105 GPa) and minimum value is for Ti-12Mo-6Zr-3Fe with 1300°C which is 95 GPa which is 9.5% less than Ti-12Mo which is better for biomaterial application. Poisson's coefficient is for all alloys listed above is either 0.33 or 0.34.

From the hardness column it is shown that hardness is increasing after addition of Zr and Fe. % increase in hardness is much higher than Ti-Mo binary alloy. Minimum hardness value is for Ti-12Mo which is 283 HV and maximum is for Ti-12Mo-6Zr-1Fe at 1250°C sintering temperature which is 542 HV. Value of hardness for Ti-12Mo is approx. 48% less than Ti-12Mo-6Zr-1Fe.

So, combination of less elastic modulus and higher hardness is found in case of quaternary alloys as shown in table 4.5 which is better for biomaterial applications.

#### **4.1.6. Surface fracture characterization**

##### **4.1.6.1. Ti-Mo base alloy sintered at 1250 °C**

From the figure 4.1(A), it is confirmed that there is formation of dimple which shows its ductile character but in figure 4.1(D) more brittle surface are seen.

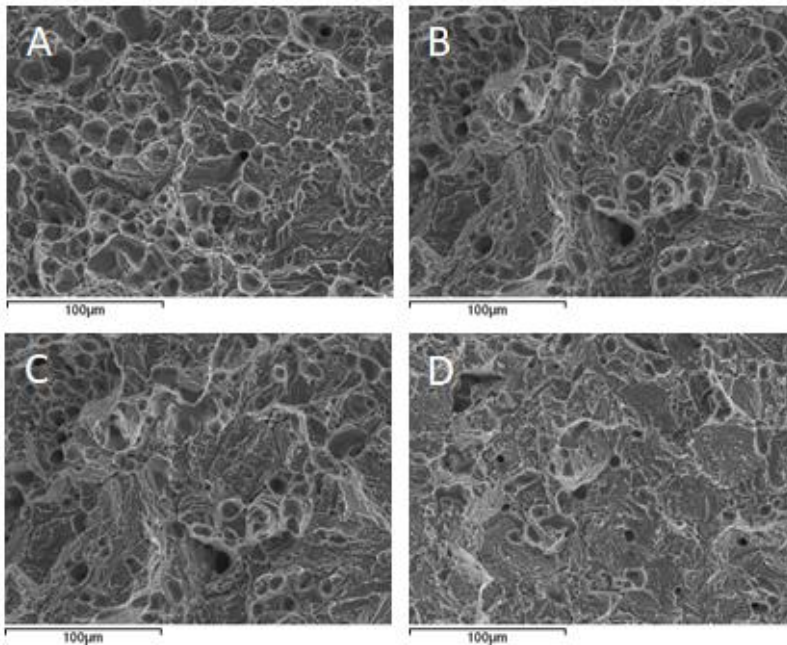


Figure 4.1: Fractography analysis of A) Ti-12Mo B) Ti-15Mo C) Ti-12Mo-6Zr (D) Ti-15Mo-6Zr with 500x magnification

It is seen the fracture is of mixed type like brittle and ductile for all the alloys. Brittleness is more in case of Ti-15Mo-6Zr which is clearly shown in figure 4.1 (D).

#### 4.1.6.2. Fractography analysis of Ti-Mo-Zr-Fe quaternary alloys sintered at 1250 °C

From figure 4.2 (B) it is clearly shown that nature of fracture surface of Ti-12Mo-6Zr-2Fe is mixed type (brittle and ductile) and when % of Fe increases brittle nature of alloy increases shown in 4.2 (C) and (D). as it can be seen easily that Ti-12Mo-6Zr-4Fe is a brittle alloy among the quaternary alloys.

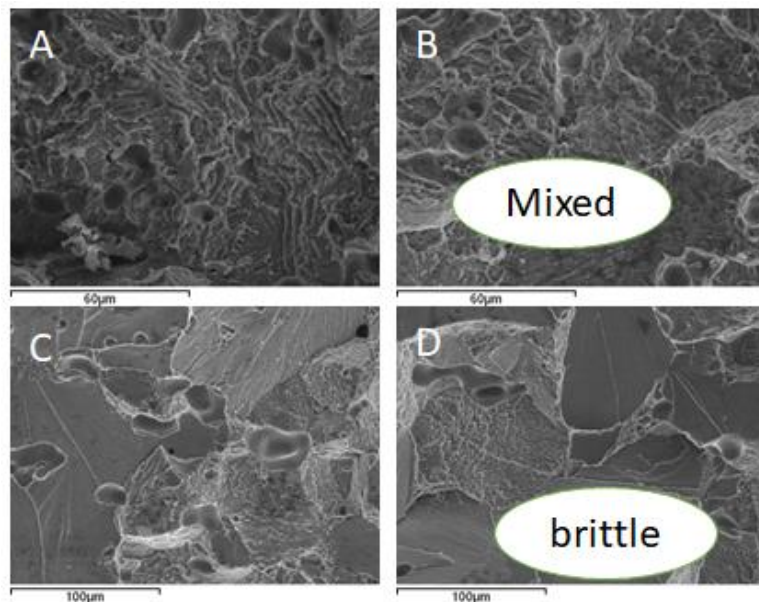


Figure 4.2: Fractography analysis of (A) Ti-12Mo-6Zr-1Fe B) Ti-12Mo-6Zr-2Fe with magnification 250x and (C) Ti-12Mo-6Zr-3Fe (D) Ti-12Mo-6Zr-4Fe with 500x magnification

#### 4.1.7. Grain size analysis:

Grain size of Ti-12Mo, Ti-12Mo-6Zr and Ti-12Mo-6Zr-xFe at 1250°C are shown in table 4.6.

Table 4.6: Grain Size Analysis of Ti-Mo alloy sintered at 1250 °C

Alloys	Grain Size (µm)	SD
Ti-12Mo	68	9
Ti-12Mo-6Zr	61	5
Ti-12Mo-6Zr-1Fe	60	16
Ti-12Mo-6Zr-2Fe	80	15
Ti-12Mo-6Zr-3Fe	73	4
Ti-12Mo-6Zr-4Fe	81	5

Maximum grain size is calculated for Ti-12Mo-6Zr-4Fe and lowest grain size is for Ti-12Mo-6Zr-1Fe. But normally with addition of Fe, grain size is increased, which is confirmed by table 4.6.

Grain size of Ti-12Mo is more than Ti-12Mo-6Zr and Ti-12Mo-6Zr-1Fe but lesser than Ti-12Mo-6Zr-2Fe, Ti-12Mo-6Zr-3Fe and Ti-12Mo-6Zr-4Fe; which is clearly shown in figure 4.4.

Lower grain size after mixing is better for further use and it's recommended by the metallurgist so in our alloy Ti-12Mo-6Zr-1Fe is better option and maximum grain size is for Ti-12Mo-6Zr-4Fe, which is approx. 35% more in comparison to grain size of Ti-12Mo-6Zr-1Fe.

#### **4.1.8. Microstructure characterization**

##### **4.1.8.1. Ti-Mo base alloys sintered at 1250 °C**

Microstructure of Ti-12Mo, Ti-15Mo, Ti-12Mo-6Zr and Ti-15Mo-6Zr are shown in figure 4.3, where one can see that grains are of mixed type, as some are very large, and some grains are small. Grain boundaries are clearly shown in microstructure images and there is some black spot found which is porosity found in the sample.

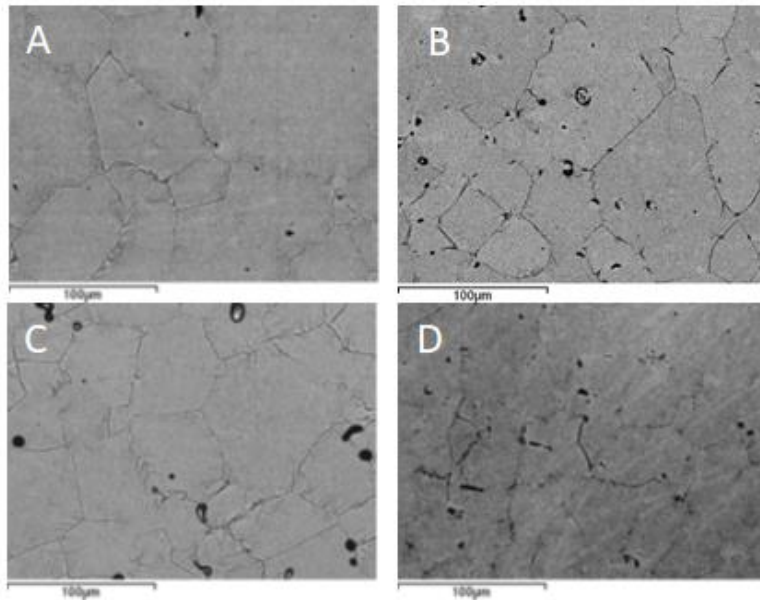


Figure 4.3: Microstructure of Ti-Mo base alloy with magnification 500X BS (a) Ti-12Mo (b)Ti-15Mo (c) Ti-12Mo-6Zr (d)Ti-15Mo-6Zr

Elemental composition of different Ti-Mo binary alloys was obtained by EDS analysis, which is tabulated in table 4.7 by which we can confirm that mixing of the element is homogeneous as the element mixing % before sintering and after sintering is almost same which is clearly shown in table 4.7.

Table 4.7: Elemental Composition calculated by smart map analysis

Alloys	Ti (% w/w)	Mo (% w/w)	Zr (% w/w)
Ti-12Mo	$87.10 \pm 0.18$	$12.90 \pm 0.12$	N/A
Ti-12Mo-6Zr	$80.73 \pm 0.13$	$12.84 \pm 0.42$	$6.43 \pm 0.15$
Ti-15Mo	$85.23 \pm 0.21$	$14.77 \pm 0.01$	N/A
Ti-15Mo-6Zr	$77.22 \pm 0.18$	$16.35 \pm 0.23$	$6.43 \pm 0.02$

#### 4.1.8.2. Microstructure analysis of Ti-Mo-Zr-Fe Quaternary alloys sintered at 1250°C

Microstructure of Ti-12Mo-6Zr-xFe (x=1, 2, 3, 4) are shown in figure 5.4. Grains are irregular which means some grains are large and some small which clearly shown in figure 4.4 (A) and 4.4 (B), some smaller and bigger porosity are also found which is shown in figure 4.4 (C) and 4.4 (D).

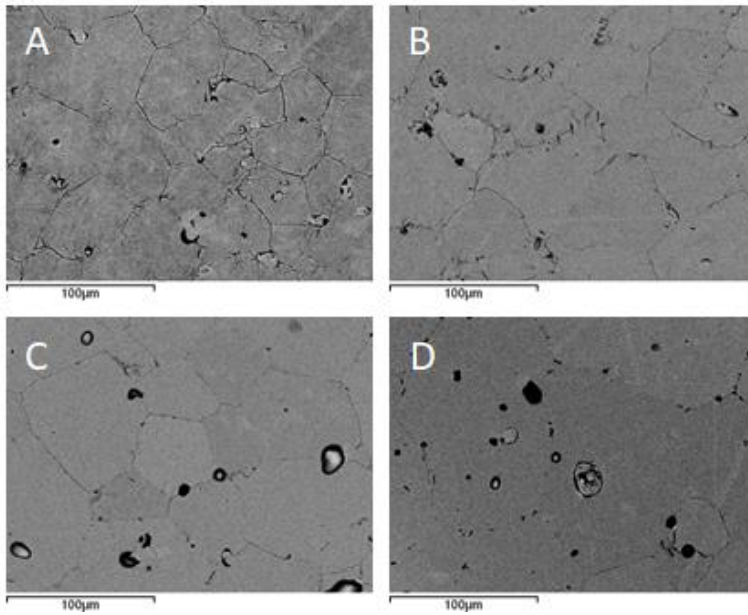


Figure 4.4: Microstructure of Ti-Mo quaternary alloy with magnification 500X BS (A) Ti-12Mo-6Zr-1Fe (B) Ti-12Mo-6Zr-2Fe (C) Ti-12Mo-6Zr-3Fe (D) Ti-12Mo-6Zr-4Fe at 1250°C

Porosity found for Ti-12Mo-6Zr-3Fe and Ti-12Mo-6Zr-4Fe are of both types i.e. open porosity and close porosity which is clearly shown in figure 4.4 (C) and (D).

#### **4.1.8.3. EDS analysis of Ti-12Mo-6Zr-2Fe**

From figure 4.5, it is seen that mixing of elements inside Ti-12Mo-6Zr-2Fe are not homogenous. It may be due to lack of diffusion.



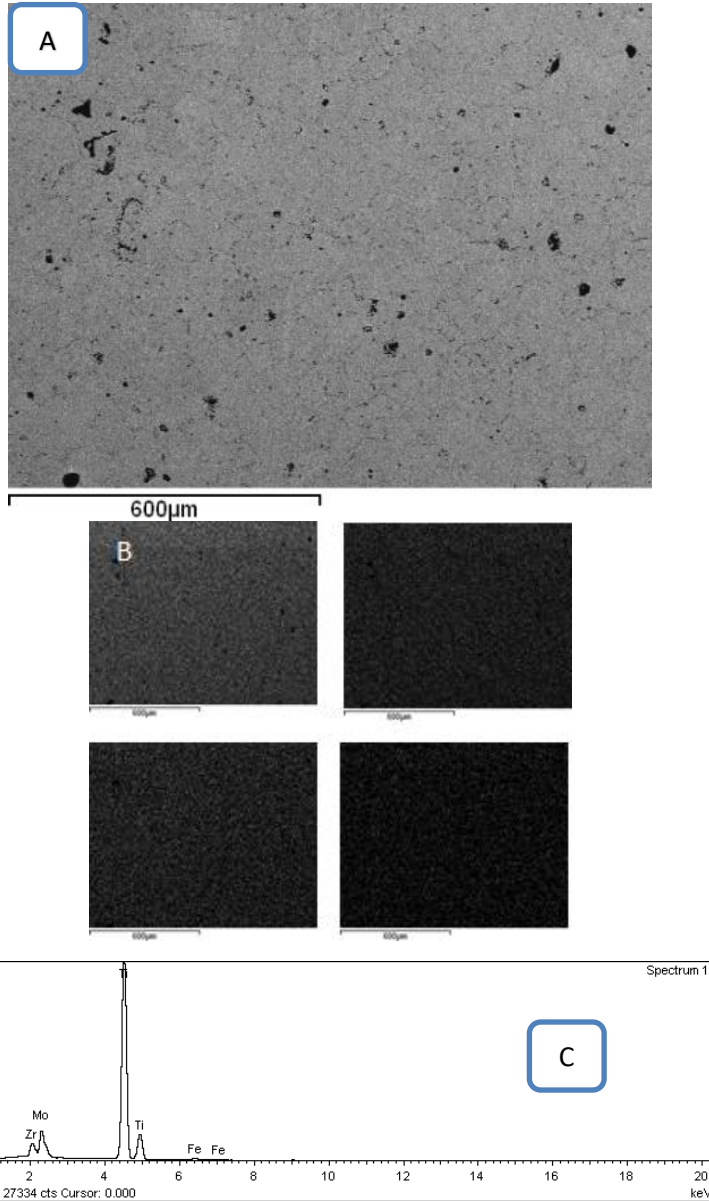


Figure 4.5: Smart map analysis of Ti-12Mo-6Zr-2Fe with 500x BS (A) General mixing of the alloying element (B) map of Ti , Mo K , Zr L and Fe K elemental mixing and (C) Spectrum obtained with EDS analysis

Elemental composition of different Ti-12Mo-6Zr-xFe (x=1, 2, 3, 4) are calculated by smart map analysis with SEM images which is shown in table 4.8. We can easily quantify the percentage of different elements like Ti, Mo, Zr and Fe after sintering of samples in different quaternary alloys. From the spectrum, it is clearly seen that the curve of Ti is very high and other elements also appeared like Mo, Zr and Fe.

Table 4.8: Elemental Composition calculated by smart map analysis of Ti-12Mo-6Zr-XFe.

Alloys	Ti (%w/w)	Mo (%w/w)	Zr (%w/w)	Fe (%w/w)
Ti-12Mo-6Zr-1Fe	79.68±0.18	12.89±0.07	6.49±0.08	0.94±0.02
Ti-12Mo-6Zr-2Fe	78.96±0.48	12.75±0.42	6.33±0.13	1.95±0.06
Ti-12Mo-6Zr-3Fe	77.70±0.21	13.04±0.01	6.43±0.12	2.84±0.08
Ti-12Mo-6Zr-4Fe	76.47±0.18	13.18±0.23	6.46±0.02	3.9±0.04

From the EDS analysis it is clearly shown that the composition after mixing is approx. same as the starting composition of the mixing. For example, Ti-12Mo-6Zr-1Fe have 79.68% of Ti (Starting 81% approx.), Mo is 12.89 % after sintering (Starting 12%) and so on.

#### **4.1.9: XRD Analysis**

XRD analysis are shown in figure 4.6 which indicates the peaks of  $\alpha$  and  $\beta$  and by this we can also calculate the % of both the phases.  $\alpha$ -phase are denoted by blue line and  $\beta$ -phase are denoted by red line.

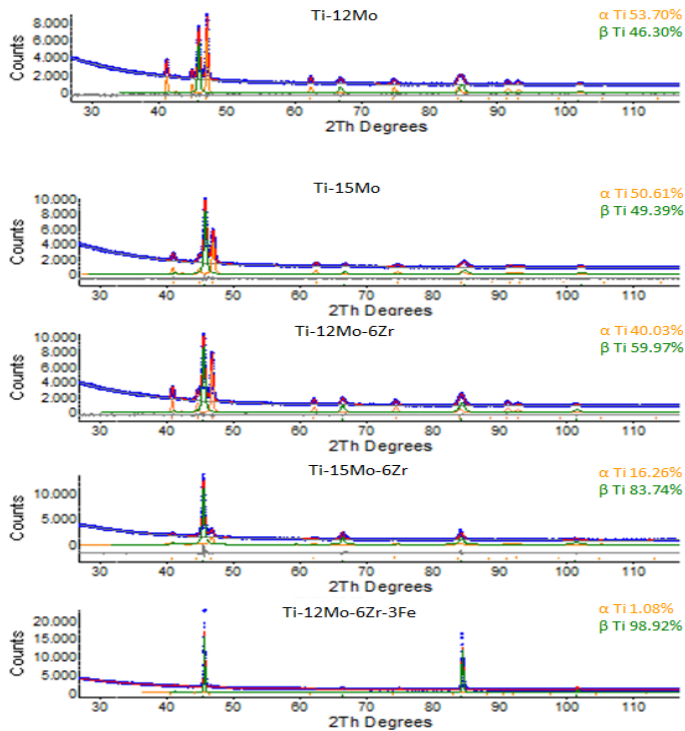


Figure 4.6: Phase analysis by XRD analysis of Ti-Mo alloys sintered at 1250°C

In table 4.9 we summarized the % of both the phases calculated with XRD analysis by which we can see that addition of more % of Mo enhances % of  $\beta$ -phase, addition of Zr also increases the % of  $\beta$  phase as Ti-12Mo-6Zr has 49.39% of  $\beta$  in comparison to Ti-12Mo and also addition of Fe improves  $\beta$ -phase as for Ti-12Mo-6Zr-3Fe % of  $\beta$  phase is 98.92% which is near to 100%.

Table 4.9: Phase analysis by XRD analysis sintered at 1250 °C

Alloy	$\alpha$ -phase	$\beta$ -phase
Ti-12Mo	53.7	46.3
Ti-12Mo-6Zr	40.03	59.97
Ti-15Mo	50.61	49.39
Ti-15Mo-6Zr	16.26	83.74
Ti-12Mo-6Zr-3Fe	1.08	98.92

Ti-12Mo have approx. both  $\alpha$ -phase and  $\beta$ -phase almost equal which is clearly tabulated in table 4.9 and addition of Zr improves  $\beta$ -phase stability as we can see for Ti-12Mo-6Zr and same in case of Ti-15Mo-6Zr. When we add Fe to Ti-12Mo-6Zr  $\beta$ -phase stability improves more and it tends to approx. 100%  $\beta$ -phase as we can see in table 4.9.

#### 4.1.10: EBSD analysis

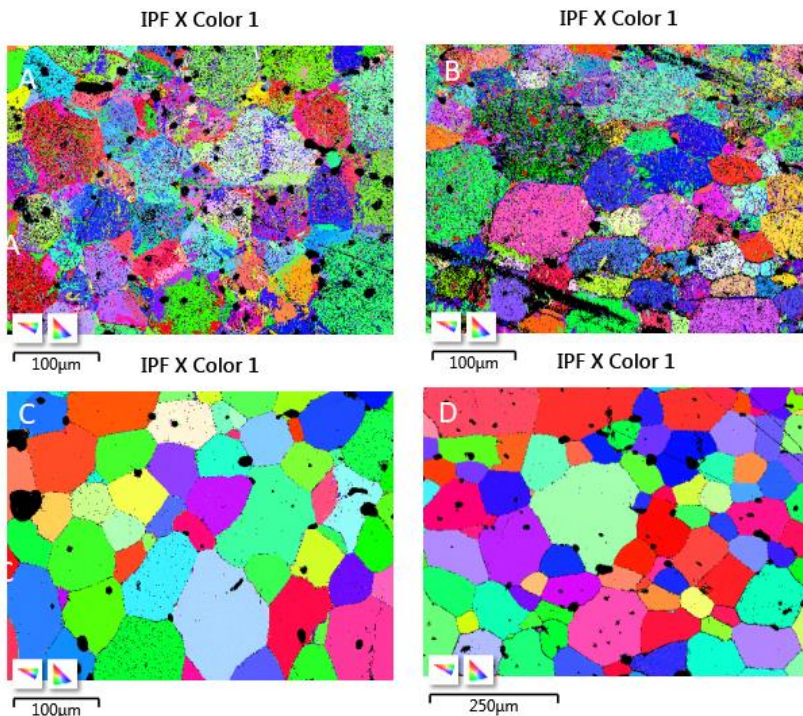


Figure 4.7: IPF X mixed image by EBSD analysis of (A) Ti-12Mo (B) Ti-12Mo-6Zr (C) Ti-12Mo-6Zr-3Fe at 1250°C (D) Ti-12Mo-6Zr-3Fe at 1300 °C

Structure of Ti-12Mo-6Zr-3Fe at both temperatures have more regular grain structure; but found porosity which is black colour in figure 5.7 (C) and (D).

Phase fraction with EBSD analysis, is summarized in table 4.10; by which we can see the % of both phase  $\alpha$  and  $\beta$  without zero solution. Zero solution includes dirt and porosity.

Figure 4.7 shows the IPF X colour of different alloys like Ti-12Mo, Ti-12Mo-6Zr, Ti-12Mo-6Zr-3Fe at 1250°C, Ti-12Mo-6Zr-3Fe at 1300 °C which shows the grain structure of the alloys. There are difficulties in preparation of samples, due to lots of dirt appeared in the structure. % of  $\beta$  for Ti-12Mo-6Zr-3Fe with both temperatures is approx. 100%, which signifies that addition of Fe increases the % of  $\beta$ .

Table 4.10: Phase fraction for different alloys with EB

Alloys	% Ti $\alpha$	% Ti $\beta$	% Ti $\beta$ with XRD
Ti-12Mo	41.25	58.75	46.3
Ti-12Mo-6Zr	29.75	70.25	59.97
Ti-12Mo-6Zr-3Fe @ 1250°C	0.96	99.04	98.92
Ti-12Mo-6Zr-3Fe @ 1300°C	0.24	99.76	NA

## 4.2. Mechanical Alloying (MA):

We have work with MA for better homogeneity and for this we have to explore with different combination of parameters for betterment of our alloys.

### 4.2.1: MA for Ti-12Mo-6Zr-2Fe with different compaction pressure

#### 4.2.1.1. Mechanical properties with short milling time

Total porosity is found by Archimedes's test. In table 5.11, relative sintered density by mechanical alloying (MA) at 600 MPa is less than 900MPa. This is starting of the compaction pressure with 600 MPa and then for improvement the mechanical properties we have to increase the compaction pressure to 900 MPa for further analysis. When total porosity is very high in case of 600 MPa , it results in reducing the total porosity and increasing compaction pressure 50%. When compaction pressure increases from 600 MPa to 900 MPa for MA method, in this case porosity decreases 6% approx. Total porosity also affects the strength, if total porosity is high than strength is less and vice versa.

Table 4.11 Relative density of Ti-12Mo-6Zr-2Fe with different conditions

Alloy	Relative sintered Density	Flexural strength (MPa)
Ti-12Mo-6Zr-2Fe MA @ 600 MPa	84.17 ± 0.82	329 ± 7
Ti-12Mo-6Zr-2Fe MA @ 900 MPa	89.83 ± 0.43	637 ± 13

An increase in compaction pressure (from 600 MPa to 900 MPa) also enhances the bending strength from 329 MPa to 637 MPa (approx 95%) , which is denoted in table 4.11.

Elastic modulus is the main mechanical property for designing biomaterials. Table 4.12 shows the elastic modulus found by Ultrasonic test of Ti-12Mo-6Zr-2Fe with MA at 600 MPa and 900 MPa compaction pressure. Modulus of elasticity is determined with MA at 600 MPa giving least value and better option as biomaterial.

Table 4.12 Elastic modulus of Ti-12Mo-6Zr-2Fe with different conditions

Alloys	Avg. E(Gpa)	Avg.v
Ti-12Mo-6Zr-2Fe MA @600 MPa	66.34±10.00	0.300±0.042
Ti-12Mo-6Zr-2Fe MA @900 MPa	81.98±2.43	0.320±0.011

#### 4.2.1.2. Fractography analysis

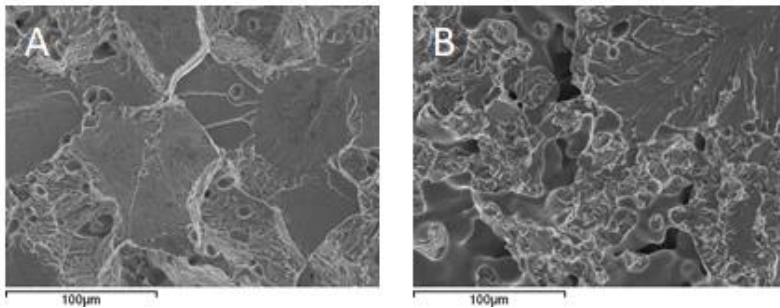


Figure.4.8: Fractography image of Ti-12Mo-6Zr-2Fe (A) with MA method under 900 MPa compaction pressure (B) with EB method under 600 MPa compaction pressure

Fracture surface with EB have more ductile nature in comparison to MA which is clearly shown in figure 4.8. Figure 4.8 (A) have brittle surface and 4.8 (B) have dimple formation, which shows ductile character for EB alloys.

#### 4.2.1.3. Micro-Structural analysis

From the figure 4.9, it is seen that the microstructure of Ti-12Mo-6Zr-2Fe prepared by MA method at 600 MPa, bigger porosity appears due to plastic deformation occurs in MA. While increasing pressure for MA method, then pore size gets decreased, but number of grain boundary upturns.

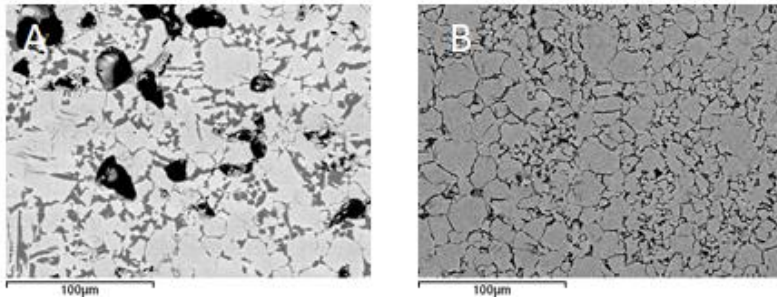


Figure 4.9: Microstructure of Ti-12Mo-6Zr-2Fe: Mechanical alloying method with (A) 600 MPa compaction pressure and (B) with 900 MPa compaction pressure

The porosity of the samples and the percentage of phases were obtained from images taken by optical microscopy using an image analysis program (See Table 4.13). EB samples show less porosity than MA samples. It is shown that MA with 900 MPa have less internal porosity and more  $\beta$ -phase in comparison to sample prepared with 600 MPa.

Table 4.13: Phase distribution and internal porosity

Process	Alloy	% Internal Porosity	<u>Phases Distribution by XRD</u>	
			% Alpha	% Beta
MA_600 MPa	Ti-12Mo-6Zr-2Fe	21.43 $\pm$ 3.38	24.13 $\pm$ 2.29	75.87 $\pm$ 2.29
MA_900 MPa	Ti-12Mo-6Zr-2Fe	9.86 $\pm$ 2.61	16.17 $\pm$ 1.81	83.83 $\pm$ 1.81

#### 4.2.1.4. EBSD analysis of Ti-12Mo-6Zr-2Fe with MA at 900 MPa

Figure 4.10 shows the IPF X and phase color of Ti-12Mo-6Zr-2Fe with MA at 900 MPa, due to more porosity and dirt; grain boundary is not visible.

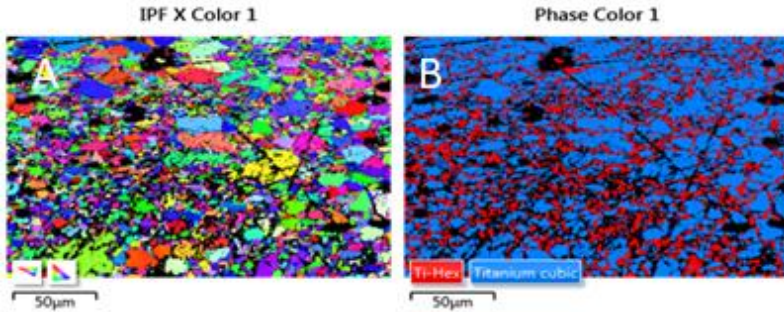


Figure 4.10: (A) IPF X color image and (B) phase color of Ti-12Mo-6Zr-2Fe with MA at 900 MPa

Table 4.14: Phases analysis with EBSD for Ti-12Mo-6Zr-2Fe with MA at 900 MPa

Phase Name	Phase Fraction (%)
$\alpha$ -Ti	21.23
$\beta$ -Ti	50.14
Zero Solutions	28.63

#### 4.2.2. MA with short milling time

This stage is for betterment or improvement of the property than before. Different parameters (exploring different milling speed and different milling time) are explored. One binary alloy and quaternary alloy (Ti-15Mo and Ti-15Mo-6Zr-2Fe) are chosen. For Mechanical Alloying, it is intended to know powder characteristics after mixing like fluidity, granulometric analysis and powder cut.

##### 4.2.2.1. Fluidity test:

Fluidity test results for Ti-Mo alloy with different combinations of milling speed and milling time are listed in table 4.15, where one can see fluidity with milling speed 180 RPM and milling time 52 min. for Ti-15Mo are highest in all the combination and for Ti-15Mo-6Zr-2Fe also too.



Table 4.15: Fluidity (For Ti-15Mo and Ti-15Mo-6Zr-2Fe) with different milling condition

Alloy	rpm- Time (min)	Powder Wt (gr)	Time for Fluid meter (S)	Fluidity
Ti-15Mo	300_45	23.701	21	1.13
	300_37	21.219	19	1.12
	300_52	21.957	20	1.10
	240_45	17.275	16	1.08
	180_45	23.814		Not possible
	180_52	24.616	21	1.17
	240_52	21.499	21	1.02
	180_60	24.427	4.5(with bigger one)	5.43
	Ti-15Mo-6Zr-2Fe	180_45	23.492	
180_52		24.112	19	1.27
210_45		23.982		Not possible

These binary alloy and quaternary alloy with different milling speed and milling time are explored. Fluidity is determined with fluid meter. The best flow of powder is for 240 rpm -52 min for both alloys. Some powder is very sticky like elemental blend powders (like powders with 180 rpm- 45 min), in which determination of fluidity is not possible for both alloys. Some powders get welded with each other, for which fluidity is not able to be checked with Hall fluid meter. Hence, overall fluidity is measurable for some combination of parameters (300-37, 300-45, 300-52 and 180-52).

#### 4.2.2.2. Granulometry:

Granulometry results for Ti-15Mo MA (with different parameters) and for Ti-15Mo-6Zr-2Fe (MA with different parameters) are shown in table 4.16.

Development of new high-performance Titanium alloys with Fe-addition for dental implants

Table 4.16: Particle size analysis (For Ti-15Mo and Ti-15Mo-6Zr-2Fe) with different milling conditions

Alloy	Condition (rpm-min)	D (0.1) (µm)	D (0.5) (µm)	D (0.9) (µm)	
Ti-15Mo	300-37	194	368	621	
	300-45	33	74	294	
	300-52	221	316	450	
	180-45	11	32	85	
	180-52	26	138	524	
	180-60	47	283	582	
	240-45	111	338	600	
	240-52	232	384	614	
	Ti-15Mo-6Zr-2Fe	180-45	16	43	202
		180-52	20	49	306
210-45		26	54	145	

Graph obtained from granulometry for different combination of milling speed and milling time are shown in figure 4.11. Maximum particle size obtained is for Ti-15Mo with 300 rpm – 52 min; zf stands for Ti-15Mo-6Zr-2Fe. Graph shows D (0.1), D (0.5), D (0.9). With the same parameter of milling time and milling time Ti-15Mo have larger grains in comparison to Ti-15Mo-6Zr-2Fe which seen in table 4.16.

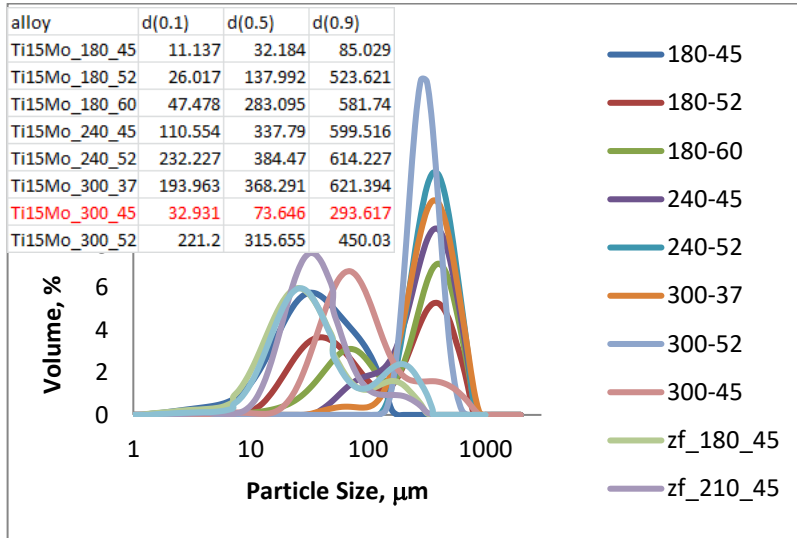


Figure 4.11: Granulometry for Ti-15Mo and Ti-15Mo-6Zr-2Fe (MA, P & S)

#### 4.2.2.3. Mechanical properties:

Table 4.17: Green density (%), sintered density (%) and bending strength of (For Ti-15Mo and Ti-15Mo-6Zr-2Fe) with different milling conditions

Alloy	Condition	Green density (%)	Sintered density (%)	Bending strength (MPa)
Ti-15Mo	300-45	76.36±0.55	90.55±0.91	604.67±143.22
	300-37	74.94±0.1	85.78±0.32	410.28±43.93
	300-52	75.8±0.67	82.36±0.88	371.72±61.50
	180-45	78.58±0.58	86.64±0.23	1597.74±179.47
	180-52	78.38±0.59	97.81±0.45	1261.08 ± 79.07
	180-60	77.1±0.59	95.91±95.91	1062.51±274.08
	240-45	74.66±0.6	85.49±1.4	400.01 ±41.38
	240-52	76.14±0.88	92.44±0.69	525.09 ± 91.07
Ti-15Mo-6Zr-2Fe	180-45	78.12±0.45	98.97±0.53	431.85 ± 119.50
	210-45	77.55±0.6	95.92±0.66	427.56 ± 57.57
	180-52	78.24±0.17	98.79±0.16	667.63 ± 57.04

Green density, sintered density and bending strength for Ti-15Mo and Ti-15Mo-6Zr-2Fe are enlisted in table 4.17. From this table, we can say that this property is better

in case of 180 rpm-52 min as we can see that sintered density is 97.81% and flexural strength is also higher with this. For Ti-15Mo-6Zr-2Fe also, with 180 rpm-52 min, sintered density is higher and bending strength are also high. So, for further research we will use this parameter.

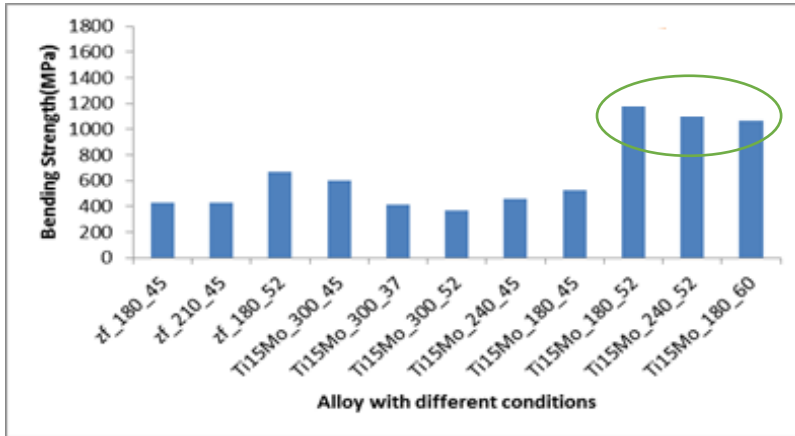


Figure 4.12: Bending strength of Ti-15Mo with different combination of parameters

Here zf stands for Ti-15Mo-6Zr-2Fe. Maximum bending strength is for Ti-15Mo (with 180 rpm and 45 min) and the value noted is 1597 MPa which is confirmed by figure 4.12.

Table 4.18: Elastic modulus (GPa) (For Ti-15Mo) with different milling conditions

Alloys	Condition	Elastic modulus (GPa)	$\nu$
Ti-15Mo	300-45	$81.34 \pm 6.55$	$0.29 \pm 0.035$
	300-37	$63.69 \pm 3.70$	$0.3 \pm 0.007$
	300-52	$62.90 \pm 2.78$	$0.31 \pm 0.041$
	240-45	$63.57 \pm 1.60$	$0.32 \pm 0.098$
	180-45	$75.61 \pm 3.00$	$0.37 \pm 0.008$
	180-52	$101.22 \pm 1.06$	$0.32 \pm 0.038$
	240-52	$73.53 \pm 1.65$	$0.37 \pm 0.004$
	180-60	$94.5 \pm 0.17$	$0.33 \pm 0.003$
Ti-15Mo-6Zr-2Fe	180-45	$76.89 \pm 4.15$	$0.35 \pm 0.089$
	210-45	$83.43 \pm 1.67$	$0.34 \pm 0.056$
	180-52	$98.75 \pm 2.34$	$0.31 \pm 0.063$

For this experiment, binary alloy Ti-15Mo with more variation of parameters is started and followed by quaternary alloy Ti-15Mo-6Zr-2Fe with less variation than before. The value of bending strength for Ti-15Mo-6Zr-2Fe is very less in comparison to Ti-15Mo; which is shown in figure 4.12.

Elastic modulus of Ti-15Mo with different milling conditions are listed in table 4.18. The value of elastic modulus with milling time 300 RPM and 52 Min. are the lowest but porosity is highest (table 4.17) and bending strength is lower.

### 4.2.3: Mechanical alloying with 180 rpm-52 min. for different alloys

#### Granulometry Analysis:

Particle size with granulometry test are tabulated in table 4.19; by where one can see the values of D (0.1) ( $\mu\text{m}$ ), D (0.5) ( $\mu\text{m}$ ) and D (0.9) ( $\mu\text{m}$ ).

Table 4.19: Particle size analysis of Ti-Mo with 180 RPM-52 Minutes

Alloy	rpm-min	D (0.1) ( $\mu\text{m}$ )	D (0.5) ( $\mu\text{m}$ )	D (0.9) ( $\mu\text{m}$ )
Ti-12Mo	180-52	18.623	47.734	121.112
Ti-12Mo-6Zr	180-52	19.183	49.997	135.366
Ti-15Mo-6Zr	180-52	20.975	52.942	146.499
Ti-15Mo-6Zr-4Fe	180-52	27.193	72.947	273.247

Unimodal characteristics for all alloys are found representing that mixing of powders are very homogeneous and belongs to one proper region.

#### Green Density (%), Sintered density and bending strength:

Green density, sintered density and bending strength of different Ti-Mo alloys are listed in table 4.20. Maximum bending strength obtained for Ti-12Mo which is 1292.31 MPa and least obtained for Ti-15Mo-6Zr-4Fe which is 476.28 MPa.

Table 4.20: Green density, sintered density and bending strength of Ti-Mo with 180 rpm-52 min

Alloy	Green density (%)	Sintered density (%)	Bending Strength (MPa)
Ti-12Mo	78.92 $\pm$ 3.86	94.32 $\pm$ 0.93	1292.31 $\pm$ 57.59
Ti-12Mo-6Zr	74.79 $\pm$ 3.03	96.30 $\pm$ 0.05	1127.15 $\pm$ 240.47
Ti-15Mo-6Zr	77.51 $\pm$ 1.22	96.48 $\pm$ 0.38	1169.65 $\pm$ 82.87
Ti-15Mo-6Zr-4Fe	76.53 $\pm$ 1.07	98.19 $\pm$ 0.05	476.28 $\pm$ 32.45

Sintered density or porosity with Archimedes' test method is analysed. Porosity is directly related to bending strength and microstructure. If porosity is very low, then bending strength and microstructure seems to be better. Here, for Ti-15Mo-6Zr-2Fe these properties are better than another alloy.

#### **Ultrasonic and hardness test:**

Elastic modulus and hardness result for different Ti-Mo alloys with milling parameters 180 rpm-52 min is listed in table 4.21. The least value for elastic modulus obtained for Ti-12Mo-6Zr is 83.40 GPa. Hardness value is approx. 180 HV for all alloys.

Table 4.21: Elastic modulus of Ti-Mo with 180 RPM-52 Minutes

Alloys	E (GPa)	Average $\nu$	Hardness (HV)
Ti-12Mo	95.48 $\pm$ 3.38	0.3300 $\pm$ 0.0130	182.2 $\pm$ 7.9
Ti-12Mo-6Zr	83.40 $\pm$ 3.32	0.3700 $\pm$ 0.0095	183.8 $\pm$ 11.6
Ti-15Mo-6Zr	94.87 $\pm$ 2.96	0.3400 $\pm$ 0.0088	180.6 $\pm$ 24.4
Ti-15Mo-6Zr-4Fe	101.27 $\pm$ 0.86	0.3400 $\pm$ 0.0016	183.6 $\pm$ 19.1

#### **4.2.4: Mechanical alloying with Process control agent (PCA):**

After work with different combination with short milling time and without PCA for Ti-Mo alloys, we have found lots of heat in the milling jar. So, for minimizing the heat we must work with PCA. In this stage of experiment, process control agent (PCA- Stearic acid (1% by mass) is employed for controlling the heat generation.

#### **Powder utility:**

This is calculated by the ratio of powder obtained after milling and weight of initial powder. From the table 4.22, it is evident that final weight of powder/ initial weight of powder is very less in case of 24 h milling time. Milling time is to be changed to obtain more powder after milling.

Table 4.22: Powder utility (%) of Ti-15Mo-6Zr-2Fe with 1% PCA

Condition	Initial powder weight (g)	Final powder weight (g)	Ratio	%
6h-5 mm Dia.	49.77	44.10	0.89	88.61
6h-10mm Dia	49.77	39.38	0.79	79.12
24h-5 mm Dia	24.88	5.70	0.23	22.91
24h-10 mm Dia	24.88	6.40	0.26	25.72

**Fluidity test:**

Fluidity test was done after the mixing of powder which is shown in table 4.23. The maximum value obtained for Ti-15Mo-6Zr-2Fe with 6h-10 mm Dia. is maximum which is 1.575.

Table 4.23: Fluidity of Ti-15Mo-6Zr-2Fe with 1% PCA

Condition	Final weight (g)	Time elapsed (S)	Fluidity (g /s)
6 h-5 mm dia.	44.1	32	1.378
6 h-10 mm dia.	39.38	25	1.575
24 h-5 mm dia.	5.7	5	1.14
24h-10 mm dia.	6.4	Not possible (particles are not regular)	-

**Granulometry test:**

Granulometry test done after the mixing of powder which is shown in table 4.24.

Table 4.24: Particle size analysis of Ti-15Mo-6Zr-2Fe with 1% PCA

Condition	D (0.1) $\mu\text{m}$	D (0.5) $\mu\text{m}$	D (0.9) $\mu\text{m}$
6h-5 mm	20.082	45.838	101.190
6h-10 mm	28.679	69.643	204.169
24h-5 mm	317.879	489.91	751.404
24h-10 mm	37.611	70.993	141.315

From the granulometry test table, the biggest particle size obtained was subjected to condition 24h-5 mm. This is due to large time and with high impact for long time with 5 mm ball size.

**SEM analysis of milling powder (after milling):**

From figure 4.13 we can see the powder cut characteristics after milling. Powders got agglomerated with each other's and forms bigger particle size, which is clearly shown by the figure. With the higher milling time (24 h) particle size gets bigger due to more agglomeration which is clearly seen in figure 4.13 (C) and 4.13 (D).

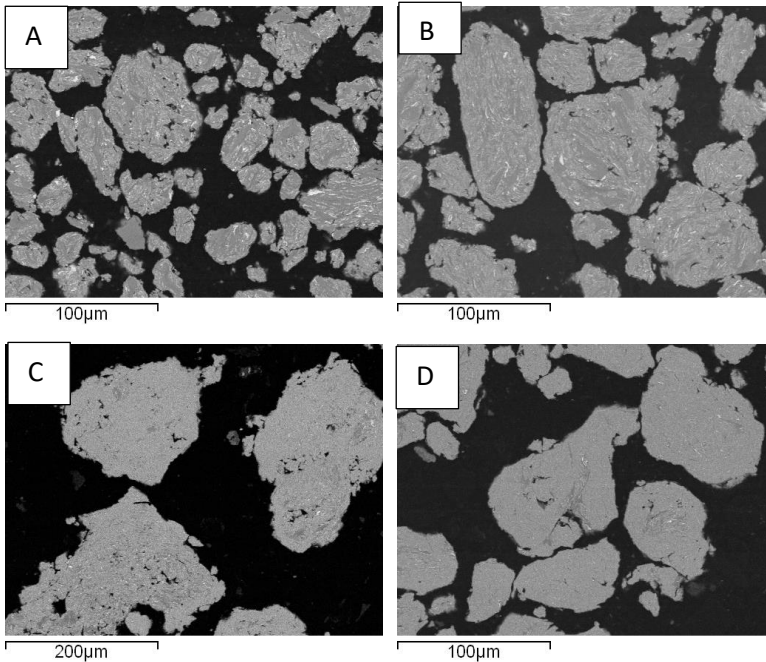


Figure 4.13: SEM analysis of mechanical alloying powder with (a) 6h-5mm (b) 6h-10 mm (c) 24h-5 mm (d) 24h-10mm

After SEM of powder cut of the milled powder, we have done elemental analysis with help of Energy dispersive X-ray spectroscopy (EDS) tool, which is tabulated in table 4.25.

Table 4.25: Elemental analysis of Ti-15Mo-6Zr-2Fe with 1% PCA by SEM image

Condition	Ti K (%w/w)	Fe K (%w/w)	Zr L (%w/w)	Mo L (%w/w)
6h-5 mm	78.43	1.33	6.39	13.85
6h-10 mm	79.30	1.35	5.94	7.4
24h-5 mm	75.11	2.15	6.95	15.78
24h-10 mm	75.00	1.86	16.46	9.30



### **Mechanical Test result of sintered part:**

We worked with different milling time and different ball size with process control agent (PCA), but powder weight obtained after milling with 24h was very less in both ball size (5 mm and 10 mm) Diameter, so it's difficult to make sintered samples with 24h. So, we worked with 6h with both ball size (5 mm and 10 mm) Diameter. We worked with 5 samples with milling time of 6h and milling ball size of 5 mm diameter and 4 samples with milling time of 6h and milling ball size of 5 mm (which depends on powder obtained after milling). Bending strength tests were possible for only 6h conditions with both ball sizes 5- and 10-mm. Mechanical properties are tabulated in table 4.26 which includes sintered density, bending strength, elastic modulus and eccentricity of the sintered samples.

Table 4.26: Mechanical properties of sintered Ti-15Mo-6Zr-2Fe with 1% PCA by SEM image

Condition	Sintered density	Bending strength (MPa)	Elastic modulus (GPa)	$\nu$
6H-5 mm	95.61±0.43	309.66	100.36±5.74	0.3230±0.0029
6H-10 mm	87.31±0.71	576.29	89.32±0.85	0.3001±0.0061

### **4.3: Spark Plasma Sintering (SPS) Results:**

For obtaining full density alloy, SPS is a better technology for enhancement of its density. After analysing microstructure, it is confirmed that alloys produced from SPS technology have full density. But the flexural strength is very low for ternary alloy and quaternary alloys. Process could have been improved for better results. We have mixed powder for SPS alloy with milling condition 180 rpm-52 min without PCA. For each alloy sintering temperatures are 1100°C.

#### **4.3.1: Mechanical test result:**

For getting the mechanical properties, we have done different mechanical test like sintered density, bending strength, elastic modulus test which is tabulated in table 4.27. Relative density is approx. 100% with each condition for different alloys. Bending strength is maximum for Ti-15Mo with 1150 °C which is 1006.66 MPa; for ternary and quaternary alloys bending strength is much lower than binary alloys as clearly shown in table 4.27. Elastic modulus is minimum for Ti-15Mo with 1100 °C which is 88.24 GPa.

Table 4.27: Different mechanical test of Ti-Mo alloys by SPS with different temperatures

Alloys	Temperature (°C)	Relative Density (%)	Bending Strength (MPa)	Elastic modulus (GPa)
Ti-15Mo	1100	97.64	921.08	88.24
	1150	98.28	1006.66	98.02
	1200	98.25	863.09	97.50
Ti-15Mo-6Zr	1100	97.99	378.64	95.35
	1150	98.32	409.16	97.64
	1200	98.57	414.07	92.75
Ti-15Mo-6Zr-2Fe	1100	97.72	339.34	106.08
	1150	97.24	335.93	101.15
	1200	97.16	301.89	103.87

**4.3.2: Microhardness of Ti-Mo alloys with different conditions:**

Table 4.28: Micro hardness of Ti-Mo alloys by SPS with different temperatures

Alloys	Temperature (°C)	Microhardness (HV)
Ti-15Mo	1100	275 ± 48
	1150	350 ± 50
	1200	334 ± 25
Ti-15Mo-6Zr	1100	377 ± 23
	1150	401 ± 26
	1200	452 ± 31
Ti-15Mo-6Zr-2Fe	1100	465 ± 41
	1150	477 ± 34
	1200	469 ± 48

Microhardness of Ti-Mo alloys are shown in table 4.28; the value of microhardness for Ti-15Mo-6Zr-2Fe sintered at 1150 °C is maximum among all which value is 477

HV and minimum is for Ti-15Mo at sintering temperature of 1100 °C which is 275 HV.

#### 4.3.3: DRX analysis of SPS samples with different conditions

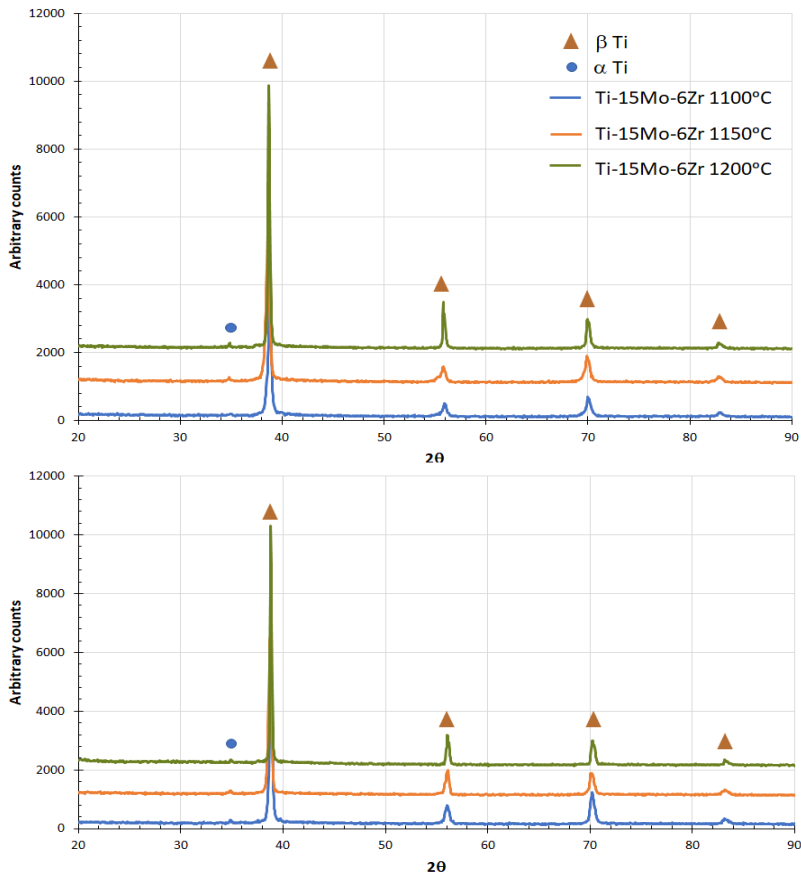


Figure 4.14: DRX analysis of Ti-Mo SPS samples with different Temperature (a) of Ti-15Mo-6Zr (b) Ti-15Mo-6Zr-2Fe

DRX analysis done for Ti-Mo alloys by SPS with different sintering temperature is shown in figure 4.14. Ti- beta and Ti-alpha are found in the DRX analysis, highest peaks are obtained for beta-phase.

**4.3.4: EBSD analysis of Ti-Mo alloys by SPS with different conditions:**

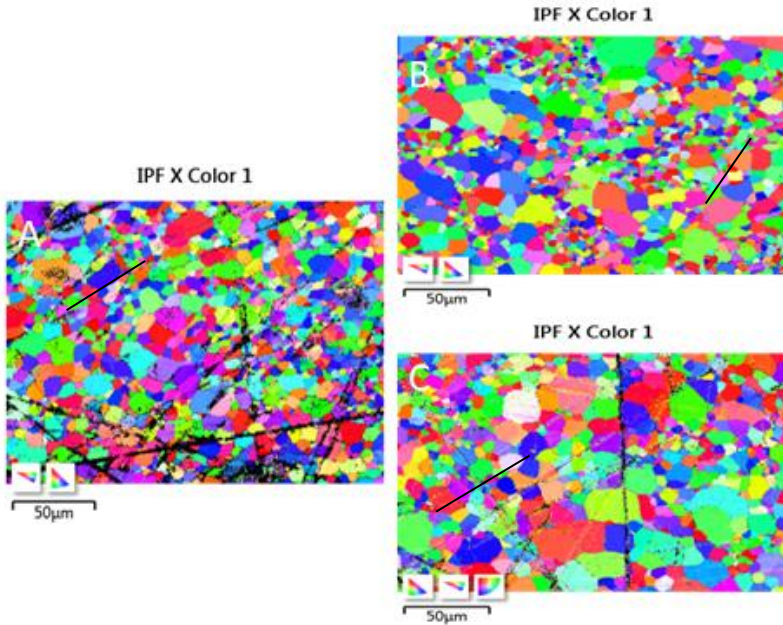


Figure 4.15: IPF X analysis of SPS samples (A) Ti-15Mo with 1100°C (B) Ti-15Mo-6Zr-2Fe with 1100°C (C) Ti-15Mo-6Zr-2Fe with 1200°C

IPF X analysis of different Ti-Mo alloys prepared with SPS method are shown in figure 4.15. We analysed with Ti-15Mo sintered at 1100°C, Ti-15Mo-6Zr-2Fe with 1100°C and Ti-15Mo-6Zr-2Fe sintered at 1200°C. Black line is due to dirt in the sample (preparation is difficult). Agglomeration activity found in these samples which is clearly shown in figure 4.15.

Phase fraction for SPS samples obtained from EBSD analysis is shown in table 4.29.  $\beta$  % for each condition is the highest, which is approx. 98% but for Ti-15Mo-6Zr sintered at 1200 °C is 89.32 which is lowest  $\beta$  %. For some alloys we have also find  $\alpha$ '' phase like for Ti-15Mo-6Zr sintered at 1200 °C and for Ti-15Mo-6Zr-2Fe sintered at 1200 °C.

Phase fraction for different samples with method obtained from EBSD analysis is summarized in table 4.29. From table it is found that binary alloys have  $\alpha$  and  $\beta$ -phase and for quaternary alloys have almost  $\beta$ -phase.

Table 4.29: Phase analysis table of Ti-Mo alloys with different parameters

Alloys	% Ti $\alpha$ phase	% Ti $\beta$ phase	% Ti $\alpha''$
Ti-12Mo EB	41.25	58.75	0.00
Ti-12Mo-6Zr EB	27.67	72.33	0.00
Ti-12Mo-6Zr-2Fe MA	29.75	70.25	0.00
Ti-12Mo-6Zr-3Fe EB 1300°C	0.24	99.76	0.00
Ti-12Mo-6Zr-3Fe EB 1250°C	0.96	99.04	0.00
Ti-15Mo SPS 1100°C	2.19	97.81	0.00
Ti-15Mo SPS 1150 °C	0.82	99.18	0.00
Ti-15Mo SPS 1200 °C	2.69	97.31	0.00
Ti-15Mo-6Zr SPS 1100 °C	0.96	99.04	0.00
Ti-15Mo-6Zr SPS 1200 °C	0.11	89.32	10.57
Ti-15Mo-6Zr-2Fe SPS 1100 °C	0.05	99.95	0.00
Ti-15Mo-6Zr-2Fe SPS 1200 °C	0.06	94.19	5.75

Table 4.30: Grain size with EBSD table of Ti-Mo alloys with different parameters

Alloys	$\alpha$ phase ( $\mu\text{m}$ )	$\beta$ phase ( $\mu\text{m}$ )	Overall ( $\mu\text{m}$ )
Ti-12Mo EB	6.21	7.47	6.85
Ti-12Mo-6Zr EB	4.97	6.59	6.89
Ti-12Mo-6Zr-2Fe MA	3.38	4.97	4.25
Ti-12Mo-6Zr-3Fe EB 1300°C	-	8.46	8.46
Ti-12Mo-6Zr-3Fe EB 1250°C	-	9.98	9.98
Ti-15Mo SPS 1100°C	2.89	4.92	4.88
Ti-15Mo SPS 1150 °C	2.08	5.47	5.46
Ti-15Mo SPS 1200 °C	2.86	5.77	5.72
Ti-15Mo-6Zr SPS 1100 °C	2.32	4.58	4.57
Ti-15Mo-6Zr SPS 1200 °C	-	5.38	5.38
Ti-15Mo-6Zr-2Fe SPS 1100 °C	-	4.66	4.66
Ti-15Mo-6Zr-2Fe SPS 1200 °C	-	6.8	6.8

For Ti-12Mo-6Zr-3Fe with 1250°C and 1300°C have 99.04 and 99.75 %  $\beta$ -phase, which is almost 100%. SPS improves  $\beta$ -phase which shown in table 4.29.

Grain size of alloys with different process and other parameters are tabulated in table 5.30. Mostly binary alloys have both  $\alpha$  and  $\beta$  grains but for quaternary alloys; only have  $\beta$  grains. Size is bigger for  $\beta$  grains normally for binary alloys which can see by table 5.30. Grains are normally in range of (6-8)  $\mu\text{m}$ . Biggest grain is for Ti-12Mo-6Zr-3Fe with EB sintered at 1300 °C which value is 9.98  $\mu\text{m}$ . Normally EB have larger grain with respect to MA and SPS process.

#### 4.4 Corrosion Test:

From the corrosion we have calculated  $I_{\text{corr}}$  ( $\text{A}/\text{cm}^2$ ),  $E_{\text{corr}}$  (V),  $\beta_c$  (V/dec),  $\beta_a$  (V/dec), OCP (V),  $R_p$  ( $\text{k}\Omega.\text{cm}^2$ ) and  $V_{\text{corr}}$  ( $\mu\text{m}/\text{year}$ ) which is tabulated in 4.31 and 4.32.

Table 4.31: Corrosion result with different parameters  $I_{\text{corr}}$  ( $\text{A}/\text{cm}^2$ ),  $E_{\text{corr}}$  (V),  $\beta_c$  (V/dec) and  $\beta_a$  (V/dec) for different process

Sample	$I_{\text{corr}}$ ( $\text{A}/\text{cm}^2$ )	$E_{\text{corr}}$ (V)	$\beta_c$ (V/dec)	$\beta_a$ (V/dec)
Ti-12Mo-6Zr-2Fe MA 600	1.49E-06	-0.42	0.104	0.133
Ti-12Mo-6Zr-2Fe MA 900	2.25E-07	-0.40	0.102	0.135
Ti-12Mo-6Zr-1Fe EB 1250	1.87E-07	-0.38	0.138	0.100
Ti-12Mo-6Zr-2Fe EB 1250	2.36E-08	-0.23	0.136	0.105
Ti-12Mo-6Zr-3Fe EB 1250	1.28E-07	-0.35	0.117	0.116
Ti-12Mo-6Zr-4Fe EB 1250	1.71E-08	-0.11	0.128	0.107
Ti-12Mo-6Zr-1Fe EB 1300	2.63E-07	-0.32	0.119	0.114
Ti-12Mo-6Zr-2Fe EB 1300	1.80E-07	-0.31	0.119	0.114
Ti-12Mo-6Zr-3Fe EB 1300	1.04E-07	-0.23	0.128	0.107
Ti-12Mo-6Zr-4Fe EB 1300	1.21E-07	-0.35	0.139	0.100
Ti-15Mo 180-52_MA	1.72E-07	-0.30	0.121	0.112
Ti-15Mo-6Zr-2Fe 180-52	1.82E-07	-0.34	0.116	0.116
Ti-15Mo-6Zr-2Fe 6h+5mm	2.08E-07	-0.28	0.114	0.119
Ti-15Mo-6Zr-2Fe 6h+10mm	4.08E-06	-0.59	0.108	0.126
Ti-15Mo SPS-1150	2.61E-08	-0.30	0.128	0.106
Ti-15Mo-6Zr-SPS-1150	2.15E-08	-0.13	0.132	0.104
Ti15Mo6Zr2Fe-SPS-1150	2.82E-08	-0.19	0.134	0.103

$I_{\text{corr}}$  value is minimum in case of SPS process which is better for biomaterials.  $E_{\text{corr}}$  and Open circuit potential is more with SPS process which also tabulated in 4.31 and 4.32.  $R_p$  ( $\text{k}\Omega.\text{cm}^2$ ) is also maximum for SPS process which is better.

Table 4.32: Corrosion result with different parameters OCP (V),  $R_p$  ( $k\Omega.cm^2$ ) and  $V_{corr}$  ( $\mu m/year$ ) for different process

Sample	OCP (V)	$R_p$ ( $k\Omega.cm^2$ )	$V_{corr}$ ( $\mu m/year$ )
Ti-12Mo-6Zr-2Fe MA 600	-0.19	16932	12
Ti-12Mo-6Zr-2Fe MA 900	-0.32	112353	1.9
Ti-12Mo-6Zr-1Fe EB 1250	-0.37	135042	1.4
Ti-12Mo-6Zr-2Fe EB 1250	-0.24	1.13E+06	0.18
Ti-12Mo-6Zr-3Fe EB 1250	-0.34	196827	0.99
Ti-12Mo-6Zr-4Fe EB 1250	-0.18	1.48E+06	0.13
Ti-12Mo-6Zr-1Fe EB 1300	-0.32	96128	2
Ti-12Mo-6Zr-2Fe EB 1300	-0.30	140355	1.4
Ti-12Mo-6Zr-3Fe EB 1300	-0.26	243887	0.8
Ti-12Mo-6Zr-4Fe EB 1300	-0.34	209075	0.93
Ti-15Mo 180-52 MA	-0.31	146771	1.3
Ti-15Mo-6Zr-2Fe 180-52	-0.34	139179	1.4
Ti-15Mo-6Zr-2Fe 6h+5mm	-0.25	121412	1.7
Ti-15Mo-6Zr-2Fe 6h+10mm	-0.40	6194	32
Ti-15Mo-SPS-1150	-0.39	966998	0.2
Ti-15Mo-6Zr-SPS-1150	-0.14	1175912	0.17
Ti-15Mo-6Zr-2Fe-SPS-1150	-0.27	894550	0.22

Corrosion test result for Mechanical alloying samples with PCA and without PCA. Current density is lower with Ti-15Mo-6Zr-2Fe in comparison to Ti-15Mo as shown in figure 4.16(A) which we shown in the format of  $\log(i)$  vs E. Process control agent (PCA) results shown in figure 4.17(A) and (B) which have inferior results in comparison to alloys without PCA.

Development of new high-performance Titanium alloys with Fe-addition for dental implants

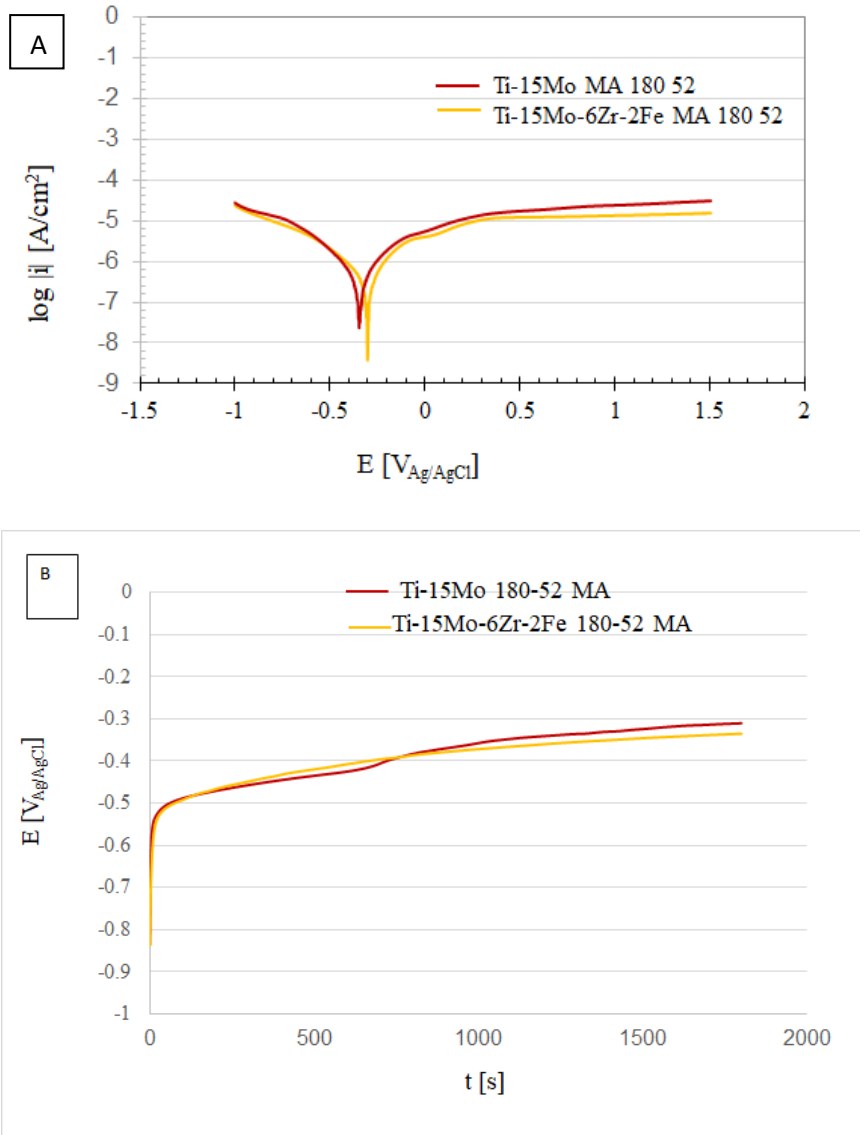


Figure 4.16: Different graphs for corrosion results of MA samples (A) Log(i) vs E for samples without PCA (B) E vs t for samples without PCA



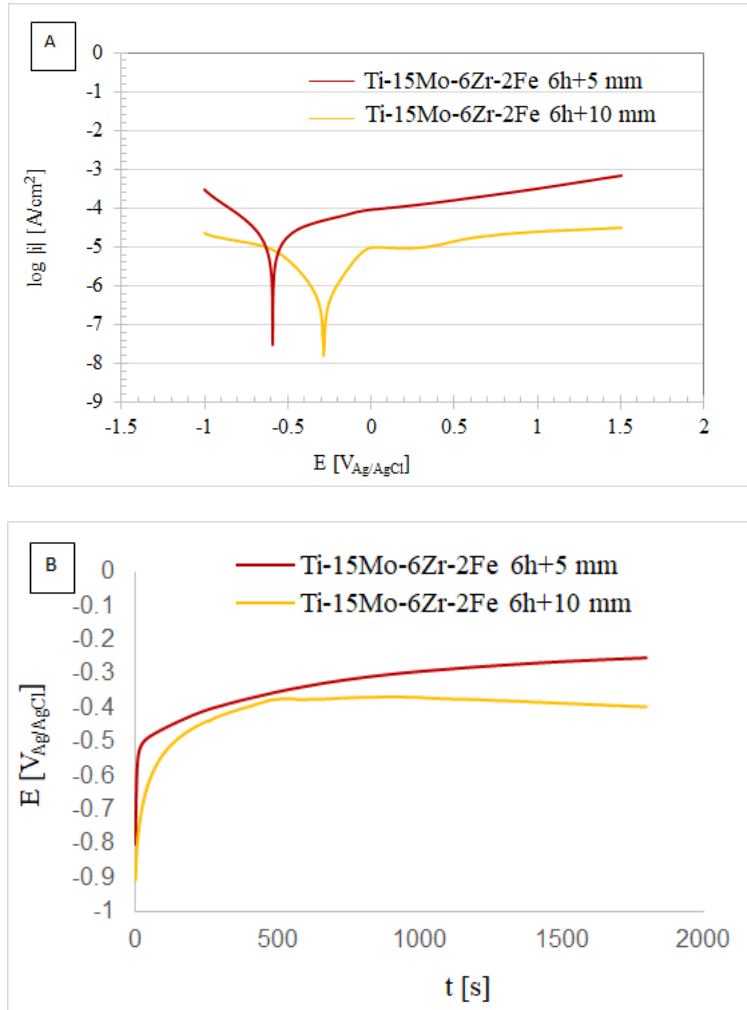


Figure 4.17: Different graphs for corrosion results of MA samples (A) Log(i) vs E for samples with PCA (B) E vs t for samples with PCA

Table 4.33 summarizes the value of ion release rate  $C$  [ $\mu\text{g/L cm}^2 \text{ h}$ ] of each element in the alloy. For biomaterial application, it should be low. For example, within all the alloys  $Ti-12Mo-6Zr-2Fe$  with elemental blend (EB) method have least ion release rate for Ti atom which is better for the implant. Overall EB and SPS have better results in comparison to MA samples.

Development of new high-performance Titanium alloys with Fe-addition for dental implants

Table 5.33: Ion-release rate of different particle with different parameters for corrosion

SAMPLE	METHOD	PARAMETERS	Ion release rate C [ $\mu\text{g}/\text{Lcm}^2 \text{ h}$ ]			
			Ti	Mo	Zr	Fe
Ti-12Mo-6Zr-1Fe	EB	ST: 1250°C	3.82 ± 0.27	1.27 ± 0.10	0.28 ± 0.03	0.12 ± 0.05
Ti-12Mo-6Zr-3Fe	EB	ST: 1250°C	5.25 ± 0.56	1.38 ± 0.15	0.37 ± 0.04	0.12 ± 0.03
Ti-12Mo-6Zr-1Fe	EB	ST: 1300°C	4.06 ± 0.16	1.56 ± 0.10	0.30 ± 0.01	0.09 ± 0.01
Ti-12Mo-6Zr-2Fe	EB	ST: 1300°C	1.06 ± 0.11	1.58 ± 0.06	0.08 ± 0.02	0.01 ± 0.01
Ti-12Mo-6Zr-3Fe	EB	ST: 1300°C	3.39 ± 0.12	0.93 ± 0.01	0.24 ± 0.01	0.11 ± 0.04
Ti-12Mo-6Zr-4Fe	EB	ST: 1300°C	2.57 ± 0.81	1.12 ± 0.01	0.18 ± 0.06	0.09 ± 0.04
Ti-12Mo-6Zr-2Fe	MA	CP: 600 MPa 300 rpm-45 min.	6.46 ± 1.83	2.27 ± 0.07	0.82 ± 0.05	0.18 ± 0.13
Ti-12Mo-6Zr-2Fe	MA	CP: 900 MPa 300 rpm-45 min.	1.75 ± 0.27	1.60 ± 0.00	0.15 ± 0.03	0.00 ± 0.00
Ti-15Mo	MA	CP: 900 MPa 300 rpm-45 min.	2.97 ± 0.21	0.99 ± 0.01	0.20 ± 0.00	0.01 ± 0.01
Ti-15Mo-6Zr-2Fe	MA+PCA	6h+5 mm	3.81 ± 1.74	1.74 ± 0.03	0.28 ± 0.13	0.09 ± 0.08
Ti-15Mo-6Zr-2Fe	MA+PCA	6h+10 mm	9.83 ± 0.94	2.98 ± 0.38	0.75 ± 0.07	0.20 ± 0.02
Ti-15Mo	SPS	ST: 1150°C, 5min.+50 MPa	2.21 ± 0.29	0.73 ± 0.05	0.01 ± 0.01	0.01 ± 0.01
Ti-15Mo-6Zr	SPS	ST: 1150°C, 5min.+50MPa	3.33 ± 0.60	0.99 ± 0.16	0.22 ± 0.03	0.01 ± 0.01
Ti-15Mo-6Zr-2Fe	SPS	ST: 1150°C, 5min.+50 MPa	2.53 ± 1.55	1.16 ± 0.18	0.17 ± 0.11	0.06 ± 0.06
Ti-15Mo-6Zr-2Fe	MA	180 RPM-52 min	2.11 ± 0.36	0.78 ± 0.13	0.21 ± 0.01	0.06 ± 0.01

Table 4.34 summarizes the value of (Velocity:  $\text{mg}/\text{dm}^2 \cdot \text{day}$ ) of each element in the alloy. This velocity is calculated with the help of ion release rate. For biomaterial application, it should be low. For example, within all the alloys Ti-12Mo-6Zr-2Fe sintered at 1300°C with elemental blend (EB) method have lowest ion velocity. Overall EB and SPS have better results in comparison to MA samples. MA with PCA have more corrosion velocity which is inferior for biomaterials.

Table 4.34: Corrosion velocity with ion-release rate

SAMPLE	METHOD	PARAMETERS	Velocity: mg/dm <sup>2</sup> ·day				
			Ti	Mo	Zr	Fe	sum
Ti-12Mo-6Zr-1Fe	EB	ST: 1250°C	0.4582	0.1519	0.0334	0.0141	0.6576
Ti-12Mo-6Zr-3Fe	EB	ST: 1250°C	0.6294	0.1658	0.0445	0.0146	0.8543
Ti-12Mo-6Zr-1Fe	EB	ST: 1300°C	0.4878	0.1866	0.0356	0.0102	0.7203
Ti-12Mo-6Zr-2Fe	EB	ST: 1300°C	0.1274	0.1894	0.0095	0.0012	0.3276
Ti-12Mo-6Zr-3Fe	EB	ST: 1300°C	0.4065	0.1115	0.0284	0.0130	0.5594
Ti-12Mo-6Zr-4Fe	EB	ST: 1300°C	0.3078	0.1345	0.0215	0.0102	0.4741
Ti-12Mo-6Zr-2Fe	MA	CP: 600 MPa 300 rpm-45 Min.	0.7756	0.2726	0.0987	0.0220	1.1689
Ti-12Mo-6Zr-2Fe	MA	CP: 900 MPa 300 rpm-45 Min.	0.2099	0.1922	0.0183	0.0003	0.4207
Ti-15Mo	MA	CP: 900 MPa 300 rpm-45 Min.	0.3560	0.1188	0.0249	0.0069	0.5067
Ti-15Mo-6Zr-2Fe	MA+PCA	6H+5 mm	0.457	0.2084	0.0335	0.0104	0.7091
Ti-15Mo-6Zr-2Fe	MA+PCA	6H+10 mm	1.180	0.358	0.090	0.0239	1.6518
Ti-15Mo	SPS	ST: 1150°C, 5min.+50MPa	0.266	0.088	0.001	0.0010	0.3550
Ti-15Mo-6Zr	SPS	ST: 1150°C, 5min.+50MPa	0.400	0.1185	0.027	0.0019	0.5466
S3: Ti-15Mo-6Zr-2Fe	SPS	ST: 1150°C, 5min.+50MPa	0.303	0.1390	0.021	0.0068	0.470
Ti-15Mo-6Zr-2Fe	MA	180 RPM-52 min	0.254	0.093	0.001	0.002	0.349

So overall, we have results for EB, MA and SPS powder metallurgy method with different combination of compaction pressure (CP), sintering temperature (ST), milling speed and milling time for MA samples.

*Development of new high-performance Titanium alloys with Fe-addition for dental implants*

# Chapter 5: Discussion of the result

When the % of Mo is 5% alloy is equiaxed  $\alpha$  and when Mo is more than 10% the alloy is equiaxed  $\alpha$  crystal grain and needle type  $\beta$ -phases are found but when Mo is more than 15% only equiaxed  $\beta$ -phases are found which is confirmed by Chen *et al.* (Chen *et al.*, 2006), so for this reason we use (12,15)% for our research. Some authors like Lu *et al.* (Lu *et al.*, 2013a) also suggested that when Mo is more than 10%, the phase is mainly  $\beta$ . Presence of  $\beta$ -stabilizer element made zirconium as a non-neutral element and pass to act as on stabilizing  $\beta$ -phase in that alloy. (Ho, Ju and Chern Lin, 1999; Correa *et al.*, 2018). There is a significant strengthening effect of Fe to Ti-based alloys, and Mo is effective in stabilizing  $\beta$ -phase (Bao *et al.*, 2014).

From table 4.1 relative green density of Ti-15Mo is maximum within all the base alloys which is approx. 78.10 % and least value is for Ti-12Mo-6Zr which is 77.50% which is approx. 0.8% less than Ti-15Mo. Increment in % of Mo increases the green density which is clear from figure 5.1 and addition of Zr also reduces the green density which is shown in figure 4.1.

From table 4.1 it is clearly shown that addition of Fe decreases green density up to 2 % but when % of Fe increases beyond 3% green density improves and green density also affects sintered density. Some author like Yang *et al.* (Yang *et al.*, 2012); who worked with Ti-Fe-Si, also discussed about green and sintered density and they confirmed that when % of Fe is more than 3% sinterability increases.

Shrinkage (volume loss) is maximum for Ti-12Mo-6Zr which is clearly shown in figure 5.1, value is 19.50% and the minimum is for Ti-15Mo which is 18.30% which is approx. 5.4% less than Ti-12Mo-6Zr. Elshalakany *et al.* (Elshalakany *et al.*, 2017) also claimed that volumetric shrinkage for their alloy (Ti-15Mo-6Zr-xCr) is between 16-20% which is like our alloy. Delvat *et al.* (Delvat *et al.*, 2008) also claimed that dimensional loss of Ti-20Mo and Ti-40Mo are between (20-23)%. Our alloy is better than their alloy because less dimensional loss after sintering is better.

Shrinkage for quaternary alloys decreases with addition of Fe to Ti-12Mo-6Zr shown in figure 5.1. The value for Ti-12Mo-6Zr-4Fe is the least for our alloy; it means

addition of more % of Fe decreases the value of shrinkage.

Addition of Zr increases the value of Shrinkage from 18.5% to 19.5% for Ti-12Mo to Ti-12Mo-6Zr and when Fe is added to Ti-12Mo-6Zr; shrinkage values decrease as % of Fe increases from 1-4%. For Ti-15Mo-6Zr also shrinkage value increases from 18.4 to 19.4%. So, overall range for our alloy is from 18.5-19.5%.

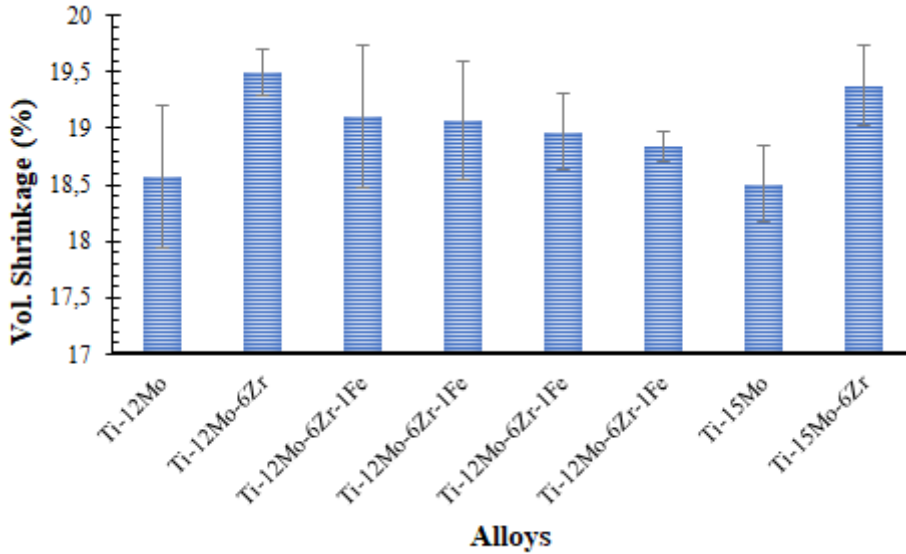


Figure 5.1: Shrinkage of Ti-Mo alloy

Sintered density is the main geometrical property of the alloy which is prepared by powder metallurgy route with press and sintering method. Porosity (100- relative sintered density) is approx. the inverse of the relative sintered density of the sample i.e. if the relative density is higher, porosity is lower and vice versa. We also calculated the value of sintered density ( $\text{gr}/\text{cm}^3$ ) by the help of relative sintered density and theoretical density, which is shown in table 4.2. For Ti-15Mo sintered density is  $4.77 (\text{gr}/\text{cm}^3)$  in our case which is prepared by elemental blend and sintering temperature  $1250\text{ }^\circ\text{C}$  but some author Martins et al. (Martins Júnior *et al.*, 2011) claimed that for Ti-15Mo is  $4.97 (\text{g}/\text{m}^3)$  which used hot-swaging method; which is more than theoretical density of Ti-15Mo which is  $4.92 (\text{g}/\text{cm}^3)$ .

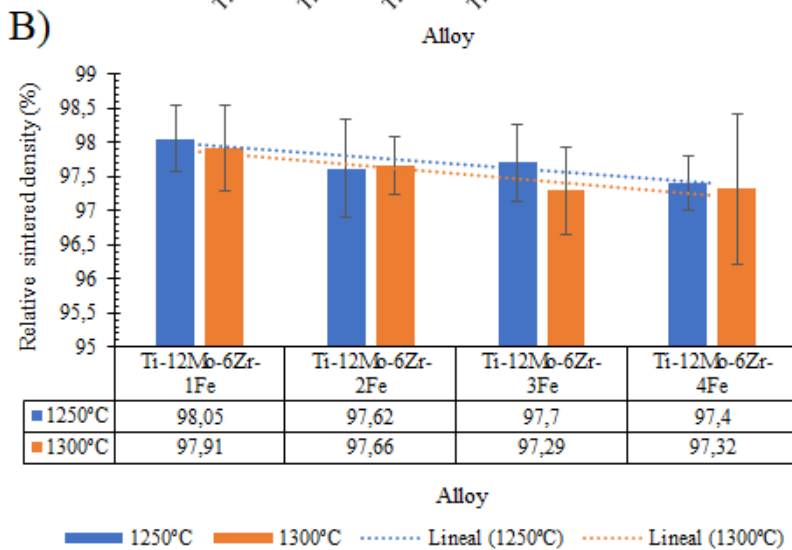
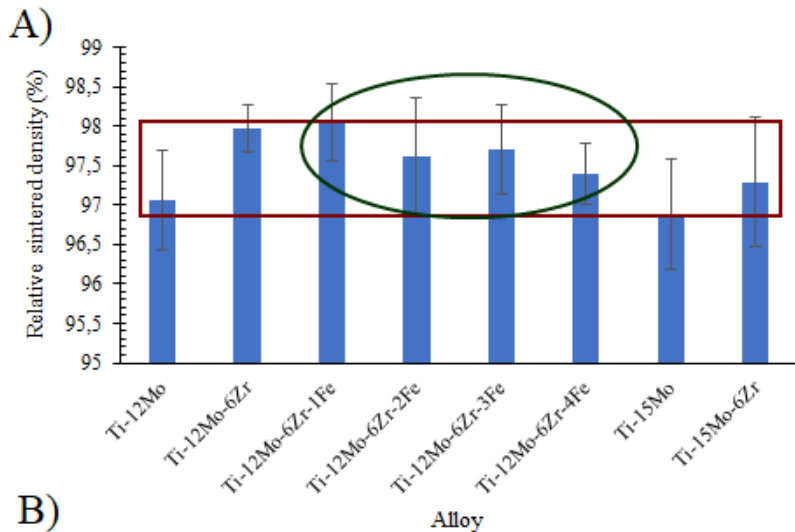


Figure 5.2:(A) Relative sintered density of Ti-Mo alloy (B) Relative sintered density of Ti-Mo-Zr-xFe at different temp.

Addition of Zr improves the relative sintered density for Ti-12Mo from (97-98) % approx. 1.01% more than the relative sintered density of Ti-12Mo, Ti-15Mo-6Zr have also higher sintered density of Ti-15Mo from 96.8 to 97.5%. Addition of Fe

increases relative sintered density with 1% of Fe from 97.9 to 98% and more % of Fe decreases relative sintered density which is shown in figure 5.2 (A). The range for relative sintered density is (97-98) % which is denoted by the box. Majumdar et al. (Majumdar *et al.*, 2010) who worked with Mo-0.6Ti-0.2Zr-0.02C by powder metallurgy route at 1800 °C claimed that sintered density for the alloy is 97% of the theoretical density.

The relative density has a linear co-relation with Fe content and sintering temperature which is shown in figure 5.2 (B). Relative density is lower in the case of 1300 °C for all the alloy but this is little bit higher in the case of Ti-12Mo-6Zr-2Fe which is shown in figure 5.2 (B). Liu et al. (Liu *et al.*, 2017) also reported the same as the increasing % of Fe causes of decrement of relative sintered density.

The range of relative sintered density for Ti-12Mo-6Zr-xFe with both temperature is between (97.33-98.05) which is also tabulated and graphically shown in figure 6.3. Minimum relative density is for Ti-12Mo-6Zr-4Fe is for both the sintering temperature which is 97.4 and 97.32% for 1250 °C and 1300 °C relatively and maximum is for Ti-12Mo-6Zr-1Fe with both temperature which is 98.05 and 97.91% for 1250 °C and 1300 °C relatively. Maximum sintered density is same for Ti-12Mo-6Zr-4Fe with both temperature which is 4.89 (gr/cm<sup>3</sup>).

Bending strength is maximum for Ti-15Mo which is 2161 MPa. Addition of Zr and Fe decreases the value of bending strength which is clearly shown by the value of Ti-12Mo-6Zr in comparison to Ti-12Mo and Ti-15Mo-6Zr in comparison to Ti-15Mo which shows the effect of Zr on Ti-Mo alloy which causes decrement of the value of bending strength. More % of Mo (from 12-15) causes increment of bending strength shown by the figure 5.3 (A).

Addition of Fe to Ti-12Mo-6Zr also decreases the value of bending strength. More % of Fe decreases the value of bending strength shown by the value of Ti-12Mo-6Zr-1Fe to Ti-12Mo-6Zr-4Fe which shows decreasing trend of the bending strength with the more % of Fe. The range for the bending strength for our alloy is very high which is from (650-2150) MPa which is denoted by the box in figure 6.4. Ho et al. (Ho *et al.*, 2009) claimed that bending strength of Ti-10Zr-1Mo is 1177 MPa which is 20% more than Ti-10Zr and 40% more than bending strength of C.P Ti (Davis, 2003); which is 844 MPa. Addition of Zr reduced the value of bending strength which is also confirmed by Ho et al. (Ho *et al.*, 2009). Addition of Zr reduced the value of bending strength approx. 5% in case of Ti-12Mo but 20% decrement in case



of Ti-15Mo which is clearly shown in figure 6.4. Addition of Fe also decreases the value of bending strength to (24-40) % which is also shown in figure 5.3 (A). So, addition of Zr and Fe reduced the value of bending strength. Chen et al. (Chen *et al.*, 2006) claimed the compression strength of Ti-xMo (x=5-20) (1546-1876) MPa which is similar to our alloy Ti-12Mo and Ti-15Mo bending strength value.

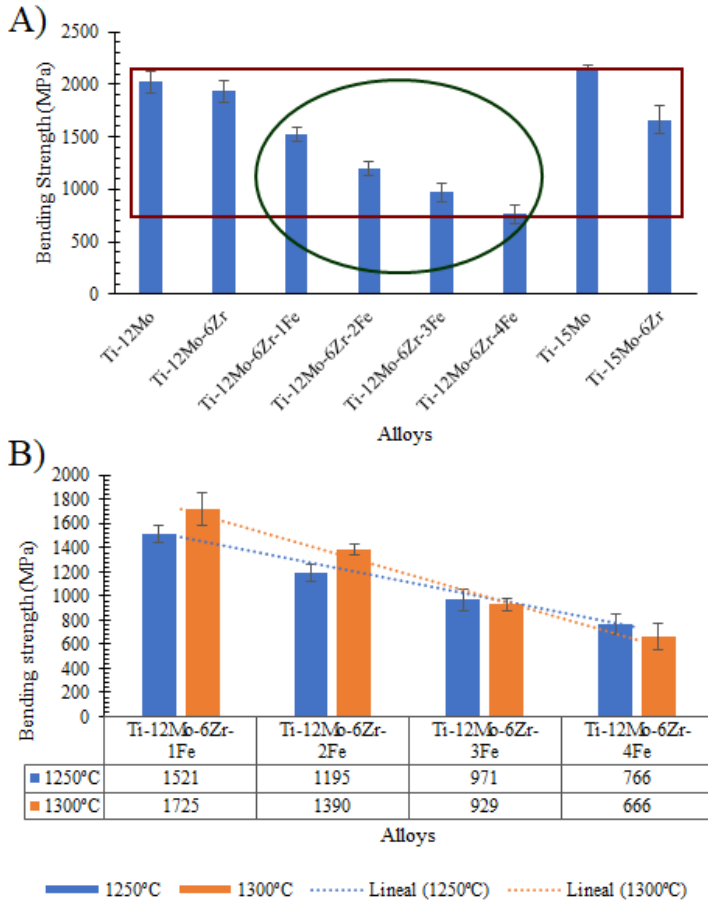


Figure 5.3: (A) Bending strength of Ti-Mo alloy (B) Bending strength of Ti-Mo-Zr-xFe at different temperatures

Bending strength shows linear trend with the addition of Fe and with the both temperature, which is clearly shown by figure 5.3 (B). Bending strength is more with higher temperature for Ti-12Mo-6Zr-1Fe and Ti-12Mo-6Zr-2Fe. The value is less with higher temperature for Ti-12Mo-6Zr-3Fe and Ti-12Mo-6Zr-4Fe which is clearly shown in figure 6.5. Value is least for Ti-12Mo-6Zr-4Fe for both temperature which is 766 and 666 MPa for 1250°C and 1300°C respectively and maximum is for Ti-12Mo-6Zr-1Fe for both sintering temperature which is 1521 and 1725 MPa for 1250°C and 1300°C respectively. (Ho, Wu, Hsu, *et al.*, 2012) also claimed that bending strength for Ti-10Zr and Ti-10Zr-xMo have higher bending strength (1472-2098) MPa which is higher than bending strength of Ti C.P which is 844 MPa.

Elastic modulus is the main mechanical properties for biomaterial; and should be lower/ like bone which should be in between (17-28) GPa; which is suggested by different scientists Niinomi *et al.* (Niinomi, 1998; Nag, Banerjee and Fraser, 2007; Geetha *et al.*, 2009; Ho, Wu, Hsu, *et al.*, 2012). Minimum value is for Ti-12Mo-6Zr-3Fe with both sintering temperature (1250°C and 1300°C) which is approx.95 GPa and maximum is for Ti-12Mo which is approx.105 GPa. Elastic modulus for Ti-15Mo is lower than Ti-12Mo; maybe the decrement of elastic modulus in Ti-15Mo is due to  $\beta$ -character of more % of Mo which is also confirmed by different scientist (Chen *et al.*, 2006; Lu *et al.*, 2013b). Addition of Fe causes decrement in elastic modulus and the nature is decreasing order for Ti-12Mo-6Zr-xFe (x=1-3) but for Ti-12Mo-6Zr-4Fe elastic modulus is more than Ti-12Mo-6Zr-3Fe and trend change. The range of elastic modulus is between (95-105) GPa for our alloys which is denoted by rectangle box in figure 5.4 (A). In previous studies elastic modulus of  $\beta$ -alloy is in between (55-124) GPa (Nag *et al.*, 2005; Geetha *et al.*, 2009). These values are less than  $\alpha$  and ( $\alpha + \beta$ ) alloys (Martins Júnior *et al.*, 2011).

Elastic modulus (EM) shows linear trend with sintering temperature and % of Fe but with Ti-12Mo-6Zr-3Fe there is a change in trend. For higher temperature elastic modulus is more in case of Ti-12Mo-6Zr-1Fe, Ti-12Mo-6Zr-2Fe and Ti-12Mo-6Zr-4Fe. EM is less with higher temperature in case of Ti-12Mo-6Zr-3Fe; shown in figure 5.4 (B) and tabulated below the graph. The least value is for Ti-12Mo-6Zr-3Fe which is 95GPa and it's more suitable as bio-material application due to less requirement of elastic modulus which is confirmed by Niinomi, Geetha *et al.* and Martins *et al.* (Niinomi, 1998; Geetha *et al.*, 2009; Martins Júnior *et al.*, 2011). Elastic modulus value for Ti-Mo alloy is much less than stainless steel(210 GPa),Co-

Cr alloys(240 GPa) pure Ti, Ti-6Al-4V(120 GPa)(Niinomi, 1998) and so on (Geetha *et al.*, 2009; Correa *et al.*, 2018).

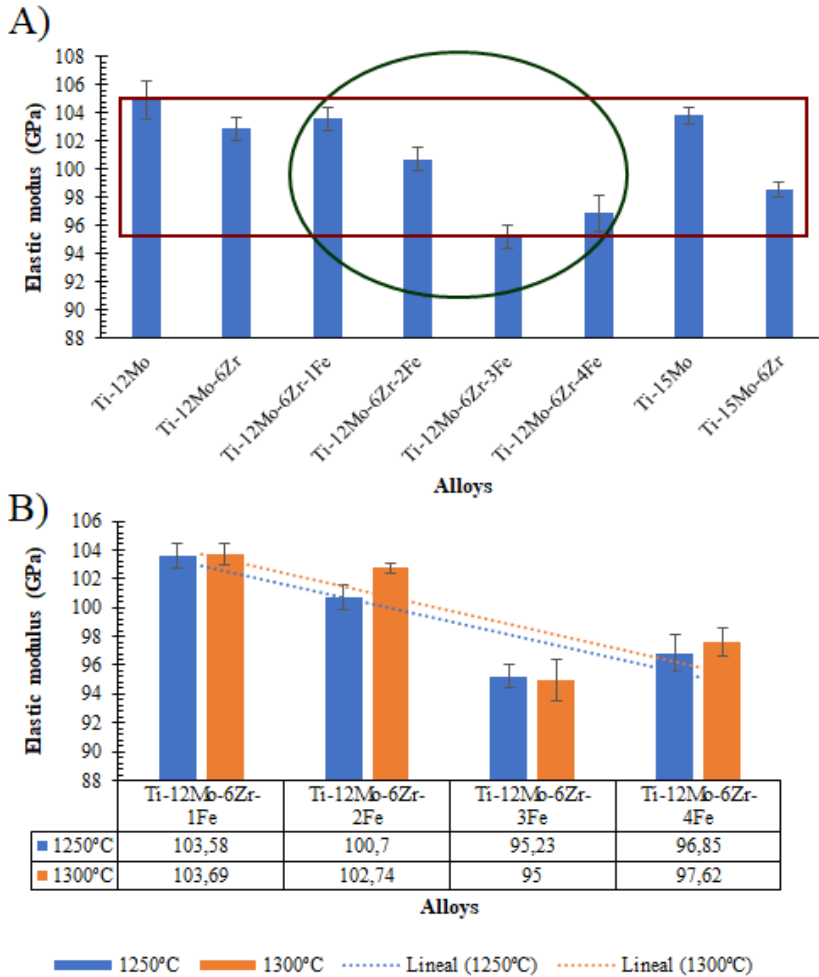


Figure 5.4: (A) Elastic modulus of Ti-Mo alloy (B) Elastic modulus of Ti-Mo-Zr-xFe at different temperatures

Ti-Mo alloys have normally lower elastic modulus who claimed elastic modulus increases upto 6% (for Ti-6Mo is 112 GPa) and then decreases the value till 8% of Mo (82.98 GPa) for Ti-Mo alloy (Zhang *et al.*, 2015). Elastic modulus for Ti-10Zr-

Development of new high-performance Titanium alloys with Fe-addition for dental implants

5Mo and Ti-10Zr-12.5Mo is 87 and 96 GPa respectively (Ho, Wu, Kuang, *et al.*, 2012) which is similar to elastic modulus for Ti-12Mo-6Zr-3Fe with both sintering temperature which is 95 GPa and also this is less than Ti C.P (99 GPa). Elastic modulus with higher content of Mo shows lower value which is also confirmed by Correa *et al.* (Correa *et al.*, 2018). Ti-35Nb-4Sn-6Mo-9Zr have elastic modulus of 68 GPa which is claimed by Dai *et al.* (Dai *et al.*, 2013). Ti-12Mo-5Ta have elastic modulus less than our alloy which is claimed by Gordin *et al.* (Gordin *et al.*, 2005).

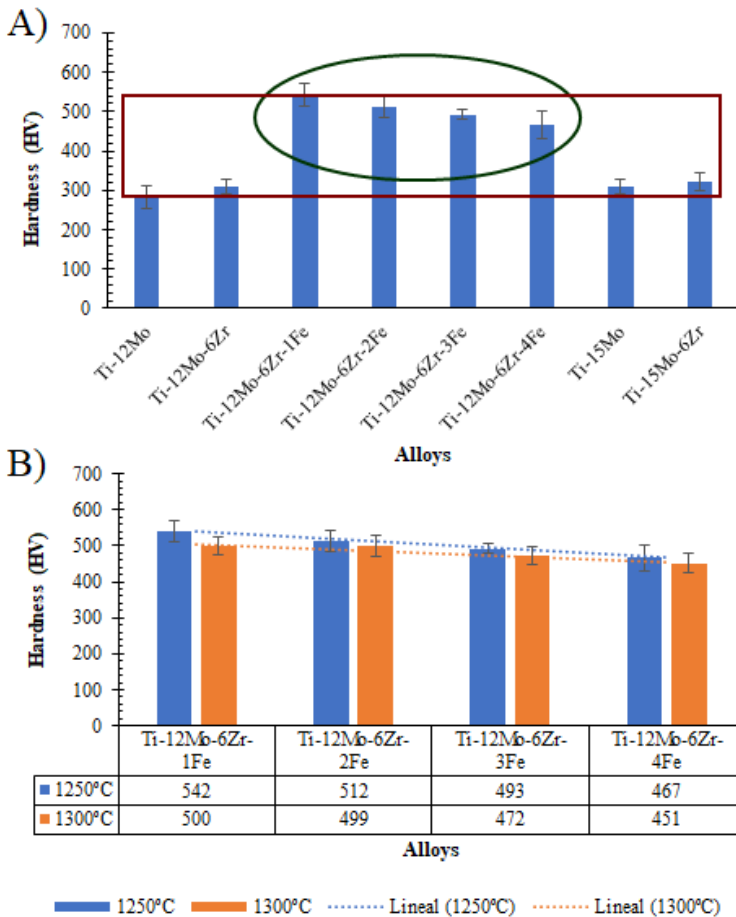


Figure 5.5: (A) Hardness of Ti-Mo alloy (B) Hardness of Ti-Mo-Zr-xFe at different temperatures

Hardness is also an important property for biomaterial application alloys. Hardness is least for Ti-12Mo which is 283 HV and maximum is for Ti-12Mo-6Zr-1Fe (sintered at 1250 °C) which is 542 HV. So, the range of hardness for our alloy is between (283-542) HV which is denoted by rectangle box in figure 5.5 (A). Addition of Zr increases the value of hardness in both binary alloy Ti-12Mo and Ti-15Mo i.e hardness for Ti-12Mo-6Zr (309 HV) is more than Ti-12Mo (283 HV); which is less than 10% and similar is for Ti-15Mo-6Zr. Addition of Fe also increases hardness value with Ti-12Mo-6Zr and for Ti-12Mo-6Zr-1Fe (542 HV) is approx. 64% more than the value of Ti-12Mo-6Zr. More % of Fe decreases the value of hardness shown in figure 5.4 (A).

Ti-12Mo-6Zr-xFe has a decreasing trend of hardness from (x=1-4). Kuroda et al. (Kuroda, Buzalaf and Grandini, 2016) claimed that hardness of Ti-Mo alloys are more than CP Ti, it's due to solid solution hardening effect due to addition of Mo and Zr (Ho, Ju and Chern Lin, 1999). More % of Mo increases the value of hardness, it's due to formation of  $\alpha''$  phase which has higher value of hardness than  $\alpha'$  phase which is confirmed by Kuroda et al.(Kuroda, Buzalaf and Grandini, 2016); maybe for this reason Ti-15Mo have more hardness value than Ti-12Mo. Ti-12Mo-6Zr-4Fe have the less value of hardness in comparison to other quaternary alloys; maybe this is due to more % of  $\beta$ -phase in case of Ti-12Mo-6Zr-4Fe which is also confirmed by Kuroda et al. (Kuroda, Buzalaf and Grandini, 2016). Ti-15Mo have micro-hardness approx. 325 HV after swaging which is claimed by Martins et al.(Martins Júnior *et al.*, 2011).

Hardness shows linear trend with temperature and % of Fe which is clearly shown in figure 5.5 (B). Higher temperature shows less hardness in comparison to lower sintering temperature. More % of Fe has less value of hardness in both cases. So Ti-12Mo-6Zr-4Fe with 1300°C has least hardness among all the quaternary alloys and value is 451 HV. Effect of Fe addition have more effect than sintering temperature. Zardiackas et al. (Zardiackas, Mitchell and Disegi, 2017) claimed that hardness for Ti-15Mo manufactured with multiple vacuum melting technique have hardness value of 291.4 HV which is similar to Ti-15Mo (309 HV) with elemental blend techniques but elastic modulus claimed by Zardiackas et al. (Zardiackas, Mitchell and Disegi, 2017) for Ti-15Mo is 77.7 GPa which is much lower than our alloy Ti-15Mo (103 GPa); it may be due to change in manufacturing process. Micro-hardness for Ti-15Zr-7.5Mo and Ti-15Zr-15Mo which is prepared by argon arc melting are 479 and 398 HV respectively which is claimed by Correa et al. (Correa *et al.*, 2016)

and the value for Ti-15Mo-7.5 Mo is similar value to Ti-12Mo-6Zr-2Fe with 1250°C and 1300°C which is 467 and 451 HV respectively. Elastic modulus for Ti-15Zr-7.5Mo and Ti-15Zr-15Mo which is prepared by argon arc melting are 114 and 74 GPa which is claimed by Correa et al. (Correa *et al.*, 2016) and value of Ti-15Mo-7.5Mo is more in comparison with all the alloys.

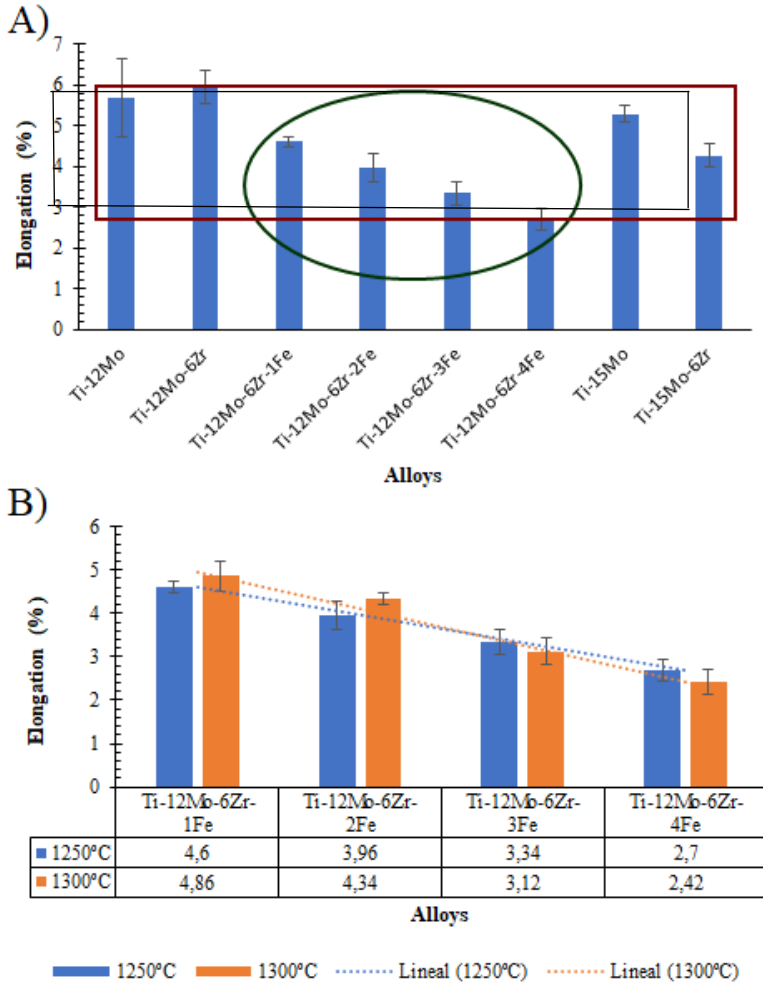


Figure 5.6: (A) Elongation to fracture of Ti-Mo alloy (B) Elongation to fracture of Ti-Mo-Zr-xFe at different temperatures

Elongation is also a main property for all the biomaterials, and it should be in the range of (10-20%) but with powder metallurgy techniques, there is problem in elongation. Elongation is maximum in case of Ti-12Mo-6Zr which is 5.95%. Addition of Zr has different behaviour with Ti-12Mo and Ti-15Mo; for Ti-12Mo the value of elongation increases from (5.67 to 5.95) but for Ti-15Mo the value of elongation decreases with Zr so the value of elongation for Ti-15Mo-6Zr (4.27%) is less than elongation of Ti-15Mo (5.28%). Addition of Fe shows continue decrement with higher % of Fe from (4.60- 2.70%). For our alloys the least value is for Ti-12Mo-6Zr-4Fe with 1300 °C which is 2.42%. The range of elongation for our alloy is between (2.70-5.95) % which is denoted by rectangular box in figure 5.6 (A). TMZF(Ti-12Mo-6Zr-2Fe) annealed have elongation is (18-22)% (Wang, 1996) which is much higher than our elongation values and this is due to different in process.

Addition of Fe shows linear decreasing trend for both the temperature (1250°C and 1300°C) shown in figure 5.6 (B). Ti-28Nb-13Zr-0.5Fe with quenching have the lowest young's modulus (58 MPa) & yield strength (780 GPa) & higher fracture plasticity (13% ) elongation (Cui and Guo, 2009). Ti-15Mo have with multiple vacuum melting techniques have elongation to fracture 20.9% (Zardiackas, Mitchell and Disegi, 2017).

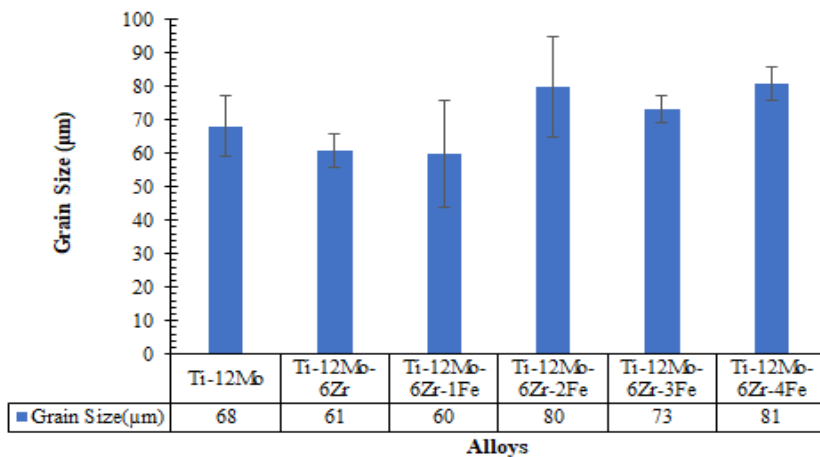


Figure 5.7: Grains size of Ti-Mo alloy

Elongation to fracture for Ti-6Al-4V as cast have 14.6% which is also more than Ti-Mo alloys by powder metallurgy due to brittle/less ductile character with powder metallurgy. Elongation for Ti-6Al-4V with elemental blend is in the range of (8-19)% with hydride-dihydride (HDH) and hunter sponge fines (SP) (Fujita *et al.*, 1996). Elongation of Ti-6Al-4V with conventional elemental blend (EB) is 6%(Liu *et al.*, 2006) which is comparable to our alloys which is also prepared by Elemental blend.

Grain size for Ti-Mo alloys is in range (60-81)  $\mu\text{m}$  shown in figure 5.7. Normally quaternary alloys have more grain size in comparison to binary alloy and ternary alloy but for Ti-12Mo-6Zr-1Fe grain size is in range of 60  $\mu\text{m}$ . Min et al.(Min *et al.*, 2010) claimed that for Ti-15Mo and Ti-15Mo-1Fe grain size is in range of 130  $\mu\text{m}$ .

Ti-6Al-7Nb with powder metallurgy has grain size is in range of (134  $\pm$  17)  $\mu\text{m}$  at sintering temperature 1250°C which is claimed by Bolzoni et al. (Bolzoni *et al.*, 2013) and this value is much more than our alloy.

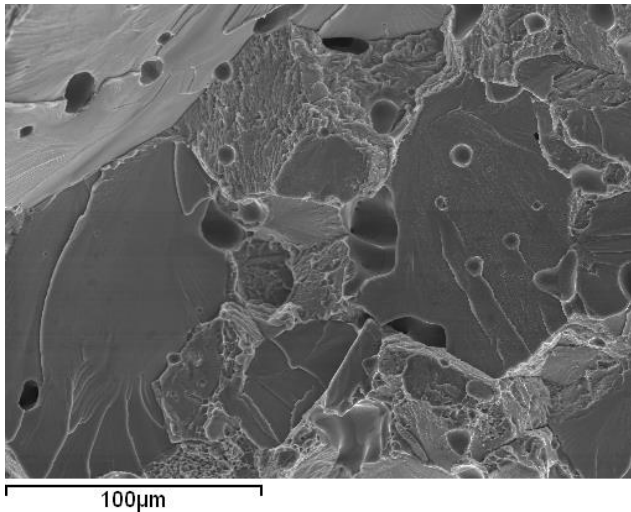


Figure 5.8: Fractography of Ti-12Mo-6Zr-4Fe

Fractography image of Ti-12Mo-6Zr-4Fe reveals that the fracture with higher % of Fe has mainly brittle fracture which is clearly shown in figure 5.8. Formation of dimples in case of binary and ternary alloys so the fracture is mixed type i.e; (brittle+ductile) fracture which is shown in result part (Figure 4.1). Addition of Fe causes



more cleavage planes and smooth fractured surface which causes more brittleness. As per increment of % of Fe have more brittle surface; shown in figure 4.2. Zr-12Mo-xTi prepared by vacuum arc melting have mixed type of fracture i.e; brittle and plastic mechanism which is confirmed by Nie et al. (Nie *et al.*, 2014). Ti-15Mo-6Zr prepared by powder metallurgy technique have cleavage facets which indicates reduced ductility and Ti-15Mo-6Zr-xCr have few dimples and cleavage structure which causes mixed type of fracture brittle and plastic mechanism which confirmed by Elshalakany et al. (Elshalakany *et al.*, 2017). Fracture characteristics of these alloys are like our alloys which is prepared by powder metallurgy technique. Ti-8Mo-12Fe prepared with powder metallurgy using vacuum sintering between 1423k-1523k have brittle structure confirmed by Tsai et al. (Tsai *et al.*, 2012).

Grain size is irregular i.e some are bigger, and some are smaller.  $\beta$ -phase are found mostly in the alloy, but  $\alpha$ -phase are found on the grain boundary of the alloy. Mixing of the element is homogeneous which is confirmed by the EDS analysis which is also confirmed by figure 4.5. Increase in % of Fe causes more porosity which also seen in figure 4.4. Porosity is normally circular in shape and some are also irregular shape. Ti-12Mo and Ti-15Mo have less porosity found on the surface in comparison to Ti-12Mo-6Zr and Ti-15Mo-6Zr which can see by figure 4.3.

Number of grains decreases with higher % of Fe for Ti-12Mo-6Zr-xFe (x=1-4) alloy and grain size increases which is seen in figure 4.4.  $\beta$ -phase increases with higher % of Fe and addition of Zr and Fe to Ti-Mo and Ti-Mo-6Zr also improves the  $\beta$ -phase which is confirmed by XRD analysis (as shown in figure 5.6) and EBSD analysis (tabulated in 4.29). For quaternary alloys like Ti-12Mo-6Zr-3Fe;  $\beta$ -phases reaches almost 100%. Average  $\beta$ -phases decreased with higher % of Fe with elemental blend techniques and from EDX analysis; it is also confirmed the good distribution of alloying element from my previous paper (Mohan *et al.*, 2017). Due to solubility of alloying element in Zr, the alloy Zr-12Mo-xTi have equiaxed  $\beta$  crystal grain can be observed (Nie *et al.*, 2014). Microstructure of CP Ti mainly have single-phase  $\alpha$  grains. Ti-35Nb-5.7Ta-7.2Zr (TNTZ) with solution treated at 800°C followed by water quenched (WQ) reveals the presence of equiaxed  $\beta$ -grains (Majumdar, Singh and Chakraborty, 2008). Ti-15Mo is  $\beta$ -alloy with single-phase micro-structure, Ti-6Al-7Nb is ( $\alpha$ +  $\beta$ ) alloy which confirmed by Zardiackas et al. (Zardiackas, Mitchell and Disegi, 1997).

$\alpha$ -phases found mainly on the boundaries as well as the interior of the grain for Ti-15Mo alloy after ageing. The micro-structure of Ti-13Mo-7Zr-3Fe consists primarily

mainly of  $\beta$ -grains with grain boundary  $\alpha$  and some intra-granular  $\alpha$ -precipitation at a relatively coarser scale (Nag *et al.*, 2005). The above microstructure is similar to our alloy with  $\beta$ -grain mainly and  $\alpha$ -phase at grain-boundary for Ti-Mo-Zr-Fe in our case.

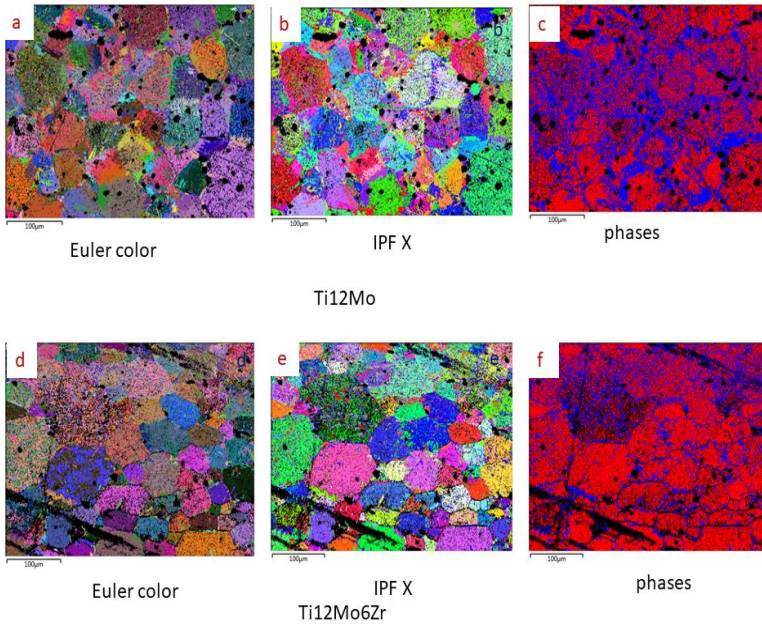


Figure 5.9: Euler color image of Ti12Mo (a) IPF X image of Ti12Mo (c) Phases image of Ti12Mo (d) Euler color image of Ti12Mo6Zr (e) IPF X image of Ti12Mo6Zr (f) Phases image of Ti12Mo6Zr

EBSD images of Ti12Mo and Ti12Mo6Zr are shown in figure 5.9, which includes Euler colours, IPF X and phases of the after- sinter. The grains are equiaxed and grain size is different. Some big grains are found near the small grains. Blue lines in phases image indicate the % of  $\alpha$  inside the alloy. So, it can be clearly seen that in case of Ti12Mo; more % of  $\alpha$  available in comparison to Ti12Mo6Zr. That means here Zr acts as  $\beta$ -stabilizer which also confirmed by XRD image of Ti12Mo6Zr in figure 6. With the help of AzTec software we calculated the grain size of Ti12Mo & Ti12Mo6Zr. Overall grain size for Ti12Mo is 6.89  $\mu\text{m}$ ,  $\alpha$  grain size is 4.97  $\mu\text{m}$  and  $\beta$  grain size is 8.59  $\mu\text{m}$ . In case of Ti12Mo6Zr Overall grain size is 6.85  $\mu\text{m}$ ,  $\alpha$  grain size is 6.21  $\mu\text{m}$  and  $\beta$  grain size is 7.47  $\mu\text{m}$ . So, for both alloy grain size for  $\beta$ -grain is larger than  $\alpha$ - grain. In case of Ti12Mo6Zr,  $\beta$  grain size is dominating than

Ti12Mo. We also calculated % of  $\alpha$  and  $\beta$  for Ti12Mo and Ti12Mo6Zr with phases diagram as shown in figure 5.16 (c) for Ti12Mo and 6.16 (f) for Ti12Mo6Zr; so, for Ti12Mo,  $\alpha$  and  $\beta$  are 41.3 and 58.7 % and for Ti12Mo6Zr,  $\alpha$  and  $\beta$  are 27.7 and 72.3 % respectively. So, also from EBSD analysis addition of Zr enhanced the  $\beta$ % as discussed above.

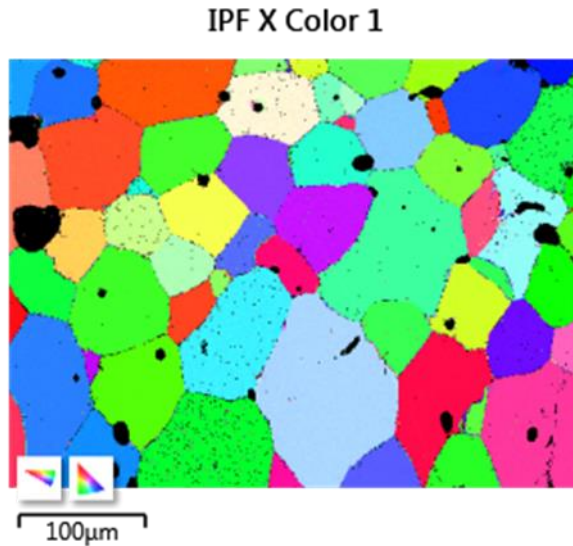


Figure 5.10: IPFX colour image by EBSD analysis of Ti-12Mo-6Zr-3Fe at 1250°C

For Ti-Mo quaternary alloys, mainly phases are  $\beta$ -phases. From the analysis for Ti-12Mo-6Zr-3Fe with both the sintering temperature 1250°C and 1300°C;  $\beta$ -phase available are 99.04% and 99.74% means approx. 100%. Grain size for Ti-12Mo-6Zr-3Fe at 1250°C is 8.46  $\mu\text{m}$  and 1300°C is 9.98  $\mu\text{m}$ . From the analysis, the standard of the element is of factory standard. From the EBSD results of Ti-12Mo-6Zr-2Cr prepared by elemental blend have  $\alpha$ -phase on the grain boundary indicated by the color key of the standard triangle (Elshalakany *et al.*, 2017). The  $(110)_\beta$  and  $(111)_\beta$  are the compact planes in  $\text{Ti}_{84}\text{Mo}_{16}$  nitride structure (Gordin *et al.*, 2010).

From the XRD analysis, it is seen that  $\alpha$ -phases peak are mainly seen for binary alloys like Ti-12Mo and Ti-15Mo but even for ternary alloys like Ti-12Mo-6Zr and Ti-15Mo-6Zr;  $\alpha$ -phase peaks disappear, for quaternary alloys also  $\alpha$ -phase

disappears which shown in figure 4.6. From the XRD analysis, addition of Zr and Fe improves  $\beta$ -phases; for quaternary alloys it is about 100% which is tabulated in 4.9.

Mo is mainly act as  $\beta$ -stabilizer and when 7.5 wt % or more with Ti-10Zr was added,  $\beta$  phase retained with a bcc crystal structure, which confirmed by XRD pattern of Ti-10Zr and Ti-10Zr-xMo alloys (Ho, Wu, Kuang, *et al.*, 2012). XRD results of Ti-15Zr-12.5Mo only exhibited peaks of  $\beta$ -phase which confirmed by Correa *et al.* (Correa *et al.*, 2018). Ti-12Mo-6Zr are strongly affected by the addition of Fe which is discussed in my previous articles (Mohan *et al.*, 2017), when % of Fe addition is 3% or more mainly phases are  $\beta$  phase (BCC crystal structure), it confirms the  $\beta$ -phase stability of Fe; which also shown in figure 4.6. From the analysis of Ti-xMo alloys, only  $\alpha$ -phase is observed in the XRD pattern when the Mo content is 5%, when the Mo content is 10% both  $\alpha$  and  $\beta$  phases are found and when the Mo contents are 15 and 20%, only  $\beta$  phase are found (Chen *et al.*, 2006).

$\beta$ -phases is confirmed by XRD analysis in each alloys Ti-15Mo, Ti-15Mo-5Zr, Ti-15Mo-1Fe and Ti-15Mo-5Zr-1Fe but the athermal  $\omega$  phase is not found (Min *et al.*, 2008). Micro-structure of CP Ti consisted of single-phase  $\alpha$  grains and the XRD patterns also confirmed that the micro-structure of Ti-35Nb-5.7Ta-7.2Zr consists of  $\beta$ -phase (Majumdar, Singh and Chakraborty, 2008).

XRD pattern of the as cast Zr-12Mo-xTi alloys, it is found that the solid-state phase of all samples at room temperature is of  $\beta$ -type Zr. It should also be clear that Ti, Zr and Mo have same structure type, space group and similar crystal lattice, which signifies that all elements maybe completely dissolved each other and form the metastable  $\beta$ -phase at high temperature (Nie *et al.*, 2014).

For homogenised the elements inside the alloy we switch to mechanical mixing procedure. Fluidity of the mechanical alloying powders with short milling time is possible in some of the cases but with PCA; fluidity is not possible. Fluidity of the Ti-15Mo and Ti-15Mo-6Zr-2Fe powders are 1.17 gr/sec and 1.27 gr/sec; shown in table 4.15. Fluidity is the basic analysis of powders for suitability of industrial uses due to its roundness of particle. Fluidity with 180 rpm and 52 min is best for both the alloys. Fluidity with PCA and higher time is more in case of 6h but with 24h milling time fluidity calculation is not possible due to irregular particles with more time. Due to this, we selected for further analysis with this parameter. flowability of Ti, Fe, Zr and Al powder after mechanical alloying from 8h-48h is not found, it's maybe due to humidity of the powder (Chandrasekaran and Xia, 2005).

Granulometry of mixed powder is also basic parameters to understand the powder quality. Particle size of milled powder is minimum in case of 180 rpm and 45 min, and the average particle size in this case is 32.18  $\mu\text{m}$  (shown in figure 4.11). Normally it is found that with same milling speed if we increase milling time the particle size increases and also same for milling speed increase cause more particle size it's may be due to alloy particle do agglomeration cause of more particle size which is also confirmed by Hsu et al. (Hsu *et al.*, 2013) who worked with Ti-7.5Mo; he claimed with 3h-15h milling time particle size is in range of 33.12 and 29.85  $\mu\text{m}$  and with 30h of milling time particle size became 110.12  $\mu\text{m}$ . Powder utility (listed in table 4.22) with higher milling time is very less it's due to more heat generated and more welding with inter-particles and jars. Higher milling time have more oxygen contamination and more metallic welding; due to this powder recovery is less with higher milling time which also confirmed by Nouri et al. (Nouri, Hodgson and Wen, 2011).

Lower milling time (6h) have less agglomeration in comparison to higher milling time (24h) shown in figure 4.13, it's mainly due to more particle inter-reaction with each other by higher milling time. Plastic deformation and cold welding is done with higher milling time. Particle distribution is almost homogeneous with lower milling time (tabulated in 4.25) but with higher milling time more Zr particles are agglomerated with each other. Higher milling time causes more agglomeration which also confirmed by Hosseini et al. (Hosseini-Gourajoubi *et al.*, 2015). Cold welding and agglomeration are major elements during higher milling time which also confirmed by Nouri et al. (Nouri, Hodgson and Wen, 2011; Wang *et al.*, 2016).

Green density for most of the samples are in range of (74.66-78.92) %. More milling time have normally lower relative green density and also lower sintered density listed in table 4.17, 4.20 and 4.26, it's maybe due to higher milling time causes more energy with the powder which creates more friction and more inter-particles collision (Nazari, Nouri and Hilditch, 2015) by which agglomerated particles can't move and deform effectively which inhibit dense packing. Sintered samples with higher milling time have normally lower sintered density which is due to higher milling time have larger particle size; lower milling time have less particles size which have close power particles which accelerates diffusion during sintering process and improves relative sintered density (Hsu *et al.*, 2013).

Bending strength of Ti-15Mo sintered alloy is maximum with lower milling time like with 180 RPM and 45 Min which is 1597 MPa and with 180 rpm-52 min the

value of bending strength is 1261 MPa but this value is lower in comparison with elemental blend alloys. Addition of Fe and Zr reduces the value of bending strength of ternary alloy and quaternary alloy with the same milling condition shown in table 4.17 and 4.20. Bending strength for Ti-15Mo-6Zr is 1167 MPa and with addition of (2 and 4) % Fe; bending strength decreases more; the value is 667.6 and 476.3 MPa respectively. This property is like elemental blend sintered samples. Increment in milling time with PCA reduced the value of bending strength listed in 4.26. Higher milling time decreases yield strength, it's may be due to less packing density and agglomeration phenomena occurs which is also confirmed by Nazari et al. (Nazari, Nouri and Hilditch, 2015).

Hardness value of MA samples is in range of (180.6-183.8) HV with 180 rpm -52 min. Minimum value is for Ti-12Mo-6Zr and maximum is for Ti-15Mo-6Zr. Ti-Mo alloys with hot pressing have microhardness value of 460HV<sub>0.3</sub> which is triple to Ti- $\alpha$  180 HV<sub>0.3</sub> confirmed by Sochacka et al. (Sochacka, Miklaszewski and Jurczyk, 2019). More milling causes more hardness due to more strength hardening in this case which also confirmed by Nouri et al. (Nouri, Hodgson and Wen, 2011) who worked with Ti-16Sn-14Nb with 10h and 20h milling time and he claimed 40% more hardness when he increased time from 10h-20h.

Elastic modulus is a major mechanical property for biomaterials. Elastic modulus is minimum in case of Ti-15Mo with 300 rpm-52min (62.90 GPa) which is better for our uses and with Zr and Fe addition the value increase which causes more elastic modulus to like for Ti-15Mo-6Zr-2Fe with 180 rpm-45min have 76.89 GPa. Higher milling time have no significant effects on elastic modulus but with higher ball size (10mm dia.), the elastic modulus is little bit less 89.32 GPa. The range of elastic modulus of Ti-7.5Mo with different milling time is very less (0.5-3.75) GPa claimed by (Hsu *et al.*, 2013). Al-4Cu, Al-4Cu/2TiO<sub>2</sub> and Ti-4Cu/8TiO<sub>2</sub> with 300 rpm-16h have elastic modulus increasing with higher TiO<sub>2</sub> have more elastic modulus claimed by (Ashuri and Hassani, 2014). By increasing Mo% the value of elastic modulus is more as claimed by Sochacka et al. (Sochacka, Miklaszewski and Jurczyk, 2019).

For achieving 100% sintered density we must move to move from mechanical alloying to Spark Plasma Sintering (SPS) process. So, for this process we are using mechanically alloyed powder with 180 rpm-52 min. From table 4.27, it is shown that sintered density of Ti-15Mo-6Zr with 1200 °C sintering temperature is maximum which is 98.57% as shown in figure 5.11 and for other alloy with different condition (alloy and sintering temperature) is also in range of (97.24-98.57) %.

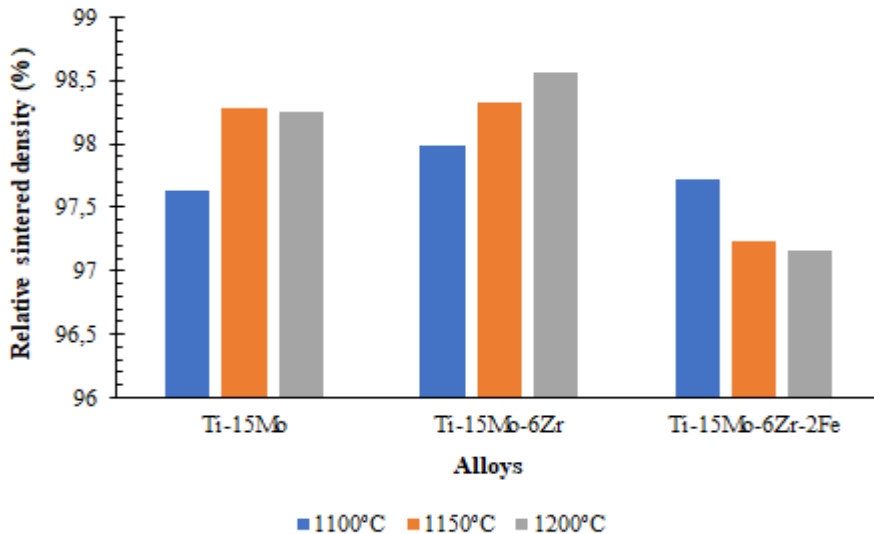


Figure 5.11: Relative sintered density of SPS samples with different sintering samples

Normally relative density increases with sintering temperature for a fixed time (5 min.) and pressure (77 MPa). The maximum relative density of 99.5% should be reached for Mo samples at a sintering temperature of 1950 °C (Mouawad *et al.*, 2012).

Relative density of Cu-Cr composites is in the range of (94.7-95.4) % which is lower than pure Cu (97.6%) and they also confirmed that by increasing the sintering temperature, higher densification can be obtained (Fang *et al.*, 2015). Al-15w% boron carbide-1.5% Co alloy produced by SPS method has (99.3±0.8)% relative sintered density in comparison to theoretical density (Ghasali, Alizadeh and Ebadzadeh, 2016)%. Ti-35Nb-7Zr with 1050 °C sintering temperature, 40 MPa and 5 Minutes holding time has a relative sintered density of 99.5% claimed by HE *et al.* (HE *et al.*, 2017). Ti-6Al-4V with 50MPa, 10 min. holding time and 1000 °C has a relative sintering density of 99.54% claimed by Eso *et al.* (Eso, Ranti and Victoria, 2019). Higher sintering has more relative sintered density for Ti-Al-Mo-Si-Ni alloy as claimed by Kanyane *et al.* (Kanyane *et al.*, 2019) and he also claimed that with higher sintering temperature, hardness value is more due to higher sintered density.

Bending strength of Ti-15Mo is higher (1006 MPa) with sintering temperature 1150 °C. Addition of Zr and Fe decreases the value of bending strength, which is clearly shown by figure 5.12. Bending strength of Ti-15Mo-6Zr-2Fe has a value of 301 MPa

with 1200 °C which is almost 70% less than value of Ti-15Mo. Bending strength is lesser due to carbon deposit on upper layer of surface. With increasing temperature bending strength decreases but with medium sintering temperature 1150 °C has more bending strength in case of Ti-15Mo and Ti-15Mo-6Zr. Addition of Zr to Ti-15Mo reduces bending strength to 40%. Lower relative sintered density also have less bending strength which also confirmed by Feng et al. (Feng *et al.*, 2004) who worked with 10% TiB reinforcement.

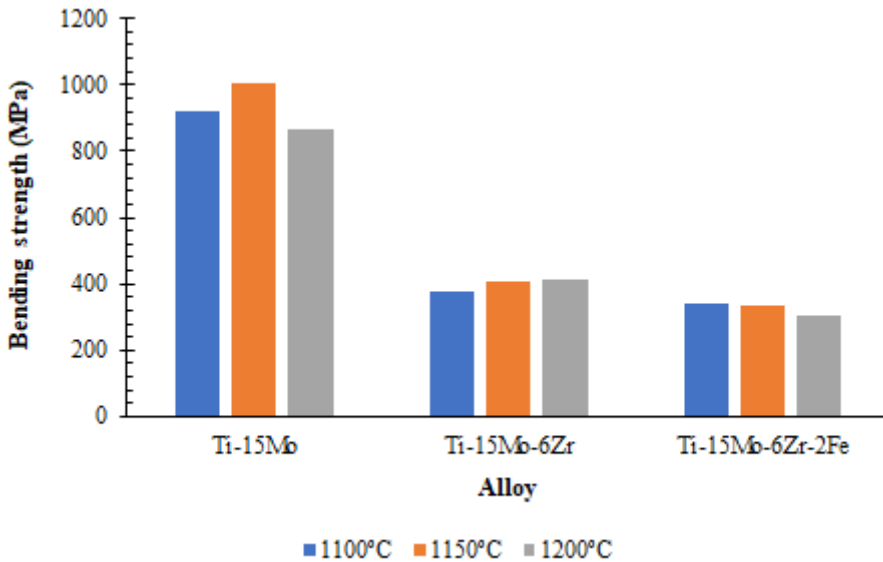


Figure 5.12: Bending strength of SPS samples with different sintering samples

Compressive flexural strength of Ti-6Al-4V with 1000°C, 50 MPa compaction pressure and 5 min holding time is 1414 MPa, he claimed with higher compaction pressure strength increases (Garbiec, Siwak and Mróz, 2016). Bending strength with elemental blend is more in comparison to both mechanical alloying and spark plasma sintering process for same alloy.

Elastic modulus for Ti-15Mo with SPS is minimum among all the alloys which is 88.24 GPa. Addition of Zr and Fe reduces the value of elastic modulus shown in figure 5.13. Maximum value is for Ti-15Mo-6Zr-2Fe with 1100 °C which is 106 GPa approx. Normally higher sintering temperature reduces elastic modulus but here in some cases it's not suitable. Some authors used less sintering temperature of 600 °C,



less holding time (3 minutes) and less compaction pressure for reduced the elastic modulus of Ti-alloy with SPS process which is 16-18 GPa claimed by Kon et al. (Kon, Hirakata and Asaoka, 2004). Ti-Fe-Mo-B with 1000 °C sintering temperature, 20 MPa pressure with SPS process have elastic modulus 137 GPa claimed by Feng et al.(Feng *et al.*, 2004).

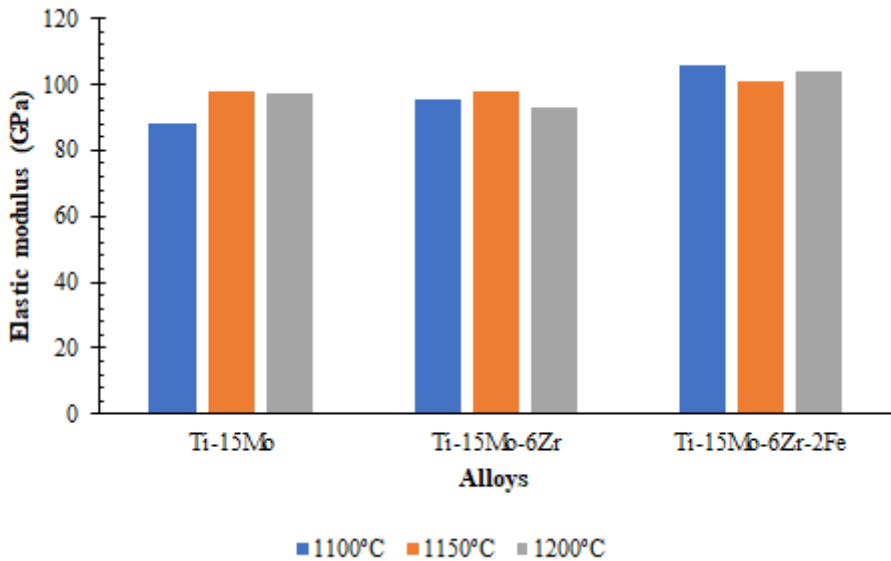


Figure 5.13: Elastic modulus of SPS samples with different sintering samples

Hardness value normally increases with addition of Zr and Fe shown in figure 6.21. Increasing in sintering temperature also improves hardness which may be due to strength hardening effect with higher sintering temperature. Hardness of Ti-15Mo is minimum which is 275 HV with 1100°C and maximum is for Ti-15Mo-6Zr-2Fe which is 477 HV with sintering temperature 1150°C. Hardness values slightly decreases with increasing in sintering temperature which claimed by Mouawad et al.(Mouawad *et al.*, 2012) who worked with Mo by SPS process (1850 °C sintering temperature, 30 min holding time and 77 MPa pressure). In our case also sintering temperature 1200 °C have lesser hardness in comparison with other but with Ti-15Mo-6Zr-2Fe, it's not valid. Some authors claimed that with lower sintering temperature less presence of  $\alpha$ -phase is more and with higher temperature more  $\beta$ -phase found and very little  $\alpha$ -phase found; due to higher  $\beta$ -phase the value of micro-

hardness is more (Bhushan *et al.*, 2018). Microhardness of Ti-6Al-4V with addition to Ni-Ta have higher micro-hardness (389 to 480.2 HV0.1), it may be due to uniform distribution of reinforced particles inside the sintered alloy (Eso, Ranti and Victoria, 2019).

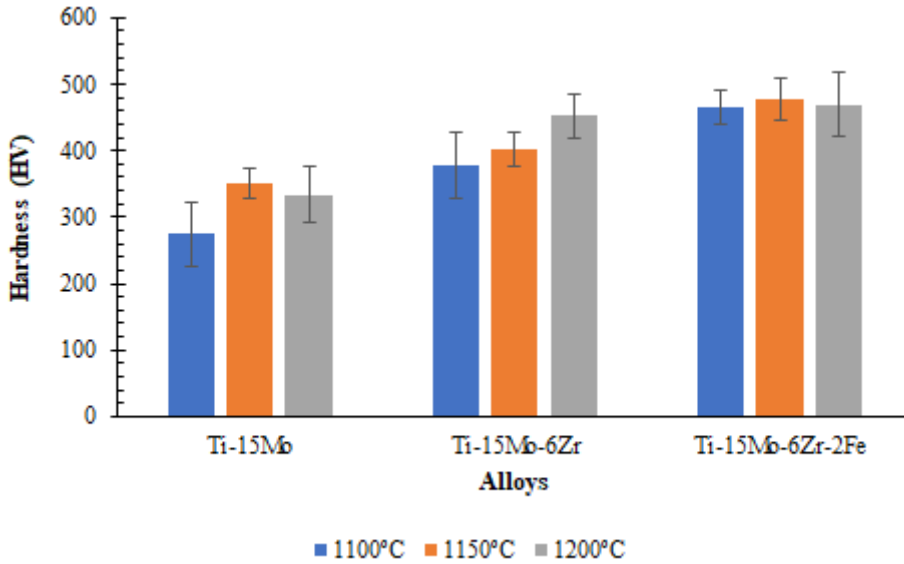


Fig.5.14: Hardness of SPS samples with different sintering samples

From the XRD analysis it is known that sintered samples of Ti-15Mo and Ti-15Mo-6Zr have both  $\alpha$  and  $\beta$  phases shown in figure 4.15. Higher sintering temperature have more  $\beta$  phases in comparison to lower sintering temperature with both samples with different sintering temperatures and some authors also confirmed this (Bhushan *et al.*, 2018) who worked with Ti-Nb-Zr-Ta.

EBSD analysis is important to know morphological character, grain structure, orientation etc. From the analysis for all alloys Ti-15Mo, Ti-15Mo-6Zr and Ti-15Mo-6Zr-2Fe with 1150 °C have higher  $\beta$ -phases in all cases. Due to highest  $\beta$ -phase present with sintering temperature 1150 °C; mechanical properties are better with this temperature in most of the cases. Grain size with SPS process is lower in comparison with other process and mostly have only  $\beta$ -phase. The value is in range of (4.88-6.8)  $\mu\text{m}$ ; tabulated in table 4.31. Fe-14Cr-0.25Y2O3-0.4Ti by SPS process with 1150 °C sintering temperature, 5 Minutes holding time have irregular grain

structure with average grain size by EBSD techniques is in range of (0.5-15)  $\mu\text{m}$  claimed by Huang et al. (Huang *et al.*, 2017) and it's similar to our results with EBSD.

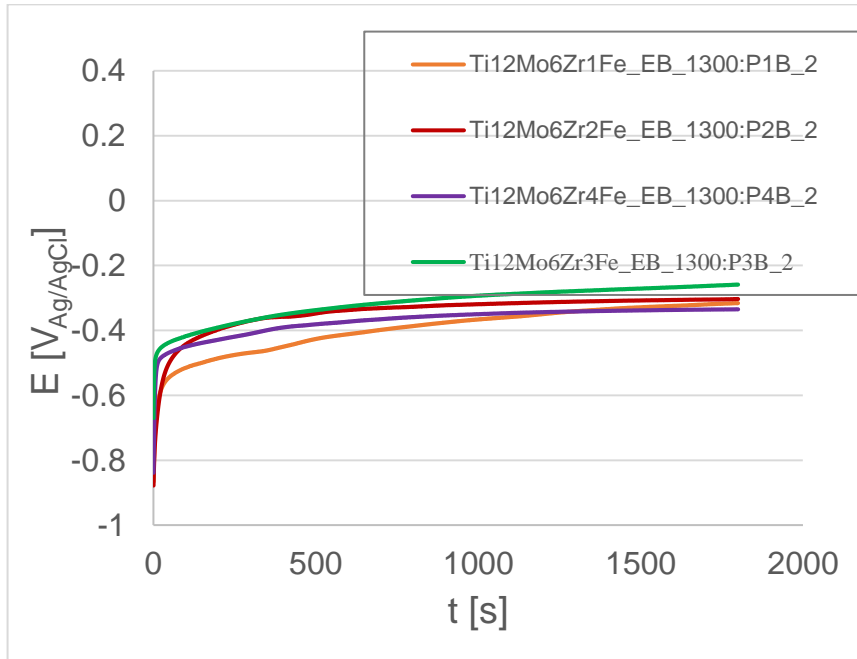


Fig.5.15:  $E_{\text{corr}}$  of EB samples with 1300 °C sintering samples

$I_{\text{corr}}$ ,  $E_{\text{corr}}$  calculated by potentiodynamic test tabulated in table 4.32 and for all of our samples  $I_{\text{corr}}$  ( $4.08 \cdot 10^{-6}$  to  $2.15 \cdot 10^{-8} \text{ A/cm}^2$ ) and  $E_{\text{corr}}$  (-0.13 to -0.59V) low in comparison to crystalline Ti ( $I_{\text{corr}} = 1.49 \cdot 10^{-5} \text{ A/cm}^2$ ,  $E_{\text{corr}} = -0.47\text{V}$ ) and for Ti-6Al-4V ( $I_{\text{corr}} = 1.06 \cdot 10^{-5} \text{ A/cm}^2$ ,  $E_{\text{corr}} = -0.46\text{V}$ ) (Niespodziana, Jurczyk and Jurczyk, 2008) which signifies that our alloy is more corrosion resistant in comparison to pre Ti and Ti-6Al-4V. With increasing Fe with same sintering temperature (1300 °C) the value of  $I_{\text{corr}}$  decreases which means addition more Fe makes the samples more corrosion resistant.  $E_{\text{corr}}$  with higher % of Fe also decreases but with 3Fe (shown in figure 5.15); the value is least which makes it more suitable. SPS samples have less  $I_{\text{corr}}$  and  $E_{\text{corr}}$  in comparison to other process like EB and MA which make SPS more corrosion resistant and more suitable alloy for biomedical application. Result by (MA + PCA) have inferior results with comparison to other results. Samples with higher  $\beta$ -phase have more corrosion resistance which also can be seen in our results and it's also confirmed by Nishimura (Nishimura, 2011); who worked with 3Mo-

5Fe-Ti and have OCP value is in range of (0.24-0.25)V and for our alloy with SPS process have -0.13 V which is very high than pure Ti (-0.71V) which makes our alloys more corrosion results due to less  $I_{\text{corr}}$ , more  $E_{\text{corr}}$  and higher OCP.

Ti-10Zr-5Nb-5Ta with casting process have  $E_{\text{corr}}$  (-0.45V); which is less than our alloy which is in range of (-0.13 - 0.59) V,(Raducanu *et al.*, 2011) mostly alloys have more value but mechanical alloying process with PCA have less value and  $I_{\text{corr}}$  ( $6.5 \cdot 10^{-5}$ ) which is more than our alloys ( $4.08 \cdot 10^{-6}$  to  $2.15 \cdot 10^{-8}$  A/cm<sup>2</sup>); our alloys are more suitable for biomedical application. For Ti-15Mo with different concentration of fluoride ions have  $I_{\text{corr}}$  is in range of ( $3.1 \cdot 10^{-7}$ ) and  $E_{\text{corr}}$  is in range of (-0.275 V)(Kumar and Narayanan, 2008) which is comparable to our results; which can be better alternative for dental implants.

Addition of more Fe (1-3) w% increases ion release rate of Ti which is not good for the biomedical application which is also discussed by Raducanu et al. (Raducanu *et al.*, 2011) but with 2Fe by elemental blend with 1300°C have less ion release rate in comparison to 2Fe. SPS have less ion release rate in comparison to mechanical alloying samples which make SPS process more suitable for biomedical applications. Samples with MA+PCA have very higher ion release rate which is not good for biomaterial.

# Chapter 6: Conclusion

## 6.1: By Elemental Blend (EB) process:

- Porosity is significantly lower at the higher sintering temperature (1300 °C), More % of Fe for Ti-12Mo-6Zr-xFe(x=1,2,3,4) means more porosity.
- Bending strength for binary (Ti-Mo) alloys is larger than in ternary (Ti-12Mo-6Zr) and quaternary alloys (Ti-12Mo-6Zr-xFe). In case of quaternary alloys (Ti-12Mo-6Zr-xFe(x=1,2,3,4); more % of Fe have less bending strength with both sintering temperatures (1250 °C and 1300 °C).
- Hardness for quaternary alloys is higher comparison to binary and ternary alloys. With higher % of Fe the value of hardness is decreasing.
- Quaternary alloys have least elastic modulus in comparison to binary and ternary alloys.
- Grain size of the sintered samples are in the range of (60-81)  $\mu\text{m}$  with optical microscopy method but with EBSD method grain size minimized to 10  $\mu\text{m}$ . Grain size is higher with optical microscopy due to grain size measured only by grain boundary but with EBSD grains measured inside the grains also like sub-grains, so value is low in comparison to optical microscopy.
- Fractography character of the sintered surface is of mixed type (ductile+ brittle).
- Fe acts as  $\beta$ -stabilizing element, Quaternary alloys have highest  $\beta$ -phase; for Ti-12Mo-6Zr-3Fe  $\beta$ -phase is (98.92%) which is almost 100%, For Ti-12Mo  $\alpha$ -phase % is 53.7 and  $\beta$ -phase % is 46.3 and for Ti-15Mo  $\alpha$ -phase % is 50.61 and  $\beta$ -phase % is 49.39 it shows that binary alloys have mixed type of structure ( $\alpha + \beta$ ) which is confirmed by XRD analysis;

- From the EBSD analysis of the samples, it is confirmed that increasing in sintering temperature improves  $\beta$ -phase % significantly.

## **6.2: By Mechanical alloying (MA) process:**

- Mechanical alloying samples have more porosity in comparison to elemental blend samples; it's due to plastic deformation occurring in mechanical alloying samples which don't allow proper compaction of the milling powders and also there is problem in diffusion of particles between each other during sintering process which causes more porosity.
- Fluidity is maximum with milling speed 180 rpm and milling time 52 min without process control agent (PCA); which makes it suitable for industrial application and further analysis.
- Particle size ( $D_{0.5}$ ) is minimum with milling speed 180 rpm and milling time 52 min without process control agent (PCA); which is 47.73  $\mu\text{m}$  for Ti-12Mo milling powder. Particle size with higher milling time and with process control agent (PCA) is very high (489  $\mu\text{m}$ ) which may be due to more agglomeration.
- Porosity is maximum with milling speed 300 rpm and milling time 52 min without process control agent (PCA) which is approx. 17.64% within all the milling combination and for more porosity elastic modulus and bending strength is also minimum within all samples with this condition.
- Bending strength and hardness is lower for MA samples in comparison to EB process. For Ti-15Mo with EB process bending strength is 2161 MPa but with MA for different combination of milling speed and milling time the maximum value is 1597 MPa. Hardness value for EB process is in range of (283-542) HV but for MA process value is in range of (180-183) HV.

- Normally elastic modulus is lower for MA samples in comparison to EB process (approx. 20-25%); it's maybe due to higher porosity of MA sintered samples in comparison to EB sintered samples.

### **6.3: By Spark plasma sintering (SPS) process:**

- Spark plasma sintering (SPS) process have very less porosity (1-2) % in comparison to elemental blend (2-3.5) % and Mechanical alloying sintered samples (8-17.64).
- Bending strength for Ti-15Mo with 1150 °C sintering temperature have highest bending strength (1006 MPa) among all SPS samples. Ti-15Mo-6Zr and Ti-15Mo-6Zr-2Fe have very less bending strength in comparison to Ti-15Mo.
- Elastic modulus is minimum (88.24 GPa) for Ti-15Mo with 1100°C within all the SPS samples.
- Hardness for Ti-15Mo alloy is less in comparison to Ti-15Mo-6Zr and Ti-15Mo-6Zr-2Fe. Ti-15Mo-6Zr-2Fe with 1150°C have highest microhardness (477 HV).
- By EBSD analysis, it is confirmed that for Ti-15Mo-6Zr-2Fe with 1100°C have 99.95% (almost 100%)  $\beta$ -phase.

### **6.4: From corrosion test:**

- Addition of Fe makes quaternary alloys (Ti-12Mo-6Zr) more corrosion resistant; for example, Ti-12Mo-6Zr-4Fe sintered at 1250°C have least  $I_{\text{corr}}$  ( $1.71 \cdot 10^{-8}$  A/cm<sup>2</sup>), higher  $E_{\text{corr}}$  (-0.11V), higher Open circuit potential(-0.18V) and lower corrosion velocity( 0.13  $\mu\text{m}/\text{year}$ ) which makes this alloy more corrosion resistant and for this reason this alloy may be a promising alloys for bio-medical applications.

- EB process have more corrosion resistant in comparison to MA samples and even in some cases it's better in comparison to SPS. But overall SPS process have more corrosion resistance in comparison to EB and MA process which make SPS process more suitable for biomedical application. Within SPS process for Ti-15Mo-6Zr at 1150 °C sintering temperature samples have better corrosion behavior in comparison to other procedure i.e. least  $I_{\text{corr}}$  ( $2.15 \times 10^{-8}$  A/cm<sup>2</sup>), higher  $E_{\text{corr}}$  (-0.13V), higher Open circuit potential (-0.14V) and lower corrosion velocity (0.17 μm/year) which is comparable to Ti-12Mo-6Zr-4Fe alloy with EB method at 1250 °C sintering temperature.
- So overall Ti-15Mo-6Zr with SPS method at 1150°C sintering temperature and Ti-12Mo-6Zr-4Fe alloy with EB method at 1250°C sintering temperature have better corrosion resistant which make this both alloy suitable for biomedical application.
- SPS have lesser ion release rate in comparison to MA samples and EB samples; which make SPS process more suitable in comparison to EB and MA process; which is suitable for our alloys.



# Chapter 7: Future Developments:

Based on the results with different fabrication process with different parameters we can do future advancement of our research:

- We can work with more sintering temperature like 1350 °C for better results.
- Transmission electron microscopy (TEM) should be performed for some selective samples like Ti-12Mo-6Zr-4Fe and for some SPS samples for detection of hcp  $\omega$ - phases.
- We can change milling time (18h,30h) and with changing Process control agent (PCA) like calcium(Ca), sodium chloride (NaCl) and wax for better understanding the effect of PCA and to maximize the powder utility and quality of milling powders for mechanical alloying techniques and with this milling powder. We can do SPS process with more alloys like for Ti-12Mo,Ti-12Mo-6Zr and Ti-12Mo-6Zr-4Fe with same sintering temperatures (1100 °C,1150 °C and 1200 °C), holding time (5 minutes) and pressure(50 MPa) for better understanding of this process; because SPS have better results in comparison to elemental blend and mechanical alloying samples.
- We can do in-vitro test (Bio-compatibility test) of some samples like SPS sample of Ti-15Mo-6Zr with 1150°C sintering temperature and Ti-12Mo-6Zr-4Fe alloy with EB method at 1250°C sintering temperature due to its better corrosion results.

Development of new high-performance Titanium alloys with Fe-addition for dental implants

# References

- Abdel-Hady, M., Hinoshita, K. and Morinaga, M. (2006) 'General approach to phase stability and elastic properties of  $\beta$ -type Ti-alloys using electronic parameters', *Scripta Materialia*, 55(5), pp. 477–480. doi: 10.1016/j.scriptamat.2006.04.022.
- Alves, V. A. *et al.* (2009) 'In situ impedance spectroscopy study of the electrochemical corrosion of Ti and Ti-6Al-4V in simulated body fluid at 25 °C and 37 °C', *Corrosion Science*. Elsevier Ltd, 51(10), pp. 2473–2482. doi: 10.1016/j.corsci.2009.06.035.
- Ashida, S., Kyogoku, H. and Hosoda, H. (2012) 'Fabrication of Ti-Sn-Cr Shape Memory Alloy by PM Process and its Properties', *Materials Science Forum*, 706–709, pp. 1943–1947. doi: 10.4028/www.scientific.net/MSF.706-709.1943.
- Ashuri, H. and Hassani, A. (2014) 'Characterization of severely deformed new composites fabricated by powder metallurgy including a stage of mechanical alloying', *Journal of Alloys and Compounds*. Elsevier B.V., 617, pp. 444–454. doi: 10.1016/j.jallcom.2014.08.031.
- Bao, Y. *et al.* (2014) 'High strength, low modulus and biocompatible porous Ti-Mo-Fe alloys', *Journal of Porous Materials*, 21(6), pp. 913–919. doi: 10.1007/s10934-014-9837-0.
- Basu, B. (no date) 'Some fundamentals on Spark Plasma Sintering as a processing tool to fabricate Biomaterials', *Materials Science*, p. 44.
- Benjamin, J. (1976) 'Mechanical alloying', *Scientific American*, pp. 40–48. doi: 10.1016/S0026-0657(00)86280-3.
- Bertrand, E. *et al.* (2010) 'Synthesis and characterisation of a new superelastic Ti-25Ta-25Nb biomedical alloy', *Journal of the Mechanical Behavior of Biomedical Materials*. Elsevier Ltd, 3(8), pp. 559–564. doi: 10.1016/j.jmbbm.2010.06.007.
- Bhushan, B. *et al.* (2018) 'Fabrication and Characterization of a New Range of  $\beta$ -type Ti-Nb-Ta-Zr-xHaP (x=0, 10) Alloy by Mechanical Alloying and Spark Plasma Sintering for Biomedical Applications', *Materials Today: Proceedings*. Elsevier Ltd, 5(14), pp. 27749–27756. doi: 10.1016/j.matpr.2018.10.010.
- Bolzoni, L. *et al.* (2013) 'Mechanical behaviour of pressed and sintered CP Ti and

Ti-6Al-7Nb alloy obtained from master alloy addition powder', *Journal of the Mechanical Behavior of Biomedical Materials*. Elsevier, 20, pp. 149–161. doi: 10.1016/j.jmbbm.2012.08.022.

Brailovski, V. *et al.* (2011) 'Bulk and porous metastable beta Ti-Nb-Zr(Ta) alloys for biomedical applications', *Materials Science and Engineering C*. Elsevier B.V., 31(3), pp. 643–657. doi: 10.1016/j.msec.2010.12.008.

Chandrasekaran, M. and Xia, Z. S. (2005) 'Effect of alloying time and composition on the mechanical properties of Ti alloy', *Materials Science and Engineering A*, 394(1–2), pp. 220–228. doi: 10.1016/j.msea.2004.11.056.

Chen, Y. Y. *et al.* (2006) 'Microstructures and properties of titanium alloys Ti-Mo for dental use', *Transactions of Nonferrous Metals Society of China (English Edition)*, 16(SUPPL.), pp. 2–6. doi: 10.1016/S1003-6326(06)60308-7.

Correa, D. R. N. *et al.* (2016) 'Tribocorrosion behavior of  $\beta$ -type Ti-15Zr-based alloys', *Materials Letters*. Elsevier, 179, pp. 118–121. doi: 10.1016/j.matlet.2016.05.045.

Correa, D. R. N. *et al.* (2018) 'Development of Ti-15Zr-Mo alloys for applying as implantable biomedical devices', *Journal of Alloys and Compounds*. Elsevier B.V., 749, pp. 163–171. doi: 10.1016/j.jallcom.2018.03.308.

Cui, W. F. and Guo, A. H. (2009) 'Microstructures and properties of biomedical TiNbZrFe ??-titanium alloy under aging conditions', *Materials Science and Engineering A*, 527(1–2), pp. 258–262. doi: 10.1016/j.msea.2009.08.057.

Dai, S. J. *et al.* (2013) 'Influence of Zr content on microstructure and mechanical properties of implant Ti-35Nb-4Sn-6Mo-xZr alloys', *Transactions of Nonferrous Metals Society of China (English Edition)*, 23(5), pp. 1299–1303. doi: 10.1016/S1003-6326(13)62597-2.

Dalmau, A. *et al.* (2015) 'Electrochemical behavior of near-beta titanium biomedical alloys in phosphate buffer saline solution', *Materials Science and Engineering C*. Elsevier B.V., 48, pp. 56–62. doi: 10.1016/j.msec.2014.11.036.

Davis, J. (2003) 'Handbook of Materials for Medical Devices', *ASM International*, pp. 205–216. doi: 10.1361/hmmd2003p001.

Delvat, E. *et al.* (2008) 'Microstructure, mechanical properties and cytocompatibility of stable beta Ti-Mo-Ta sintered alloys', *Journal of the Mechanical Behavior of Biomedical Materials*, 1(4), pp. 345–351. doi: 10.1016/j.jmbbm.2008.01.006.

Drahansky, M. *et al.* (2016) 'We are IntechOpen , the world ' s leading publisher of Open Access books Built by scientists , for scientists TOP 1 %', *Intech*, i(tourism), p. 13. doi: <http://dx.doi.org/10.5772/57353>.

Ekpenyong, C.E., Udokang, N.E., Akpan, E.E., Samson, T. . (2012) 'Double Burden , Non-Communicable Diseases And Risk Factors Evaluation In Sub-Saharan Africa : The Nigerian Experience .', *European Journal of Sustainable development*, pp. 249–270.

Elshalakany, A. B. *et al.* (2017) 'Microstructure and Mechanical Properties of Ti-Mo-Zr-Cr Biomedical Alloys by Powder Metallurgy', *Journal of Materials Engineering and Performance*, 26(3), pp. 1262–1271. doi: 10.1007/s11665-017-2531-z.

Engineering, A. and York, N. (1994) 'Densification and strengthening of silver-reinforced hyd roxya patite- matrix composite prepared by sintering', *Scanning*, 5, pp. 533–542.

Eso, O., Ranti, S. and Victoria, F. (2019) 'ScienceDirect Synthesis of Ni-Ta on Ti-6Al-4V Alloy Using Spark Plasma Sintering', *Materials Today: Proceedings*. Elsevier Ltd., 18, pp. 2250–2256. doi: 10.1016/j.matpr.2019.07.006.

Fang, Q. *et al.* (2015) 'Microstructures and mechanical properties of spark plasma sintered Cu–Cr composites prepared by mechanical milling and alloying', *Materials & Design*. Elsevier Ltd, 88, pp. 8–15. doi: 10.1016/j.matdes.2015.08.127.

Fellah, M. *et al.* (2015) 'Experimental study of new titanium alloy Ti-6Al-4Fe for biomedical application', pp. 540–550.

Feng, H. *et al.* (2004) 'Microstructure and mechanical properties of in situ TiB reinforced titanium matrix composites based on Ti-FeMo-B prepared by spark plasma sintering', *Composites Science and Technology*, 64(16), pp. 2495–2500. doi: 10.1016/j.compscitech.2004.05.013.

Fujita, T. *et al.* (1996) 'Microstructure and properties of titanium alloy produced in the newly developed blended elemental powder metallurgy process', *Materials Science and Engineering A*, 213(1–2), pp. 148–153. doi: 10.1016/0921-5093(96)10232-X.

Gao, Z. *et al.* (2012) 'Preparation and Characterization of Ti-10Mo Alloy by Mechanical Alloying', *Metallography, Microstructure, and Analysis*, 1(6), pp. 282–289. doi: 10.1007/s13632-012-0045-5.

Garbiec, D., Siwak, P. and Mróz, A. (2016) 'Effect of compaction pressure and heating rate on microstructure and mechanical properties of spark plasma sintered Ti6Al4V alloy', *Archives of Civil and Mechanical Engineering*. Politechnika Wroclawska, 16(4), pp. 702–707. doi: 10.1016/j.acme.2016.04.009.

García-Moreno, O. *et al.* (2011) 'Alumina reinforced eucryptite ceramics: Very low thermal expansion material with improved mechanical properties', *Journal of the European Ceramic Society*, 31(9), pp. 1641–1648. doi: 10.1016/j.jeurceramsoc.2011.03.033.

Geetha, M. *et al.* (2009) 'Ti based biomaterials, the ultimate choice for orthopaedic implants - A review', *Progress in Materials Science*. Elsevier Ltd, 54(3), pp. 397–425. doi: 10.1016/j.pmatsci.2008.06.004.

Ghasali, E., Alizadeh, M. and Ebadzadeh, T. (2016) 'Mechanical and microstructure comparison between microwave and spark plasma sintering of Al-B<sub>4</sub>C composite', *Journal of Alloys and Compounds*. Elsevier B.V, 655, pp. 93–98. doi: 10.1016/j.jallcom.2015.09.024.

Gordin, D. M. *et al.* (2005) 'Synthesis, structure and electrochemical behavior of a beta Ti-12Mo-5Ta alloy as new biomaterial', *Materials Letters*, 59(23), pp. 2959–2964. doi: 10.1016/j.matlet.2004.09.064.

Gordin, D. M. *et al.* (2010) 'Microstructural characterization of nitrided beta Ti-Mo alloys at 1400 °C', *Materials Characterization*. Elsevier Inc., 61(3), pp. 376–380. doi: 10.1016/j.matchar.2009.12.010.

Guo, S. *et al.* (2013) 'Microstructural evolution and mechanical behavior of metastable  $\beta$ -type Ti–25Nb–2Mo–4Sn alloy with high strength and low modulus', *Progress in Natural Science: Materials International*. Elsevier, 23(2), pp. 174–182. doi: 10.1016/j.pnsc.2013.03.008.

Guo, S. *et al.* (2014) 'Effect of sintering processing on microstructure, mechanical properties and corrosion resistance of Ti-24Nb-4Zr-7.9Sn alloy for biomedical applications', *Journal of Alloys and Compounds*. Elsevier B.V., 597, pp. 211–216. doi: 10.1016/j.jallcom.2014.01.087.

Hanawa, T. (2006) 'Recent Development of New Alloys for Biomedical Use', *Materials Science Forum*. Trans Tech Publications Ltd, 512, pp. 243–248. doi: 10.4028/www.scientific.net/MSF.512.243.

- Hao, Y. L. *et al.* (2007) 'Elastic deformation behaviour of Ti-24Nb-4Zr-7.9Sn for biomedical applications', *Acta Biomaterialia*, 3(2), pp. 277–286. doi: 10.1016/j.actbio.2006.11.002.
- Hatanaka, S. *et al.* (2010) 'Isothermal Aging Behavior in Ti-10 Cr-Al Alloys for Medical Applications', *Advanced Materials Research*, 89–91, pp. 232–237. doi: 10.4028/www.scientific.net/AMR.89-91.232.
- HE, Z. yuan *et al.* (2017) 'Mechanical and corrosion properties of Ti-35Nb-7Zr-xHA composites fabricated by spark plasma sintering', *Transactions of Nonferrous Metals Society of China (English Edition)*. The Nonferrous Metals Society of China, 27(4), pp. 848–856. doi: 10.1016/S1003-6326(17)60097-9.
- Herr, U. (1995) 'Mechanical Alloying and Milling', *Key Engineering Materials*, 103, pp. 113–124. doi: 10.4028/www.scientific.net/KEM.103.113.
- Ho, W. F. *et al.* (2009) 'Structure, mechanical properties and grindability of dental Ti-10Zr-X alloys', *Materials Science and Engineering C*. Elsevier B.V., 29(1), pp. 36–43. doi: 10.1016/j.msec.2008.05.004.
- Ho, W. F., Wu, S. C., Hsu, S. K., *et al.* (2012) 'Effects of molybdenum content on the structure and mechanical properties of as-cast Ti-10Zr-based alloys for biomedical applications', *Materials Science and Engineering C*. Elsevier B.V., 32(3), pp. 517–522. doi: 10.1016/j.msec.2011.12.003.
- Ho, W. F., Wu, S. C., Kuang, H. S., *et al.* (2012) 'Effects of molybdenum content on the structure and mechanical properties of as-cast Ti-10Zr-based alloys for biomedical applications', *Materials Science and Engineering C*. Elsevier B.V., 32(3), pp. 517–522. doi: 10.1016/j.msec.2011.12.003.
- Ho, W. F., Ju, C. P. and Chern Lin, J. H. (1999) 'Structure and properties of cast binary Ti-Mo alloys', *Biomaterials*, 20(22), pp. 2115–2122. doi: 10.1016/S0142-9612(99)00114-3.
- Hosseini-Gourajoubi, F. *et al.* (2015) 'Effect of process control agents on synthesizing nano-structured 2Mg-9Ni-Y catalyst by mechanical milling and its catalytic effect on desorption capacity of MgH<sub>2</sub>', *Advanced Powder Technology*. The Society of Powder Technology Japan, 26(2), pp. 448–453. doi: 10.1016/j.appt.2014.11.017.
- Hsu, H.-C. *et al.* (2013) 'Processing and mechanical properties of porous Ti–7.5Mo alloy', *Materials & Design*, 47, pp. 21–26. doi: 10.1016/j.matdes.2012.12.043.

Huang, Y. *et al.* (2017) ‘Microstructural comparison of effects of hafnium and titanium additions in spark-plasma-sintered Fe-based oxide-dispersion strengthened alloys’, *Journal of Nuclear Materials*. The Authors, 487, pp. 433–442. doi: 10.1016/j.jnucmat.2017.02.030.

I, K. K. W., I, L. J. G. and I, J. H. D. (2017) ‘WANG ET AL. / Ti-12Mo-6Zr-2Fe FOR SURGICAL IMPLANTS’, pp. 76–87.

Ikeda, M. *et al.* (2009) ‘Isothermal Aging Behavior of Beta Titanium–Manganese Alloys’, *Materials Transactions*, 50(12), pp. 2737–2743. doi: 10.2320/matertrans.MA200902.

Ikehata, H. *et al.* (2004) ‘First-principles calculations for development of low elastic modulus Ti alloys’, *Physical Review B*, 70(17), pp. 1–8. doi: 10.1103/PhysRevB.70.174113.

Jackson-Leach, R. and Lobstein, T. (2006) ‘Estimated burden of paediatric obesity and co-morbidities in Europe. Part 1. the increase in the prevalence of child obesity in Europe is itself increasing’, *International Journal of Pediatric Obesity*, 1(1), pp. 26–32. doi: 10.1080/17477160600586614.

Kanyane, L. R. *et al.* (2019) ‘Synthesis of equi-atomic Ti-Al-Mo-Si-Ni high entropy alloy via spark plasma sintering technique: Evolution of microstructure, wear, corrosion and oxidation behaviour’, *Results in Physics*. Elsevier, 14(March), p. 102465. doi: 10.1016/j.rinp.2019.102465.

Kon, M., Hirakata, L. M. and Asaoka, K. (2004) ‘Porous Ti-6Al-4V Alloy Fabricated by Spark Plasma Sintering for Biomimetic Surface Modification’, *Journal of Biomedical Materials Research - Part B Applied Biomaterials*, 68(1), pp. 88–93. doi: 10.1002/jbm.b.20004.

Kumar, S. and Narayanan, T. S. N. S. (2008) ‘Corrosion behaviour of Ti-15Mo alloy for dental implant applications’, *Journal of Dentistry*, 36(7), pp. 500–507. doi: 10.1016/j.jdent.2008.03.007.

Kuroda, D. *et al.* (1998) ‘Design and mechanical properties of new  $\beta$  type titanium alloys for implant materials’, *Materials Science and Engineering: A*, 243(1–2), pp. 244–249. doi: 10.1016/S0921-5093(97)00808-3.

Kuroda, P. A. B., Buzalaf, M. A. R. and Grandini, C. R. (2016) ‘Effect of molybdenum on structure, microstructure and mechanical properties of biomedical Ti-20Zr-Mo alloys’, *Materials Science and Engineering: C*. Elsevier B.V., 67, pp.



511–515. doi: 10.1016/j.msec.2016.05.053.

Kurtz, S. M. *et al.* (2007) ‘Future clinical and economic impact of revision total hip and knee arthroplasty’, *Journal of Bone and Joint Surgery - Series A*, 89(SUPPL. 3), pp. 144–151. doi: 10.2106/JBJS.G.00587.

Kusano, Y. *et al.* (2010) ‘Phase Constitution and Mechanical Properties of Ti-(Cr, Mn)-Sn Biomedical Alloys’, *Materials Science Forum*, 654–656(October 2015), pp. 2118–2121. doi: 10.4028/www.scientific.net/MSF.654-656.2118.

Kwasniak, P. *et al.* (2014) ‘Influence of oxygen content on the mechanical properties of hexagonal titanium: First principles calculations’, *Mater. Sci. Engng A*, 590(8), pp. 74–79.

Laheurte, P. *et al.* (2010) ‘Mechanical properties of low modulus ?? titanium alloys designed from the electronic approach’, *Journal of the Mechanical Behavior of Biomedical Materials*. Elsevier Ltd, 3(8), pp. 565–573. doi: 10.1016/j.jmbbm.2010.07.001.

Lampman, S. and International, A. S. M. (2018) ‘Titanium and Its Alloys for Biomedical Implants’, *Materials for Medical Devices*, 23, pp. 223–236. doi: 10.31399/asm.hb.v23.a0005674.

Li, X. *et al.* (2015) ‘Crystallization kinetics and spark plasma sintering of amorphous Ni<sub>53</sub>Nb<sub>20</sub>Ti<sub>10</sub>Zr<sub>8</sub>Co<sub>6</sub>Ta<sub>3</sub> powders prepared by mechanical alloying’, *Vacuum*, 114, pp. 93–100. doi: 10.1016/j.vacuum.2015.01.002.

Li, Yuhua *et al.* (2014) ‘New developments of ti-based alloys for biomedical applications’, *Materials*, 7(3), pp. 1709–1800. doi: 10.3390/ma7031709.

Liu, J. *et al.* (2017) ‘Microstructure, mechanical behavior and biocompatibility of powder metallurgy Nb-Ti-Ta alloys as biomedical material’, *Materials Science and Engineering C*. Elsevier B.V., 71, pp. 512–519. doi: 10.1016/j.msec.2016.10.043.

Liu, X. J. *et al.* (2014) ‘The effect of process control agents and ball to powder ratios on the electrochemical characteristics of mechanically alloyed SnS<sub>2</sub> anode materials’, *Powder Technology*, 259, pp. 117–124. doi: 10.1016/j.powtec.2014.03.052.

Liu, Y. *et al.* (2006) ‘Design of powder metallurgy titanium alloys and composites’, *Materials Science and Engineering A*, 418(1–2), pp. 25–35. doi: 10.1016/j.msea.2005.10.057.

Lu, J. W. *et al.* (2013a) ‘Microstructure and beta grain growth behavior of Ti-Mo alloys solution treated’, *Materials Characterization*. Elsevier Inc., 84(96), pp. 105–111. doi: 10.1016/j.matchar.2013.07.014.

Lu, J. W. *et al.* (2013b) ‘Microstructure and beta grain growth behavior of Ti-Mo alloys solution treated’, *Materials Characterization*. Elsevier Inc., 84(96), pp. 105–111. doi: 10.1016/j.matchar.2013.07.014.

Ma, L. W., Cheng, H. S. and Chung, C. Y. (2013) ‘Effect of thermo-mechanical treatment on superelastic behavior of Ti-19Nb-14Zr (at.%) shape memory alloy’, *Intermetallics*, 32, pp. 44–50. doi: 10.1016/j.intermet.2012.07.024.

Majumdar, P., Singh, S. B. and Chakraborty, M. (2008) ‘Elastic modulus of biomedical titanium alloys by nano-indentation and ultrasonic techniques-A comparative study’, *Materials Science and Engineering A*, 489(1–2), pp. 419–425. doi: 10.1016/j.msea.2007.12.029.

Majumdar, S. *et al.* (2010) ‘Preparation of Mo-Ti-Zr-C alloy tube by P/M route’, *Nuclear Engineering and Design*. Elsevier B.V., 240(5), pp. 975–979. doi: 10.1016/j.nucengdes.2009.12.019.

Martins Júnior, J. R. S. *et al.* (2011) ‘Preparation and characterization of Ti-15Mo alloy used as biomaterial’, *Materials Research*, 14(1), pp. 107–112. doi: 10.1590/S1516-14392011005000013.

Martz, E. O. *et al.* (1997) ‘Materials and Design of Spinal Implants-A Review.’, *Journal of biomedical materials research*, 38(3), pp. 267–288. doi: 10.1002/(sici)1097-4636(199723)38:3<267::aid-jbm12>3.0.co;2-8.

Min, X. H. *et al.* (2008) ‘Effect of Fe and Zr additions on omega phase formation in beta-type Ti-Mo alloys’, *Materials Science and Engineering A*, 497(1–2), pp. 74–78. doi: 10.1016/j.msea.2008.06.018.

Min, X. H. *et al.* (2010) ‘Effects of Fe addition on tensile deformation mode and crevice corrosion resistance in Ti-15Mo alloy’, *Materials Science and Engineering A*. Elsevier B.V., 527(10–11), pp. 2693–2701. doi: 10.1016/j.msea.2009.12.050.

Mishnaevsky, L. *et al.* (2014) ‘Nanostructured titanium-based materials for medical implants: Modeling and development’, *Materials Science and Engineering R: Reports*, 81(1), pp. 1–19. doi: 10.1016/j.mser.2014.04.002.

Miura, K. *et al.* (2011) ‘Acta Biomaterialia The bone tissue compatibility of a new Ti – Nb – Sn alloy with a low Young ’ s modulus’, *Acta Biomaterialia*. Acta

Materialia Inc., 7(5), pp. 2320–2326. doi: 10.1016/j.actbio.2011.02.008.

Mohammed, M. T. (2014) ‘Beta-Titanium-Alloys-The-Lowest-Elastic-Modulus-for-Biomedical-Applications-A-Review’, *International Journal of Chemical, Nuclear, Materials and Metallurgical Engg*, 8(8), pp. 772–77.

Mohan, P. *et al.* (2017) ‘Effect of Fe content, sintering temperature and powder processing on the microstructure, fracture and mechanical behaviours of Ti-Mo-Zr-Fe alloys’, *Journal of Alloys and Compounds*. Elsevier B.V, 729, pp. 1215–1225. doi: 10.1016/j.jallcom.2017.09.255.

Mouawad, B. *et al.* (2012) ‘Full densification of molybdenum powders using Spark Plasma Sintering’, *Metallurgical and Materials Transactions A*, pp. 1–8. Available at: <https://hal.archives-ouvertes.fr/hal-01081684/>.

Nag, S. *et al.* (2005) ‘Comparison of microstructural evolution in Ti-Mo-Zr-Fe and Ti-15Mo biocompatible alloys’, *Journal of Materials Science: Materials in Medicine*, 16(7), pp. 679–685. doi: 10.1007/s10856-005-2540-6.

Nag, S., Banerjee, R. and Fraser, H. L. (2007) ‘A novel combinatorial approach for understanding microstructural evolution and its relationship to mechanical properties in metallic biomaterials’, *Acta Biomaterialia*, 3(3 SPEC. ISS.), pp. 369–376. doi: 10.1016/j.actbio.2006.08.005.

Nakai, M. *et al.* (2011) ‘Self-adjustment of Young’s modulus in biomedical titanium alloys during orthopaedic operation’, *Materials Letters*. Elsevier B.V., 65(4), pp. 688–690. doi: 10.1016/j.matlet.2010.11.006.

Nazari, K. A., Nouri, A. and Hilditch, T. (2015) ‘Effects of milling time on powder packing characteristics and compressive mechanical properties of sintered Ti-10Nb-3Mo alloy’, *Materials Letters*. Elsevier, 140, pp. 55–58. doi: 10.1016/j.matlet.2014.10.143.

Nie, L. *et al.* (2014) ‘Novel ??-type Zr-Mo-Ti alloys for biological hard tissue replacements’, *Materials and Design*. Elsevier Ltd, 53, pp. 8–12. doi: 10.1016/j.matdes.2013.07.008.

Niespodziana, K., Jurezyk, K. and Jurczyk, M. (2008) ‘The synthesis of titanium alloys for biomedical applications’, *Rev. Adv. Mater. Sci*, 18, pp. 236–240. Available at: [http://www.ipme.ru/e-journals/RAMS/no\\_31808/niespodziana.pdf](http://www.ipme.ru/e-journals/RAMS/no_31808/niespodziana.pdf).

Niinomi, M. (1998) ‘Mechanical properties of biomedical titanium alloys’, *Materials Science and Engineering: A*, 243(1–2), pp. 231–236. doi: 10.1016/S0921-

5093(97)00806-X.

Niinomi, M. (2002) 'Recent metallic materials for biomedical applications', *Metallurgical and Materials Transactions A*, 33(3), pp. 477–486. doi: 10.1007/s11661-002-0109-2.

Niinomi, M. (2003a) 'Fatigue performance and cyto-toxicity of low rigidity titanium alloy, Ti-29Nb-13Ta-4.6Zr', *Biomaterials*, 24(16), pp. 2673–2683. doi: 10.1016/S0142-9612(03)00069-3.

Niinomi, M. (2003b) 'Recent research and development in titanium alloys for biomedical applications and healthcare goods', *Science and Technology of Advanced Materials*, 4(5), pp. 445–454. doi: 10.1016/j.stam.2003.09.002.

Niinomi, M., Nakai, M. and Hieda, J. (2012) 'Development of new metallic alloys for biomedical applications', *Acta Biomaterialia*. Acta Materialia Inc., 8(11), pp. 3888–3903. doi: 10.1016/j.actbio.2012.06.037.

Nishimura, T. (2011) 'Corrosion resistance of Mo-Fe-Ti alloy for overpack in simulating underground environment', *Nuclear Engineering and Design*. Elsevier B.V., 241(12), pp. 4745–4749. doi: 10.1016/j.nucengdes.2011.03.032.

Van Noort, R. (1987) 'Titanium: The implant material of today', *Journal of Materials Science*, 22(11), pp. 3801–3811. doi: 10.1007/BF01133326.

Nouri, A., Hodgson, P. D. and Wen, C. (2011) 'Effect of ball-milling time on the structural characteristics of biomedical porous Ti-Sn-Nb alloy', *Materials Science and Engineering C*. Elsevier B.V., 31(5), pp. 921–928. doi: 10.1016/j.msec.2011.02.011.

O'Brien, R. C. *et al.* (2009) 'Spark Plasma Sintering of simulated radioisotope materials within tungsten cermets', *Journal of Nuclear Materials*. Elsevier B.V., 393(1), pp. 108–113. doi: 10.1016/j.jnucmat.2009.05.012.

Oldani, C. R. and Dominguez, a a (2007) 'Simulation of the mechanical behavior of a HIP implant. Implant fixed to bone by cementation under arbitrary load', *Journal of Physics: Conference Series*, 90, p. 012007. doi: 10.1088/1742-6596/90/1/012007.

Oshida, Y. (2013) *10 - Fabrication Technologies, Bioscience and Bioengineering of Titanium Materials (Second Edition)*. doi: <http://dx.doi.org/10.1016/B978-0-444-62625-7.00010-8>.

- Park, C. H. *et al.* (2017) ‘Multifunctional Beta Ti Alloy with Improved Specific Strength’, *Shape Memory and Superelasticity*. Springer International Publishing, 3(4), pp. 373–380. doi: 10.1007/s40830-017-0124-1.
- Raducanu, D. *et al.* (2011) ‘Mechanical and corrosion resistance of a new nanostructured Ti-Zr-Ta-Nb alloy’, *Journal of the Mechanical Behavior of Biomedical Materials*. Elsevier Ltd, 4(7), pp. 1421–1430. doi: 10.1016/j.jmbbm.2011.05.012.
- Sabeena, M. *et al.* (2016) ‘Microstructural characterization of transformation products of bcc ?? in Ti-15 Mo alloy’, *Journal of Alloys and Compounds*. Elsevier B.V, 658, pp. 301–315. doi: 10.1016/j.jallcom.2015.10.200.
- Shen, Z. *et al.* (2002) ‘Spark plasma sintering of alumina’, *Journal of the American Ceramic Society*, 85(8), pp. 1921–1927. doi: 10.1111/j.1151-2916.2002.tb00381.x.
- Sochacka, P., Miklaszewski, A. and Jurczyk, M. (2019) ‘Development of  $\beta$ -type Ti-x at. % Mo alloys by mechanical alloying and powder metallurgy: Phase evolution and mechanical properties ( $10 \leq x \leq 35$ )’, *Journal of Alloys and Compounds*. Elsevier B.V, 776, pp. 370–378. doi: 10.1016/j.jallcom.2018.10.217.
- Suárez, M., Fernández, a and Menéndez, J. (2013) ‘Challenges and Opportunities for Spark Plasma Sintering: A Key Technology for a New Generation of Materials’, *Sintering Applications*, p. 319. doi: <http://dx.doi.org/10.5772/53706>.
- Sugano, D. and Ikeda, M. (2005) ‘The effect of aluminum content on phase constitution and heat treatment behavior of Ti-Cr-Al alloys for healthcare application’, *Materials Science and Engineering C*, 25(3), pp. 377–381. doi: 10.1016/j.msec.2005.01.021.
- Suryanarayana, C., Ivanov, E. and Boldyrev, V. . (2001) ‘The science and technology of mechanical alloying’, *Materials Science and Engineering: A*, 304–306, pp. 151–158. doi: 10.1016/S0921-5093(00)01465-9.
- Tane, M. *et al.* (2008) ‘Peculiar elastic behavior of Ti-Nb-Ta-Zr single crystals’, *Acta Materialia*, 56(12), pp. 2856–2863. doi: 10.1016/j.actamat.2008.02.017.
- Tarzimoghadam, Z. *et al.* (2015) ‘Microstructure design and mechanical properties in a near- $\alpha$  Ti-4Mo alloy’, *Acta Materialia*. Acta Materialia Inc., 97, pp. 291–304. doi: 10.1016/j.actamat.2015.06.043.
- Tsai, J. T. *et al.* (2012) ‘Microstructure and properties of Ti-8Mo-12Fe and Ti-8Mo-8Cu alloys with Cr<sub>3</sub>C<sub>2</sub> additives produced in the powder metallurgy processes’,

*Procedia Engineering*, 36, pp. 368–373. doi: 10.1016/j.proeng.2012.03.054.

Wang, K. (1996) ‘The use of titanium for medical applications in the USA’, *Materials Science and Engineering A*, 213(1–2), pp. 134–137. doi: 10.1016/0921-5093(96)10243-4.

Wang, S. *et al.* (2016) ‘Effect of mechanical alloying on the microstructure and properties of W–Ti alloys fabricated by spark plasma sintering’, *Powder Technology*. Elsevier B.V., 302, pp. 1–7. doi: 10.1016/j.powtec.2016.08.039.

Yang, G. and Zhang, T. (2005) ‘Phase transformation and mechanical properties of the Ti 50Zr30Nb10Ta10 alloy with low modulus and biocompatible’, *Journal of Alloys and Compounds*, 392(1–2), pp. 291–294. doi: 10.1016/j.jallcom.2004.08.099.

Yang, Y. F. *et al.* (2012) ‘The sintering, sintered microstructure and mechanical properties of Ti-Fe-Si alloys’, *Metallurgical and Materials Transactions A: Physical Metallurgy and Materials Science*, 43(12), pp. 4896–4906. doi: 10.1007/s11661-012-1272-8.

Yoda, M. *et al.* (2001) ‘Bond strength of binary titanium alloys to porcelain’, *Biomaterials*, 22(12), pp. 1675–1681. doi: 10.1016/S0142-9612(00)00329-X.

Zardiackas, L. D., Mitchell, D. W. and Disegi, J. a. (1997) ‘Characterization of Ti-15Mo beta titanium alloy [orthopedic implants]’, *Proceedings of the 1997 16 Southern Biomedical Engineering Conference*, pp. 95–98. doi: 10.1109/SBEC.1997.583223.

Zardiackas, L. D., Mitchell, I. D. W. and Disegi, J. A. (2017) ‘Copyright 9 1996 by ASTM International www.astm.org’, pp. 60–75.

Zhang, W. D. *et al.* (2015) ‘Elastic modulus of phases in Ti-Mo alloys’, *Materials Characterization*. Elsevier Inc., 106, pp. 302–307. doi: 10.1016/j.matchar.2015.06.008.

Zhao, C., Zhang, X. and Cao, P. (2011) ‘Mechanical and electrochemical characterization of Ti-12Mo-5Zr alloy for biomedical application’, *Journal of Alloys and Compounds*. Elsevier B.V., 509(32), pp. 8235–8238. doi: 10.1016/j.jallcom.2011.05.090.

Zhao, X. *et al.* (2012) ‘Beta type Ti-Mo alloys with changeable Young’s modulus for spinal fixation applications’, *Acta Biomaterialia*. Acta Materialia Inc., 8(5), pp. 1990–1997. doi: 10.1016/j.actbio.2012.02.004.

Zhentaoy, Y. and Lian, Z. (2006) 'Influence of martensitic transformation on mechanical compatibility of biomedical ?? type titanium alloy TLM', *Materials Science and Engineering A*, 438–440(SPEC. ISS.), pp. 391–394. doi: 10.1016/j.msea.2005.12.079.

*Development of new high-performance Titanium alloys with Fe-addition for dental implants*



## List of publications:

### Journal papers:

- Mohan, P., Elshalakany, A.B., Osman, T.A., Amigo, V. and Mohamed, A., 2017. Effect of Fe content, sintering temperature and powder processing on the microstructure, fracture and mechanical behaviours of Ti-Mo-Zr-Fe alloys. *Journal of Alloys and Compounds*, 729, pp.1215-1225.

Journal of Alloys and Compounds 729 (2017) 1215–1225



Contents lists available at ScienceDirect

Journal of Alloys and Compounds

journal homepage: <http://www.elsevier.com/locate/jalcom>



### Effect of Fe content, sintering temperature and powder processing on the microstructure, fracture and mechanical behaviours of Ti-Mo-Zr-Fe alloys



P. Mohan<sup>a</sup>, Abou Bakr Elshalakany<sup>a,d</sup>, T.A. Osman<sup>c</sup>, V. Amigo<sup>a</sup>, Alaa Mohamed<sup>b,d,\*</sup>

<sup>a</sup> Institute of Materials Technology, Universitat Politècnica de València, Spain

<sup>b</sup> Egypt Nanotechnology Center, EGNC, Cairo University, 12613 Giza, Egypt

<sup>c</sup> Mechanical Design and Production Engineering Department, Cairo University, Giza, Egypt

<sup>d</sup> Production Engineering and Printing Technology Department, Akhbar El Yam Academy, Giza, Egypt

#### ARTICLE INFO

##### Article history:

Received 4 August 2017

Received in revised form

22 September 2017

Accepted 23 September 2017

Available online 25 September 2017

##### Keywords:

Elemental blend

Mechanical alloying

Biocompatibility

Mechanical properties

#### ABSTRACT

The present work studies the effect of iron on the microstructural characterization and mechanical properties of Ti12Mo6ZrxFe alloys that fabricated by two different techniques elemental blend (EB) at 600 MPa and mechanical alloying (MA) at 600 MPa and 900 MPa with different sintering temperatures. The Ti12Mo6ZrxFe ( $x = 1, 2, 3$  and 4 wt.%) alloys were investigated to develop new biomedical materials used for dental implant application. The microstructure, residual porosity and the mechanical properties of the sintered Ti12Mo6ZrxFe alloys were investigated by using optical microscopy, X-ray diffraction (XRD), Scanning Electron Microscopy (SEM), Energy dispersive X-ray (EDX), microhardness and bending stress–strain curves. The results indicated that addition of Zr and a small amount of Fe improves the  $\beta$ -phase stability and improving the properties of Ti-Mo alloy. In addition, with increasing the sintering temperatures, the microstructure became more homogeneous for  $\beta$  phase, which decreases in the modulus and strength. The Mechanical alloying allows highly homogeneous composition and particle morphology. Bending strength in EB is much higher than MA techniques. Increasing of compaction pressure during MA technique increases the bending strength and decreases the porosity. Moreover, the Ti12Mo6Zr2Fe alloys exhibited higher bending strength/modulus ratios.

© 2017 Elsevier B.V. All rights reserved.

- Elshalakany, A.B., Ali, S., Mata, A.A., Eessaa, A.K., Mohan, P., Osman, T.A. and Borrás, V.A., 2017. Microstructure and mechanical properties of Ti-Mo-Zr-Cr biomedical alloys by powder metallurgy. *Journal of Materials Engineering and Performance*, 26(3), pp.1262-1271.

JMEPEG  
DOI: 10.1007/s11665-017-2531-z

©ASM International  
1059-9495/19.00  CrossMark

## **Microstructure and Mechanical Properties of Ti-Mo-Zr-Cr Biomedical Alloys by Powder Metallurgy**

*Abou Bakr Elshalakany, Shady Ali, A. Amigó Mata, Ashraf K. Eessaa, P. Mohan, T.A. Osman, and V. Amigó Borrás*

*(Submitted May 6, 2016; in revised form January 3, 2017)*

Titanium and its alloys have been widely used as biometals due to their excellent biocompatibility, corrosion resistance and moderate mechanical properties. Ti-15Mo-6Zr-based alloys and a series of Ti-15Mo-6Zr-xCr ( $x = 1, 2, 3, 4$  wt.%) alloys were designed and fabricated by powder metallurgy for the first time to develop novel biomedical materials. The microstructure, internal porosity and mechanical properties of the sintered Ti-15Mo-6Zr and Ti-15Mo-6Zr-xCr alloys were investigated using scanning electronic microscopy (SEM) and bending and compression tests. The experimental results indicated that the microstructure and mechanical properties of these alloys changed as different Cr levels were added. The addition of small Cr levels further increased the  $\beta$ -phase stability, improving the properties of the Ti-15Mo-6Zr-xCr alloy. However, all of the alloys had good ductility, and the Ti-15Mo-6Zr-2Cr alloy had lower bending and compression moduli (31 and 23 GPa, respectively) than the Ti-15Mo-6Zr-based alloys (40 and 36 GPa, respectively). Moreover, the Ti-15Mo-6Zr-2Cr alloys exhibited higher bending and compression strength/modulus ratios, which were as large as 48.4 and 52.2, respectively; these were higher than those of the Ti-15Mo-6Zr-based alloy (41.3 and 33.6, respectively). In the search for a better implant material,  $\beta$  phase Ti-15Mo-6Zr-2Cr, with its low modulus, ductile properties and reasonably high strength, is a promising candidate.

## **Conference Papers:**

- Mohan, P., Amigó Mata, A., Elshalakany, A.B., and Amigó, V., July 2015 Effect Of Powder Processing On The Microstructure And Mechanical Properties Of Ti-Mo Alloys. V congreso Nacional de Pulvimetalurgia Girona 2015. 1,2 y 3 de Julio (pp. 388-397)

*V Congreso Nacional de Pulvimetalurgia Girona 2015. 1, 2 y 3 de julio*

### **EFFECT OF POWDER PROCESSING ON THE MICROSTRUCTURE AND MECHANICAL PROPERTIES OF TI-MO ALLOYS**

*P.Mohan<sup>1</sup>, A. Amigo<sup>1</sup>, Abou Bakr Elshalakany<sup>1,2</sup>, V.Amigo<sup>1</sup>*

*<sup>1</sup>INSTITUTE OF MATERIALS TECHNOLOGY (ITM-UPV) UNIVERSITY POLYTECHNIC OF VALENCIA, SPAIN*

*<sup>2</sup>PRODUCTION ENGINEERING AND PRINTING TECHNOLOGY DEPARTMENT, AKHBAR EL YOM ACADEMY, GIZA, EGYPT*

*pramo@doctor.upv.es, anamma@upvnet.upv.es, abahel@doctor.upv.es, vamigo@mcm.upv.es*

#### **ABSTRACT**

Ti and its alloys are mostly used biomaterials due to its unique properties like (high corrosion resistance, low elastic modulus, high mechanical strength/ density, good biocompatibility etc.).Ti  $\beta$  alloys based on the Ti-Mo alloy system shows much more interest for biomaterials researcher. Addition of Zr and small amount of Fe improves the  $\beta$ -phase stability and improving the properties of Ti-Mo alloy. These alloys produced by powder metallurgy (PM) using firstly elemental blend (EB) technique (600 MPa pressure) and then after Mechanical alloying technique (600 MPa and 900 MPa).Mechanical alloying used mainly for improving mixing and better diffusion of elements. This paper describes the microstructural characterization and mechanical properties obtained by bending test, Archimedes test and ultrasonic test of Ti-Mo-Zr-Fe alloys made by elemental blend and mechanical alloying technique. The Mechanical alloying allows highly homogeneous composition and particle morphology. Bending strength is more in elemental blend in compare to mechanical alloying technique. Increasing of compaction pressure during mechanical alloying technique increases bending strength and decreases porosity. Mainly two phases appears on sintered sample name as  $\alpha$ -phase and  $\beta$ - phase.

- Mohan, P., Amigó Mata, A. and Amigó, V., 2016. Effects of Fe and Mo Content on the Microstructure and Mechanical Properties of Ti-Mo based alloys prepared by Elemental blend and Mechanical alloying technique. In *Transactions of Powder Metallurgy Association of India* (Vol. 42, No. 1, pp. 25-31). Powder Metallurgy Assoc. of India

*V Congreso Nacional de Pulvimetalurgia Girona 2015. 1, 2 y 3 de julio*

P27

## **EFFECT OF POWDER PROCESSING ON THE MICROSTRUCTURE AND MECHANICAL PROPERTIES OF TI-MO ALLOYS**

*P.Mohan<sup>1</sup>, A. Amigo<sup>1</sup>, Abou Bakr Elshalakany<sup>1,2</sup>, V.Amigo<sup>1</sup>*

*<sup>1</sup>INSTITUTE OF MATERIALS TECHNOLOGY (ITM-UPV) UNIVERSITY POLYTECHNIC OF VALENCIA, SPAIN*

*<sup>2</sup>PRODUCTION ENGINEERING AND PRINTING TECHNOLOGY DEPARTMENT, AKHBAR EL YOM ACADEMY, GIZA, EGYPT*

*pramo@doctor.upv.es, anamma@upvnet.upv.es, abahel@doctor.upv.es, vamigo@mcm.upv.es*

### **ABSTRACT**

Ti and its alloys are mostly used biomaterials due to its unique properties like (high corrosion resistance, low elastic modulus, high mechanical strength/ density, good biocompatibility etc.). Ti  $\beta$  alloys based on the Ti-Mo alloy system shows much more interest for biomaterials researcher. Addition of Zr and small amount of Fe improves the  $\beta$ -phase stability and improving the properties of Ti-Mo alloy. These alloys produced by powder metallurgy (PM) using firstly elemental blend (EB) technique (600 MPa pressure) and then after Mechanical alloying technique (600 MPa and 900 MPa). Mechanical alloying used mainly for improving mixing and better diffusion of elements. This paper describes the microstructural characterization and mechanical properties obtained by bending test, Archimedes test and ultrasonic test of Ti-Mo-Zr-Fe alloys made by elemental blend and mechanical alloying technique. The Mechanical alloying allows highly homogeneous composition and particle morphology. Bending strength is more in elemental blend in compare to mechanical alloying technique. Increasing of compaction pressure during mechanical alloying technique increases bending strength and decreases porosity. Mainly two phases appears on sintered sample name as  $\alpha$ -phase and  $\beta$ - phase.